Novel formulation techniques for co-amorphous systems with special focus on *in situ* co-amorphisation

Dissertation

with the aim of achieving a doctoral degree

at the Faculty of Mathematics, Informatics and Natural Sciences

Department of Chemistry

Universität Hamburg

submitted by

Ina Petry

Hamburg 2019

The experimental studies and the preparation of this thesis were carried out between October 2015 and May 2019 in the Department of Chemistry at the University of Hamburg, in the division of Pharmaceutical Technology, on the initiative and under supervision of Professor Dr. Claudia S. Leopold.

Zusammenfassung

Damit ein Arzneistoff resorbiert und oral bioverfügbar werden kann, ist eine ausreichend hohe Wasserlöslichkeit Voraussetzung. Während der letzten zwei Jahrzehnte ist der Anteil an neu entwickelten Arzneistoffen, die schlecht wasserlöslich sind, stark gestiegen, sodass die Löslichkeitsverbesserung ein bedeutendes Forschungsfeld im Bereich der pharmazeutischen Entwicklung darstellt. In diesem Zusammenhang ist die Verwendung sogenannter co-amorpher Systeme ein sehr vielversprechender Ansatz, um schlecht wasserlösliche Arzneistoffe zu formulieren. Da es sich hierbei um ein vergleichsweise neues Forschungsgebiet handelt, wurden bisherige Studien vorwiegend im Labormaßstab durchgeführt. Für das weitere Verständnis sind Untersuchungen nötig, die sich mit der Verarbeitung von co-amorphen Systemen in fertige Darreichungsformen sowie der Lagerstabilität co-amorpher Systeme beschäftigen. Obwohl pharmazeutische Filmüberzüge eine naheliegende Möglichkeit darstellen, um die Stabilität co-amorpher Systeme zu erhöhen, gibt es bisher keine Erfahrungen im Überziehen dieser Systeme.

Aus diesem Grund war es ein Ziel der vorliegenden Dissertation, zu untersuchen, ob das Überziehen einer co-amorphen Formulierung möglich ist, ohne ihre physikalische Stabilität negativ zu beeinflussen. Die Ergebnisse zeigten, dass die co-amorphe Modell-Formulierung, bestehend aus einer Kombination aus Indometacin und Arginin, sowohl während des Coating-Prozesses, als auch während der anschließenden Lagerung für bis zu drei Monate stabil war. Außerdem führte der verwendete Filmüberzug zu einer deutlichen Erhöhung der Freisetzung aus der Filmtablette im Vergleich zu der nicht überzogenen Tablette.

Interessanterweise wurde in dieser Studie eine Farbveränderung der kristallinen Referenz-Formulierung bestehend aus Indometacin und Arginin während der Lagerung

bei hoher Luftfeuchte (75 % RF) beobachtet. Da die Auswertung der Festphasen-Analytik dieser Referenz-Formulierung auf eine Co-amorphisierung zwischen Indometacin und Arginin als Grund für die Farbveränderung hinwies, war es ein weiteres Ziel der vorliegenden Arbeit, diese *in situ* Co-amorphisierung genauer zu untersuchen. Die zweite Studie dieser Doktorarbeit beschäftigte sich deshalb mit der Veränderung der physikalischen und chemischen Eigenschaften physikalischer Indometacin-Arginin Mischungen während der Lagerung bei verschiedenen definierten Luftfeuchten. Die Ergebnisse zeigten, dass die physikalischen Mischungen kristallin blieben und chemisch stabil waren, wenn sie bei 28 % bzw. 58 % RF gelagert wurden. Im Gegensatz dazu wurde während der Lagerung bei 75 % RF die Entstehung von co-amorphem Indometacin-Arginin sowie chemische Hydrolyse von Indometacin beobachtet.

Auch wenn *in situ* Amorphisierung normalerweise eine Instabilität darstellt und unbeabsichtigt stattfindet, wird im Bereich der Forschung seit kurzem der Ansatz einer kontrollierten *in situ* Amorphisierung verfolgt. Dies bedeutet, dass man eine kristalline Arzneistoff-Formulierung verwendet, die erst kurz vor der Einnahme durch den Patienten „aktiviert", also amorphisiert, wird, wodurch physikalische Stabilitätsprobleme einer amorphen Formulierung während der Herstellung und Lagerung verhindert werden können. In diesem Zusammenhang wurde postuliert, dass die beobachtete *in situ* Co-amorphisierung von Indometacin und Arginin während der Lagerung bei feuchten Bedingungen für eine kontrollierte *in situ* Co-amorphisierung genutzt werden könnte. Die dritte Studie der vorliegenden Arbeit beschäftigte sich daher mit der Entwicklung einer geeigneten Filmtabletten-Formulierung, um eine kontrollierte *in situ* Co-amorphisierung in einer Arzneiform zu realisieren. Diese Studie konnte zeigen, dass die Verwendung eines magensaftresistenten, aber dennoch permeablen Überzuges für Indometacin-

Arginin oder auch Furosemid-Arginin Tabletten eine *in situ* Co-amorphisierung der jeweiligen Systeme während Immersion in saurem Medium ermöglichte.

Da diese Studie die erste war, die eine erfolgreiche *in situ* Co-amorphisierung in einer fertigen Arzneiform zeigen konnte, blieb zunächst unklar, ob es sich hierbei um einen generellen Ansatz zur *in situ* Co-amorphisierung diverser Systeme handelte, oder ob dieses Konzept nur für einzelne Systeme geeignet ist. Aus diesem Grund war es das Ziel der vierten Studie dieser Arbeit, die Übertragbarkeit dieses Konzeptes auf die Kombination eines basischen Arzneistoffes (Carvedilol) und einer sauren Aminosäure (Asparaginsäure) zu untersuchen. Die Ergebnisse zeigten, dass auch diese Filmtabletten-Formulierung während Immersion in saurem Medium *in situ* co-amorphisiert wurde. Der in der vorliegenden Arbeit entwickelte Ansatz könnte deswegen die *in situ* Co-amorphisierung verschiedener co-amorpher Systeme ermöglichen.

Abstract

A sufficiently high water solubility is a requirement for an API to be absorbed and become orally bioavailable. As over the last two decades, the number of poorly water-soluble drugs in the pharmaceutical development pipeline has tremendously increased, solubility improvement has become a very important field within pharmaceutical research and drug development. Amongst several strategies, the use of so-called co-amorphous systems has recently gained interest as formulation approach for poorly water-soluble drugs. However, as this approach is comparably new, so far research has mainly been conducted on a lab scale. Thus, investigations on down-streaming of co-amorphous systems into final dosage forms as well as further stability studies are still needed. Although the application of pharmaceutical polymer coatings might be one obvious approach to improve the stability of co-amorphous systems, no experience exists in the coating of co-amorphous formulations so far.

Therefore, one aim of this thesis was to investigate whether coating of a co-amorphous formulation is possible without negatively affecting its physical stability. Results showed that the coated co-amorphous model formulation consisting of a combination of indomethacin and arginine was stable during the coating process and during storage for up to three months at defined conditions. Furthermore, the applied coating even increased the drug release of indomethacin in comparison to the respective uncoated formulation.

Interestingly, in this study a colour change of the crystalline reference formulation comprising indomethacin and arginine was observed during storage at humid conditions (75 % RH). As solid-state analysis of this reference indicated a co-amorphisation of indomethacin and arginine as reason for the observed colour change, it was a further

aim of this thesis to investigate this *in situ* co-amorphisation behaviour. For this purpose, in a second study the solid-state properties as well as the chemical changes of the physical mixtures of indomethacin and arginine after storage at different RHs were analysed. Results showed that physical mixtures stored at 28 % and 58 % RH remained crystalline and were chemically stable, while the formation of co-amorphous indomethacin-arginine as well as basic hydrolysis of indomethacin were observed upon exposure to 75 % RH.

Although *in situ* amorphisation usually takes places accidentally and presents an in-stability, few studies recently introduced the concept of an intended *in situ* amor-phisation. As a crystalline formulation may become "activated", i.e. amorphised, directly prior to administration by the patient, physical stability problems of the amorphous form during processing and storage may be circumvented using this approach. In this context, it was assumed that the observed co-amorphisation of indomethacin and arginine during storage at humid conditions might be applied for a controlled *in situ* co-amorphisation. Therefore, the third study of this thesis dealt with the development of a film coated tablet formulation to enable such a controlled *in situ* co-amorphisation in the final dosage form. This study showed that the application of a gastro-resistant but water-permeable coating on crystalline indomethacin-arginine and also crystalline furosemide-arginine tablets enabled the formation of the respective co-amorphous system during immersion in an acidic medium.

As this study was the first showing a successful *in situ* co-amorphisation in a final dosage form, it was still unclear, whether this approach is also applicable to further compounds or is limited to only acidic APIs and basic coformers. Therefore, the aim of the fourth study of this thesis was to assess the applicability of this approach on the

combination of the basic model drug carvedilol and the acidic amino acid aspartic acid. The results showed an *in situ* co-amorphisation of carvedilol with aspartic acid during immersion of the coated tablets in the acidic medium. Therefore, the presented approach may allow the preparation of differently composed co-amorphous formulations.

Conference contributions and publications

In context with this work, the following contributions have been presented at conferences and journal articles have been published.

Conference contributions - oral presentations

Petry, I., Löbmann, K., Grohganz, H., Rades, T., Leopold, C.S.
Characterization of film-coated tablets consisting of either co-amorphous or crystalline indomethacin-arginine.
10th Annual Meeting of the Pharmaceutical Solid State Research Cluster 2016, Copenhagen, Denmark

Petry, I., Löbmann, K., Grohganz, H., Rades, T., Leopold, C.S.
How arginine in combination with moisture influences the solid-state and chemical stability of indomethacin.
11th Annual Meeting of the Pharmaceutical Solid State Research Cluster 2017, Graz, Austria

Petry, I., Löbmann, K., Grohganz, H., Rades, T., Leopold, C.S.
In situ co-amorphisation of carvedilol with aspartic acid in film-coated tablets.
12th Annual Meeting of the Pharmaceutical Solid State Research Cluster 2018, Leuven, Belgium

Conference contributions - poster presentations

Petry, I., Löbmann, K., Grohganz, H., Rades, T., Leopold, C.S.
Coated crystalline   indomethacin-arginine tablets undergo in situ amorphisation when stored at high humidity.
Meeting of the American Association of Pharmaceutical Scientists 2016, Denver, USA

Petry, I., Löbmann, K., Grohganz, H., Rades, T., Leopold, C.S.
The Influence of Arginine and Moisture on the Solid-State Properties and Chemical Stability of Indomethacin.
Meeting of the American Association of Pharmaceutical Scientists 2017, San Diego, USA

Petry, I., Löbmann, K., Grohganz, H., Rades, T., Leopold, C.S.
In vivo co-amorphisationof APIs in the stomach – a proof of concept.
11th World Meeting on Pharmaceutics,Biopharmaceutics and Pharmaceutical Technology 2018, Granada, Spain

Petry, I., Löbmann, K., Grohganz, H., Rades, T., Leopold, C.S.
In situ co-amorphisation of carvedilol with aspartic acid in film-coated tablets.
The 3rd European Conference on Pharmaceutics 2019, Bologna, Italy

Journal articles with authors` contributions and reference chapters.

Title	Journal	Authors	Contribution to the work	Percentage	Reference chapters
Solid-state properties and drug release behavior of co-amorphous indomethacin-arginine tablets coated with Kollicoat® Protect	European Journal of Pharmaceutics and Biopharmaceutics (accepted)	Petry, I. Löbmann. K. Grohganz, H. Rades, T. Leopold. C.S.	Project plan, experiments,data analysis, publication Supervisor Supervisor Supervisor Supervisor	100%	2.2.2, 2.2.3, 2.2.4, 2.2.5, 2.2.6.2, 2.2.7.1, 2.2.8, 2.2.9, 2.2.10, 2.2.11.1, 3.1
Undesired co-amorphisation of indomethacin and arginine during combined storage at high humidity conditions	International Journal of Pharmaceutics (accepted)	Petry, I. Löbmann. K. Grohganz, H. Rades, T. Leopold. C.S.	Project plan, experiments,data analysis, publication Supervisor Supervisor Supervisor Supervisor	100%	2.2.1, 2.2.6.1, 2.2.7.2, 2.2.8, 2.2.9, 2.2.11.2, 3.2
In situ co-amorphisation of arginine with indomethacin or furosemide during immersion in an acidic medium – A proof of concept study	European Journal of Pharmaceutics and Biopharmaceutics (accepted)	Petry, I. Löbmann. K. Grohganz, H. Rades, T. Leopold. C.S.	Project plan, experiments,data analysis, publication Supervisor Supervisor Supervisor Supervisor	100%	2.2.1, 2.2.3, 2.2.4, 2.2.5, 2.2.7, 2.2.9, 2.2.11.2, 3.3
In situ co-amorphisation in coated tablets – The combination of carvedilol with aspartic acid during immersion in an acidic medium	International Journal of Pharmaceutics (accepted)	Petry, I. Löbmann. K. Grohganz, H. Rades, T. Leopold. C.S.	Project plan, experiments,data analysis, publication Supervisor Supervisor Supervisor Supervisor	100%	2.2.2 2.2.3, 2.2.4, 2.2.5, 2.2.7, 2.2.9, 2.2.10, 2.2.11.1, 3.4

List of Abbreviations

API	Active pharmaceutical ingredient
ARG	Arginine
ASD	Amorphous solid dispersion
ASP	Aspartic acid
AUC	Area under the curve
BCS	Biopharmaceutical classification system
CA	Citric acid
CA-T	Carvedilol-aspartic acid tablet
CA-CT	Carvedilol-aspartic acid coated tablet
CAS	Co-amorphous system
CBA	4-chlorobenzoic acid
C-CT	Carvedilol coated tablet
cDSC	Conventional differential scanning calorimetry
C-T	Carvedilol tablet
CVD	Carvedilol
CoA	Co-amorphous
CoA FA-T	Co-amorphous furosemide-arginine tablet
CoA IA-T	Co-amorphous indomethacin-arginine tablet

CoA FUR-ARG	Co-amorphous furosemide-arginine
CoA IND-ARG	Co-amorphous indomethacin-arginine
DMA	Dynamic mechanical analysis
DSC	Differential scanning calorimetry
FA-T	Furosemide-arginine tablet
FA-CT	Furosemide.arginine coated tablet
Fig.	Figure
FTIR	Fourier-transform infrared spectroscopy
FUR	Furosemide
GIT	Gastro-intestinal tract
HCl	Hydrochloric acid
HPLC	High performance liquid chromatography
IAC-CT	Indomethacin-arginine-citric acid coated tablet
IAC-T	Indomethacin-arginine-citric acid tablet
IA-T	Indomethacin-arginine tablet
IA-CT	Indomethacin-arginine coated tablet
IND	Indomethacin
mDSC	Modulated differential scanning calorimetry
MMIA	5-methoxy-2-methyl-3-indolacetic acid

PCA	Principal component analysis
Ph. Eur.	European Pharmacopoeia
PB	Powder blend
PM	Physical mixture
PM-T	Physical mixture tablet
PM-CT	Physical mixture coated tablet
RH	Relative humidity
RF	Relative Feuchte
RT	Room temperature
SD	Standard deviation
SD CoA IND-ARG	Spray-dried co-amorphous indomethacin-arginine
SD CoA CVD-ASP	Spray-dried co-amorphous carvedilol-aspartic acid
SD-T	Spray-dried co-amorphous indomethacin-arginine tablet
SD-CT	Spray-dried co-amorphous indomethacin-arginine coated tablet
SEM	Scanning electron microscopy
T_g	Glass transition temperature
TGA	Thermogravimetric analysis
USP	United States Pharmacopeia
XRPD	X-ray powder diffractometry

Contents

1. Introduction

1.1 The Biopharmaceutics Classification System (BCS)

Among the multiple options for the administration of a pharmaceutical dosage form, the oral route represents the most preferred route of drug delivery. This aspect may be explained by the convenience and safety of this route of administration, leading to a high patient compliance [1]. In addition, the production costs of oral dosage forms are comparably low, which makes them especially attractive [1,2].

However, the oral route demands a sufficient bioavailability of the active pharmaceutical ingredients (APIs) in the respective formulation, which requires bioavailability investigations. The bioavailability describes the extent and rate in which the API is available at the target location [3,4]. For intravenously applied dosage forms it amounts to 100 %, as the already dissolved API is directly applied into the blood stream. In contrast, in an orally applied dosage form the API has to undergo three steps *in vivo* before it is able to reach the target location [5]. In a first step, if the dosage form is solid, it has to disintegrate and release the API. In a second step, the API has to dissolve in the gastrointestinal fluid, which is required for its subsequent permeation through the gastrointestinal barrier [6]. The extent and rate at which these three steps take place, determine the bioavailability of the API in the respective formulation. While the disintegration can be controlled by the selection of the excipients and the preparation technique of the formulation, the dissolution and permeation are mainly affected by the properties of the API. Therefore, the solubility and intestinal permeability of an API mainly determine its bioavailability. With the aim to correlate *in vitro* drug dissolution with *in vivo* drug absorption Amidon et al. introduced the Biopharmaceutics Classification

System (BCS) in 1995 [7]. Today, it is a generally acknowledged framework for the classification of drug substances into four different categories based on their solubility and permeability characteristics [7] (Fig. 1).
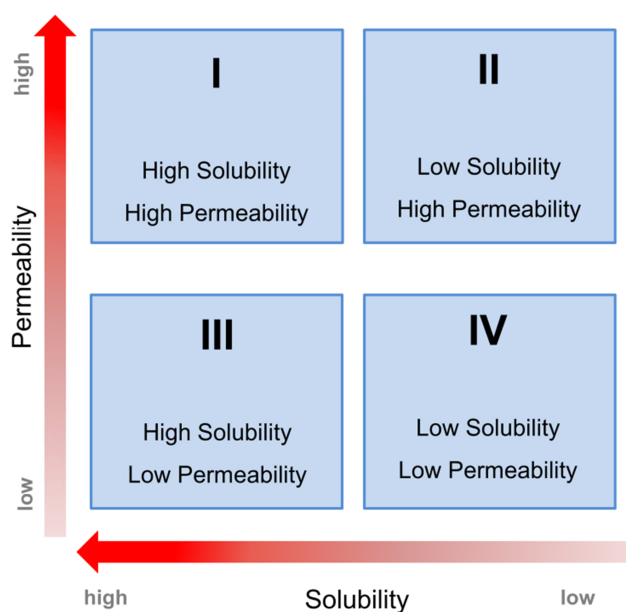
Fig. 1: Overview of the different API classes of the Biopharmaceutics Classification System (BCS).

In this context, highly soluble means that the highest dose of the API in an immediate release formulation is soluble in a maximum of 250 ml of aqueous medium (pH 1-7.5) [8]. If the highest dose needs more than 250 ml of medium to dissolve, it is considered as poorly soluble. The permeability of the API is considered as high, if it becomes absorbed by at least 90 % [8]. Permeability measurements may be conducted in humans *in vivo* or even *in vitro* using cell cultures. Such a classification of an API into one of the BCS classes may give information on its performance after oral administration. An API, which is classified as BCS class I possesses a high solubility

and a high permeability (Fig. 1). Therefore, the rate-determining step of its bioavailability is mainly the release of the API from its formulation. In contrast, the bioavailability of an API belonging to BCS class II, which shows a high permeability but a low solubility, is determined by the dissolution rate of the API. Similarly, the rate-determining step for the bioavailability of an API with high solubility but low permeability (BCS class III), is its intestinal absorption. If both, solubility and permeability are low (BCS class IV), further investigations are needed to assess the rate-determining step for the oral bioavailability. However, the oral bioavailability of an API from BCS class IV is expected to be rather low.

Over the last decades, computational high throughput screening methods have been frequently applied for the process of drug discovery, leading to an increasing number of hydrophobic and thus poorly water-soluble drug candidates in the drug development pipeline [9,10], which is estimated to be above 90 % [11]. Most of these candidates present BCS class II drugs. Therefore, their low solubility limits their bioavailability *in vivo*. As these drug candidates often have a high therapeutic potential, the solubility improvement is of particular interest in pharmaceutical research. Thus, several established techniques exist to improve the solubility of poorly water-soluble APIs, which are summarised in the literature [12–15]. Among these strategies, the conversion of the API into its amorphous form presents a promising approach to improve the solubility and thus the bioavailability of these compounds [16].

1.2 Amorphous systems

1.2.1 General aspects

The amorphous state of an API possesses a higher internal energy compared to its respective crystalline form, because of the absence of any long-range order. Thus, the physical properties of the amorphous form may differ from the respective crystalline form, e.g. the solubility and dissolution rate, which are both improved in most cases [17–19]. As crystalline solids comprise a long-range order, during dissolution thereof their defined three-dimensional structure (crystal lattice) must be disrupted. In contrast, amorphous solids lack any long-range order, which in theory results in a faster dissolution. In addition, with amorphous solids a higher maximum concentration is reached during dissolution compared to their crystalline counterpart resulting in a higher apparent solubility of the amorphous form, which is referred to as supersaturation.

However, the higher internal energy and increased molecular mobility may also lead to a physical instability of the amorphous state, which shows a tendency to recrystallise into the poorly soluble crystalline form, e.g. during processing, storage, or even dissolution [20]. Thus, the plain amorphous form of an API is unsuitable to be used in pharmaceutical dosage forms, and much effort is needed to find adequate technologies for the stabilisation of the amorphous form in the final formulation. Over the last years, different approaches have been shown to be feasible strategies to stabilise amorphous drugs, including polymer-based amorphous solid dispersions (ASDs), mesoporous silica-based glass solutions, and co-amorphous formulations [21,22]. All three strategies represent so-called glass solutions, which belong to the solid dispersions, and are shown in Fig. 2. Generally, the term *glass* represents amorphous material [19].

Therefore, a glass solution is a single amorphous phase system of the amorphous drug and an amorphous excipient [23]. Depending on the type of stabilising excipient used, it may be distinguished between the three above mentioned formulation approaches (Fig. 2).
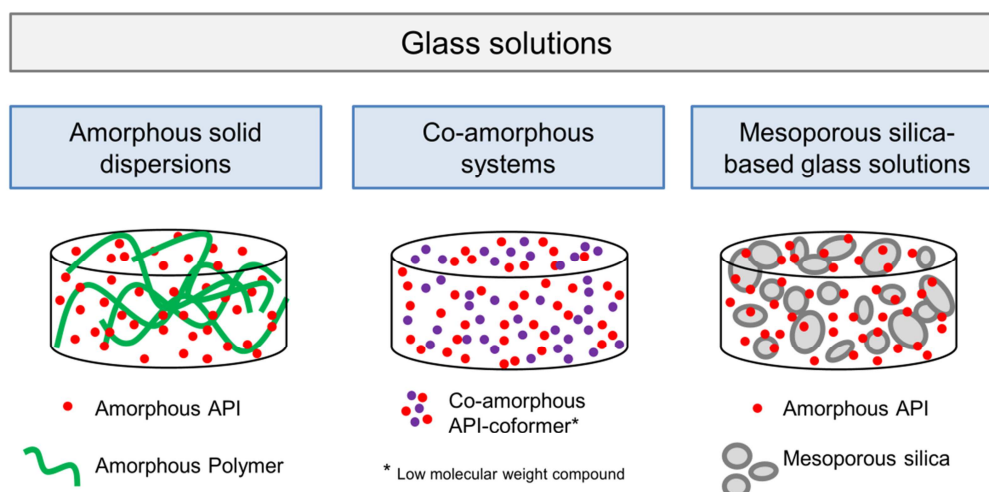
Fig. 2: Overview of the different types of glass solutions based on the selection of stabilising excipient.

Among these types of glass solutions, ASDs present the mostly investigated systems. In these systems, the amorphous form is stabilised by forming a homogeneous glass solution with a polymer. The incorporation of the amorphous API into the polymeric network reduces the mobility of the drug molecules, leading to an increase of the glass transition temperature (T_g) of the system, thus preventing recrystallisation [20,24,25]. Despite their benefits, ASDs do not represent an optimal and generally applicable formulation approach for amorphous drugs, as the physical stabilisation of the drug in the polymeric carrier over time remains a major challenge, also because of the high hygroscopicity of many polymers [26,27]. The absorption of moisture during processing

or storage of these systems may reduce the T_g, undoing the initial stabilisation of the amorphous API in the polymer. In addition, the drug solubility in the polymer is often limited, leading to large volume dosage forms, which limits the use for high dosage drugs [28].

Mesoporous silica is nano-engineered silica with a high specific surface area, as it contains many very small pores (2-50 nm diameter) [29]. In so-called mesoporous silica-based glass solutions, the amorphous API is stabilised by being adsorbed to the large surface area within the silica particle pores. As the amorphous API interacts with the functional groups of the silica, it is trapped in the pores, which limits the tendency of the amorphous form to recrystallise [30]. However, as with the ASDs, this approach shows some drawbacks, as the loading capacity of the mesoporous silica is often limited and the preparation of glass solutions thereof involves the use of organic solvents [21].

Because of the disadvantages of the two above mentioned approaches, lately the so-called co-amorphous systems (CAS) have gained attention as alternative technique to stabilise amorphous drugs [21]. In a CAS, the amorphous API is combined with at least one low molecular weight compound (coformer). The crystalline API and the crystalline coformer are amorphised together, resulting in a homogenous amorphous glass solution. If low molecular weight compounds are used instead of polymers, the amount of excipient for the stabilisation of the amorphous API in the final dosage form may be significantly reduced. In a CAS, API and coformer interact with each other on the molecular level. Thereby, the physical stability of the system is improved and the dissolution rate of the poorly soluble API is enhanced. Furthermore, the dissolution of

the API from a CAS is often not only increased compared to the crystalline form of the API, but also increased compared to the plain amorphous drug [31,32].

1.2.2 Coformer selection for co-amorphous systems

For the successful stabilisation of the amorphous API in a CAS the selection of suitable coformers is critical. During the last years, the selection of a coformer was mainly performed on a trial-and-error basis, although some recently performed studies tried to predict and systemize the coformer selection for CASs [33–35]. Although the formation of ternary co-amorphous systems is also possible [36], in most CASs the API is combined with only one coformer [33]. So far, there are many different small molecules available, which have already been shown to successfully stabilise various drugs. Thus, in a CAS the API may for example be combined with another API [37–42]. As the combination of two APIs is limited to pharmacologically useful pairs, the development of an API-API CAS is only possible in certain cases. Therefore, Löbmann et al. have introduced amino acids as more generally applicable coformers for CASs [43,44]. Also, organic acids [45–50], dipeptides [51,51,52], whey proteins [53], saccharine [54], and nicotinamide [55] have already been shown to form CASs with several drugs. Nevertheless, amino acids present the most widely investigated coformers.

Depending on the combination of API and coformer, different stabilisation mechanisms may be observed in a CAS. The molecular interactions may either result from hydrogen bonding, π-π or even ionic interactions [21,56]. Such ionic interactions between API and coformer result in the formation of a co-amorphous salt, which represents a special CAS as it combines two different formulation approaches for poorly water-soluble drugs,

namely amorphisation and salt formation [57,58]. Thus, co-amorphous salts are particularly interesting for the solubility improvement of poorly water-soluble drugs. To investigate whether a dissolution increase of a co-amorphous salt also results from the amorphisation of the drug, Kasten et al. recently compared the co-amorphous indomethacin-lysine salt with the respective crystalline salt [59]. In this study a higher dissolution rate for the co-amorphous salt than for the respective crystalline salt was found, thus demonstrating the high potential of co-amorphous salts as formulation approach for poorly water-soluble drugs. In addition, the physical stability of co-amorphous salt systems is often high resulting from the comparably strong molecular interactions of the two compounds. This observation may be confirmed by the detection of a single high glass transition temperature (T_g) in DSC thermograms, which is located above the T_gs of the individual compounds [60–62].

1.2.3 Physical stability of co-amorphous systems

The physical stability of a CAS does not only depend on the choice of coformer, but also on the molar ratio between both compounds. Usually, the 1:1 molar ratio (1:1:1 in ternary CASs) represents the most stable CAS of a distinct combination of two small molecules. This observation may be explained by the fact that the two compounds form a heterodimer [38]. To enable recrystallisation of the system, one compound would need to abandon the heterodimer. As a consequence, energy input is required for a recristallisation, whereby the physical stability of the CAS is improved compared to that of the single amorphous system. This theory is supported by many studies, in which it is described that CASs of various drugs consisting of either a 1:2 or a 2:1 ratio showed a recrystallisation of the excess drug during storage [38,63–65]. However, sometimes

small deviations from the equimolar ratio may also lead to an improved stability of a CAS [66,67]. Beyer et al. found that for the naproxen-indomethacin CAS, the 0.6:0.4 molar ratio was the most stable blend. As this ratio represents the eutectic composition of this system, the authors concluded that the eutectic point may be important for the stability of CASs. However, as detailed investigations in terms of the ideal ratio for a CAS are time-consuming, nowadays CASs are mainly prepared at an equimolar ratio, as published data suggest that the optimal ratio may be found around 50 mol % [67].

If a suitable coformer is selected and an appropriate molar ratio is determined, the CAS is physically stable during stability studies for up to months [32,37,38,43,44,68,69]. So far, most of the physical stability studies of CASs have been conducted only under dry conditions (0% RH at room temperature or higher) [33,35], which may be explained by the fact that the subject of CASs is still comparatively new. However, humidity may be critical for the long-term stability of CASs, as moisture is known to often negatively affect the physical stability of ASDs [70–73].

1.2.4 Preparation techniques for co-amorphous systems

CASs may be prepared by the same techniques, which are used for the preparation of any amorphous blends. The preparation techniques may be divided into two groups, depending on the manner, how the molecular disorder is introduced into the system. It may be distinguished between a kinetic and a thermodynamic pathway [74,75]. Fig. 3 gives an overview of these pathways, which both start with the physical mixture of the crystalline forms of API and coformer (I). By applying the thermodynamic pathway, the compounds are first converted to a non-crystalline form that is thermodynamically stable,

such as a melt or a solution (II). Thereafter, to obtain a solid co-amorphous system, in the case of a melt, it has to be cooled down so rapidly that the molecules are not able to rearrange themselves (quench-cooling). Similarly, in the case of a solution the solvent has to be removed as quickly as possible, thus allowing the precipitation of the co-amorphous form of both dissolved compounds (IV). By application of the kinetic pathway, the CAS is formed by a direct solid conversion, which is caused by a continuous mechanical stress of the crystals, e.g. by ball milling. At the beginning of the kinetic pathway, some defects are introduced into the crystal lattice (III). During further mechanical processing, the CAS is formed after a certain time period (IV) [20,21,55].
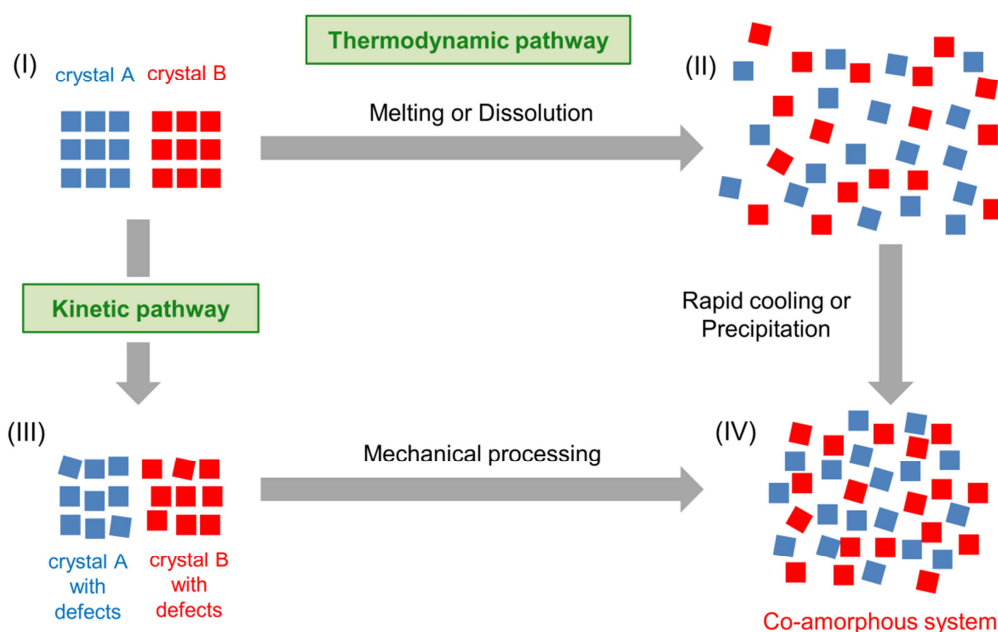
Fig. 3: Overview of the different preparation techniques for co-amorphous systems, modified from [75].

Lately, investigations have been focused on the characterisation of the different CASs only on a lab scale, because it allows a time-saving screening of different CAS combinations. Hence, mostly techniques with small sample sizes and easy handling were used, such as quench-cooling [37,38,66,76–78], ball milling [43,58,60,67,68,77,79], and solvent evaporation [69,80]. Despite their advantages for rapid screening purposes on a laboratory scale, these techniques are not suitable for a scale-up during industrial production. Thus, recently the feasibility of spray-drying for the preparation of CASs on a production scale was investigated [32,45,81–86]. In addition, melt extrusion was examined as a large-scale production technique. However, the physical stability of the resulting CAS was shown to be insufficient [85].

None of the mentioned preparation methods represents a generally suitable technique for the production of CASs. While quench-cooling and melt extrusion are only applicable to compounds that do not degrade upon melting, with ball milling it is not always possible to achieve a completely (co-) amorphous product [79]. For solvent evaporation techniques, the identification of a proper solvent may be challenging, if one or both of the compounds are poorly soluble in the feasible solvents. Furthermore, the low yields and the need of organic solvents are disadvantages of the spray-drying approach. Thus, the preparation technique for a CAS has to be chosen based on the properties of both compounds, the API and the coformer. It should also be considered that the selected preparation method can affect the physical properties of the final product, as it may influence the short-range order in the amorphous solid [20]. In addition, the process conditions have to be selected carefully, as it has been previously shown that they also affect the characteristics of the CAS [37,66,81].

1.2.5 Alternative approaches for the preparation of amorphous systems

All the currently used methods for the preparation of CASs do not present ideal techniques for a large-scale production, either because they are not scalable (quench-cooling, ball-milling), or because of drawbacks related to the use of organic solvents (spray-drying). Thus, there is still a need for novel and innovative techniques to prepare CASs.

In this context, the concept of a controlled *in situ* amorphisation seems to be promising. If amorphisation happens *in situ*, it means that a crystalline compound is amorphised without any intended external energy input. Such *in situ* amorphisations usually take place inadvertently during manufacturing processes and are initiated by heat, mechanical stress, or moisture [87]. These process-induced solid-state changes are unintended and may lead to serious changes of pharmaceutically relevant properties of the product. One example of such an unintended amorphisation leading to serious changes of the product quality is the increased degradation rate of a drug such as acetylsalicylic acid in the final formulation [88,89].

However, it was previously shown that such an *in situ* amorphisation allows to prepare amorphous pharmaceutical formulations immediately before intake by the patient, if it happens in a controlled manner [87]. As this concept involves the preparation of a crystalline formulation, which is physically stable during processing, transport and storage, *in situ* amorphisation also circumvents the stability problems usually related to other amorphous formulation approaches. Before ingestion by the patient, the formulation becomes "activated", i.e. amorphised. So far, different approaches for the *in situ* "activation" of initially crystalline formulations have been investigated. Priemel et al. showed that *in situ* amorphisation of indomethacin-Eudragit® E compacts was enabled

by immersion of the compacts in phosphate buffer pH 6.8 [90]. Similarly, Doreth et al. amorphised naproxen- and ibuprofen-Eudragit[®] E compacts by immersion in water [91]. Apart from the activation by aqueous media, the combination of humid storage conditions and microwave radiation has been shown to allow the preparation of ASDs of indomethacin [92,93] or celecoxib [94] with polyvinylpyrrolidone. Also, other glass solutions consisting of drug-polymer combinations were already prepared using microwave radiation [95–98]. In all above-mentioned studies, the *in situ* amorphisation has allowed the preparation of ASDs of the respective APIs with a polymer.

This concept of a controlled *in situ* amorphisation for the preparation of ASDs might also be beneficial for the preparation of CASs [57]. Compared to *in situ* amorphised ASDs, the amount of excipient (coformer) could be significantly reduced, making this approach applicable to solid oral formulations with a higher dosage and thus, a higher volume.

Recently, Lenz et al. prepared tablets containing crystalline indomethacin and crystalline arginine as well as a reference formulation containing only crystalline indomethacin. During drug release testing in phosphate buffer pH 4.5 an increased drug release of indomethacin from the crystalline indomethacin-arginine tablet formulation compared to the plain indomethacin tablet was observed [99]. Because upon contact with the dissolution medium a colour change of the crystalline indomethacin-arginine tablet formulation from white to yellow was observed [100], the improved drug release behaviour was attributed to an *in situ* co-amorphisation of indomethacin with arginine. Thus, this study indicated that an *in situ* amorphisation is not only limited to API-polymer combinations. However, despite its theoretical advantages, the concept of a controlled *in situ* co-amorphisation of an API with a low molecular weight excipient has not yet been investigated.

1.3 Analytical techniques for the characterisation of co-amorphous systems

1.3.1 General aspects

The analytical techniques applied for the characterisation of CASs are the same as those generally used for the analysis of amorphous systems. Table 1 gives an overview of the most frequently applied techniques. As their working principles are summarised in the literature, the following section briefly discusses the three most important analytical techniques and their application for the solid-state characterisation of CASs.

Table 1: Overview of the commonly used analytical techniques for the characterisation of amorphous systems.

	Analytical technique	**Literature**
Diffractometric techniques	X-ray powder diffractometry (XRPD)	[101]
Thermal analytical techniques	Differential scanning calorimetry (DSC)	[101]
	Dynamic mechanical analysis (DMA)	[102–104]
	Isothermal microcalorimetry (IMC)	[101]
	Dynamic vapour sorption (DVS)	[101]
Spectroscopic techniques	Raman spectroscopy	[105,106]
	Fourier-transform infrared spectroscopy (FTIR)	[105]
	Terahertz spectroscopy (THz)	[105,107]
	Solid-state nuclear magnetic resonance (ss NMR)	[108]

1.3.2 X-Ray powder diffractometry (XRPD)

X-Rays are waves of electromagnetic radiation located between ultraviolet and gamma radiation in the electromagnetic spectrum. If an X-ray beam hits a crystalline solid, it is scattered in all directions. In some cases, the scattered beams may interfere and reinforce each other, leading to diffraction. Diffraction takes place, if Bragg´s law is applicable [109,110]:

$$2d \sin\theta = n\lambda \qquad\qquad\qquad\qquad\qquad\qquad\qquad\qquad \text{(Eq. 1)}$$

where d is the inter-planar distance in the crystal, θ the angle of incidence of the x-rays, n an integer, and λ the wavelength of the x-rays.

In general, single-crystal X-ray diffraction is a powerful technique to identify the structure of a crystal. As most pharmaceutical APIs are available as powders, they are alternatively studied by X-ray powder diffractometry (XRPD). As the powder particles are randomly orientated during XRPD measurements, the obtained data contains less information compared to single-crystal X-ray diffraction [111].

However, XRPD is a frequently applied and non-destructive technique for the identification of solids and their (pseudo-) polymorphic forms, as every crystal has a unique X-ray powder pattern [110]. In addition, XRPD is also able to identify amorphous substances by the absence of distinct reflections in their diffractograms. Instead, amorphous substances show diffuse, so-called "halo" diffraction patterns. Therefore, XRPD is also frequently used to determine the degree of crystallinity of substances. Different approaches are described in the literature for the quantitative analysis of degree of crystallinity by XRPD [108,110,112].

Although XRPD is a well-established, non-destructive, and powerful technique for the differentiation between crystalline and amorphous phases, it is unable to identify whether two or more amorphous compounds are present as a single- or multi-phase system. For the analysis of CASs, XRPD should therefore be combined with other characterisation techniques [113].

1.3.3 Differential scanning calorimetry (DSC)

DSC is a frequently applied thermal analytical technique, which is used to measure the physical and chemical responses of a sample upon heating. Typically, the sample is placed into a metal pan. While running a linear temperature gradient, with DSC the difference in heat flow, which is needed to maintain the sample pan and an empty reference pan at the same temperature, is measured [114]. If an endothermic event takes place in the sample pan, it will consequently result in an increase of the heat flow into this pan. However, if the sample undergoes an exothermic process, a decrease of the heat flow compared to the reference pan may be observed. These phase transitions manifest themselves in peaks or steps in the resulting DSC thermogram (heat flux against temperature or time). Thus, thermal events, such as melting, desolvation, glass transition, chemical degradation, crystallisation, etc. may be monitored. In addition, the area under DSC peaks may also be used for enthalpy calculations [115].

In contrast to a crystal, amorphous material does not undergo melting, which is the transition of a material from a solid to a liquid state upon heating. Instead, amorphous materials show a glass transition, which describes the transition from the "kinetically frozen", so-called "glassy" state into the liquid-like rubbery state [17]. The temperature of

this glass transition (T_g) may be used to identify and characterise amorphous systems [112,116]. DSC is also a valuable technique for detection, whether an amorphous API and its coformer exist as CAS or rather as a physical mixture (PM). While the PM shows two glass transitions in the resulting DSC thermogram, with a homogenous CAS only a single T_g will be detected [117].

Because of some limitations of the conventional DSC methodology, a modulated DSC (mDSC) approach was developed in 1993 [118,119]. In an mDSC experiment, a modulated heating rate is superimposed on a constant average heating rate, which leads to a higher sensitivity and resolution of the measurement. Thus, weak transitions may be separated from other simultaneously happening thermal events [120]. As glass transitions are comparably weak thermal events, the application of mDSC for amorphous systems may be superior. Previously, the application of conventional DSC for the analysis of co-amorphous indomethacin-arginine led to a miscalculation of the T_g of the CAS, as this thermal event was overlapped by dehydration of absorbed water [18,32,43]. Therefore, mDSC is currently the preferred methodology for the analysis of CASs.

1.3.4 Fourier-transform infrared spectroscopy (FTIR)

FTIR is a vibrational spectroscopic technique. The electromagnetic spectrum of infrared (IR) spectroscopy is typically divided into near-IR (NIR: 12,500 - 400 cm^{-1}), mid-IR (MIR: 4,000 - 400 cm^{-1}), and far-IR (FIR: 400 - 20 cm^{-1}). In the present work MIR spectroscopy was applied.

The measurement principle of IR spectroscopy is based on the fact that if electromagnetic radiation (of a distinct energy) hits a sample, the sample will absorb energy, as the molecules in the sample undergo vibrations. After permeating the sample, the propagated radiation will be influenced by the optical properties of the sample, leading to signals (absorption bands) in the resulting IR spectrum. As the position, the intensity, and the width of these bands are dependent on the sample properties, FTIR may be used for the qualitative and quantitative analysis of solid or liquid substances [121–123].

Regarding the analysis of amorphous systems, FTIR spectroscopy is a valuable technique because the transformation of a crystalline compound into its amorphous form leads to the broadening and the shift of bands in the resulting IR spectrum [105]. For the characterisation of CASs it is important that FTIR spectroscopy has the potential to detect molecular interactions between two or more compounds, such as hydrogen bonding, salt formation, or π-π interactions. Therefore, FTIR is able to distinguish between crystalline or amorphous PMs of two compounds and their respective CAS. The type of molecular interaction in a CAS may be identified by specific peak shifts of those functional groups, which are interacting with each other [56].

1.4 Polymer coatings

1.4.1 General aspects

The coating of solid dosage forms is nowadays routinely performed in the pharmaceutical industry, as the application of a coating offers many advantages, such as an improved stability or a modified drug release from the dosage form. By definition, a coated dosage form consists of a solid core (e.g. a tablet), which is coated with a homogeneous cfilm [124]. While sugar-based coatings were frequently applied in the 19th century, nowadays polymers are predominantly used for film coating of solid dosage forms [125]. This trend may be explained by the advantages of the application of coating polymers, e.g. their comparably low amount required for coating, which decreases the weight of the final tablet formulation. The film coating process with polymers is also significantly faster than the coating with sugars, which enables the reduction of the production costs. Furthermore, the high variety of available polymers offers the ability of a tailor-made drug release from solid oral dosage forms. For this purpose, even polymer blend may be applied to prepare a defined functional coating [126].

The coating of a pharmaceutical dosage pursues different objectives [124,125], which are presented in Fig. 4. For once, coatings are able to mask an unpleasant taste or odor of the contained API, which is especially interesting for pediatric use [127]. Also, the smoother surface of the coated dosage form enables easier swallowing, leading to an improved patient compliance. In addition, the colouring of a formulation by application of a coating that contains dyes or pigments enables the differentiation between pharmaceutical dosage forms. Coatings may also have a protective function: a uniform film decreases the mechanical stress of the formulation during further processing, thus

reducing cracking and abrasion [125]. Besides, the coating may also function as a barrier against light, moisture, or oxygen [128]. Hence, the storage stability of formulations sensitive to these environmental conditions may be markedly improved. For these purposes, immediate release coatings are applied, which do not affect the drug release profile of the core.
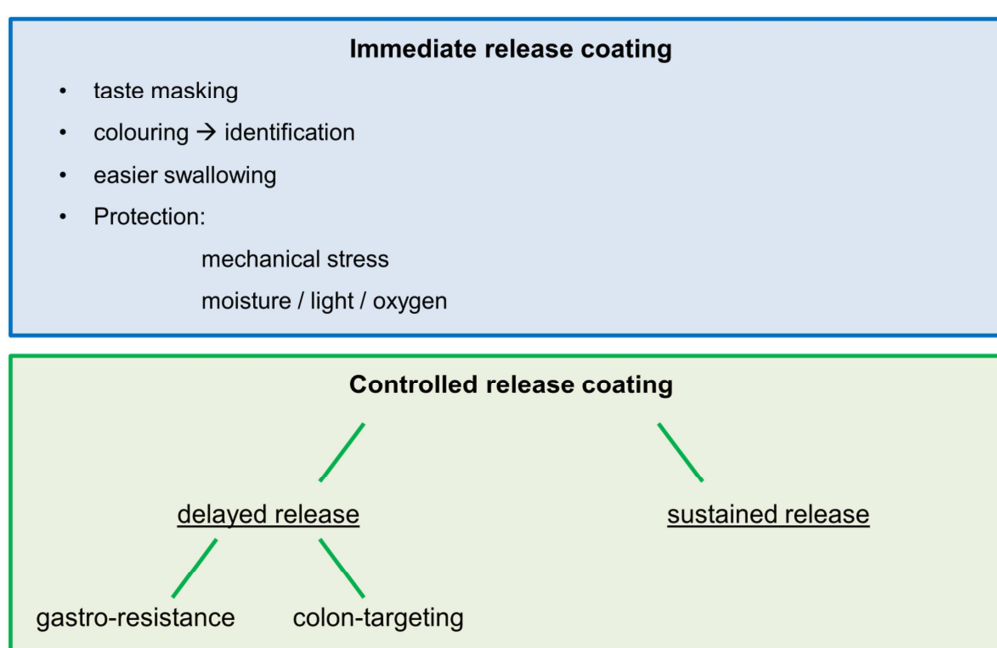
Fig. 4: Overview of the different functionalities of pharmaceutical film coatings**.**

Coatings also offer the potential for protection of amorphous systems. Because humidity was shown to be a major reason for the phase separation and recrystallisation of amorphous systems, moisture protective coatings might be able to improve the storage stability of amorphous and co-amorphous formulations. Grohganz et al. already suggested that studies are needed, which deal with the investigation of suitable processes for the coating of amorphous systems [18]. However, despite its obvious

potential, coating of amorphous and co-amorphous formulations has not yet been investigated.

However, as stated above, coatings may also be functional and used to control the drug release from the core [129]. Depending on the targeted region in the gastrointestinal tract (GIT), it may be distinguished between enteric coatings and coatings for colon drug delivery. The former resist the gastric juice and dissolve, as soon as the pH value increases upon reaching the small intestine. Such a coating is applied, if either the API has to be protected from the gastric acid (e.g. proton-pump inhibitors), or if the gastric mucosa has to be protected from irritant APIs (e.g. bisphosphonates). Coatings for colon delivery are supposed to dissolve in the lower parts of the GIT, and are used for the local treatment of colonic disorders [130].

Apart from the delay of API release by enteric polymer films, coatings may also be applied for sustained release [131]. Such a coating is supposed to allow a release of a defined amount of API during a distinct time interval. Thus, the dosing frequency may be reduced, leading to a higher patient compliance.

1.4.2 Polymers for film coating

As stated above, today many different types of polymers are used for the coating of solid dosage forms. Depending on their origin they may be classified into natural, semisynthetic, and synthetic polymers [132]. Because of the disadvantages of natural polymers, e.g. their batch-to-batch variation, semisynthetic and synthetic polymers are commonly used. While the cellulose derivatives are semisynthetic coating polymers, polymethacrylate copolymers and polyvinyl derivates belong to the class of synthetic
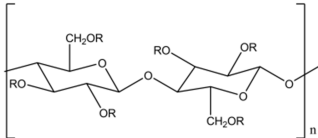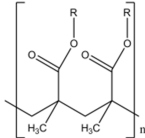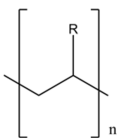
polymers. Depending on their designated functionality, it is possible to alter the side chains or the polymer backbone. In Table 2 commonly used polymers for pharmaceutical coatings are shown and characterised regarding their structure and functionality [124,125,133].

For an immediate release coating, the used polymer derivative has to be water-soluble, such as the water-soluble cellulose derivates hydroxypropyl cellulose, hydroxyethyl cellulose. Another example for a fast dissolving immediate release coating is Kollicoat® IR, a polyvinyl alcohol-polyethylene glycol graft copolymer. A special immediate release coating is Eudragit® E. Because of its basic side chains it is only soluble at pH values below 5.0, and thus, it is insoluble in the neutral saliva [132]. Therefore, it is often used for taste masking purposes. In addition, coatings of Eudragit® E show a very low permeability for water vapour, making it especially useful for the protection of moisture sensitive APIs. Another coating, which was especially developed for the moisture protection of solid dosage forms is Kollicoat® Protect. It is based on Kollicoat® IR, but additionally contains 35 - 45 % polyvinyl alcohol, making the coating more flexible and elastic. Hence, the coating is able to incorporate high amounts of solids (pigments such as talc or titanium dioxide), which in turn may function as a barrier for moisture [134].

Table 2: Overview of the commonly used polymers for pharmaceutical coatings [133].

	Cellulose derivates	Polymethacrylates	Polyvinyl derivates
Formula			
	Name / Trade name	**Name / Trade name**	**Name / Trade name**
Immediate release	- Hydroxypropyl cellulose - Hydroxyethyl cellulose - Hydroxymethyl cellulose - Hydroxypropylmethyl cellulose		- Polyvinylpyrrolidone (Kollidon®) - Polyvinyl alcohol-polyethylene glycol copolymer (Kollicoat® IR)
Saliva resistant	-	Poly (butyl methacrylate-co-(2-dimethylaminoethyl) methacrylate-co-methyl methacrylate) 1.2:1 (Eudragit® E)	-
Gastro-resistant	- Cellulose acetate succinate - Hydroxypropylmethyl cellulose acetate phthalate (HP 50®, HP 55®) - Cellulose acetate phthalate (Aquateric®)	- Poly (methacrylic acid-co-methyl methacrylate) 1:1 = Eudragit® L 1:2 = Eudragit® S - Poly (methacrylic acid-co-ethyl acrylate) 1:1 (Eudragit® L-55, Kollicoat® MAE)	- Polyvinyl acetate phthalate (Coateric®, Sureteric®)
Sustained release	- Ethyl cellulose (Aquacoat®, Surelease®)	- Poly (ethyl acrylate-co-methyl methacrylate-co-trimethylammonioethyl methacrylate chloride) 1:2:0.2 = Eudragit® RL 1:2:0.1 = Eudragit® RS - Poly (ethyl acrylate-co-methyl methacrylate) 2:1 (Eudragit® NE, Kollicoat® EMM)	- Polyvinyl acetate (Kollicoat® SR 30 D)

If a coating is supposed to resist the acidic gastric juice (pH between 1.0 and 2.5 in the fasted state [132]), acidic side chains must be introduced into the polymer backbone, such as the free carboxyl groups in the polymethacrylate derivatives Eudragit® L and S. Both types differ in the ratio between free and esterified carboxyl groups. This difference leads to a change of the required pH value for the dissolution of the coatings (> pH 6.0 for Eudragit® L and > pH 7.0 for Eudragit® S). In addition, the copolymer poly(methacrylic acid-co-ethyl acrylate) (Eudragit® L-55, Kollicoat® MAE) is available, which dissolves at a pH value of 5.5.

Sustained release coatings are not supposed to dissolve in the GIT. Instead, they have to swell pH independently, making them permeable for water and the APIs during the whole gastro-intestinal transit. Apart from cellulose and polyvinyl derivates (Table 2), polymethacrylates for sustained release coatings are Eudragit® RL and RS, where R stands for *retard*. The letters L and S describe the ratio of esters to the cationic side chains, which determine the permeability of the coating. Thus, permeation through Eudragit® RS films needs longer than through RL films. As with Eudragit® L and S, both polymer types may be combined to generate a designated drug release profile. As during the processing of Eudragit® RS and RL usually plasticizers are needed, Eudragit® NE and Kollicoat® EMM were developed, which do not require the addition of external plasticizers, because of internal plasticization of the copolymers.

1.4.3 Coating formulation development

Usually, for the preparation of a pharmaceutical coating, the selected polymer or polymers have to be used together with excipients. The choice of the excipients is linked

to the applied coating method. Although dry coating techniques have gained considerable interest for the coating of moisture sensitive solid dosage forms [135], coating from a liquid (organic or aqueous) still presents the major industrial preparation technique. This liquid contains the dissolved or dispersed coating material and is usually sprayed onto the solid cores. During evaporation of the liquid at elevated temperatures, the coating material forms the film. In general, the film formation from a polymer solution is simple compared to a polymer dispersion. As only immediate-release polymers are water-soluble, other polymer coating solutions have to be prepared with organic solvents such as ethanol, isopropanol, acetone, or mixtures thereof. However, the use of toxic and flammable organic solvents comes along with health and safety hazards and thus, with strict environmental requirements [125].

Therefore, nowadays most coatings are processed as aqueous polymer dispersions. Depending on the production technique, these dispersions are called latexes or pseudolatexes and consist of finely dispersed polymer particles (< 1 µm), leading to a stabilisation with regard to sedimentation during storage [136]. The application of such an aqueous based polymer dispersion requires special considerations regarding the film formation, which are described in detail in the literature [137,138]. Briefly, to enable formation of a homogenous film by coalescence of the polymer particles upon water evaporation, the polymer has to be highly elastic and flexible. This is the case if the process temperature is above the so-called minimum film forming temperature of the polymer. This film forming temperature is highly dependent of the properties of the polymer and the coating formulation. Often, the properties of the plain polymer are insufficient for a processing without any additives. Therefore, excipients are needed, which lead to plasticization of the polymer and allow film formation. These so-called

plasticizers are nonvolatile, high-boiling substances that change the mechanical properties of the polymer, thereby also increasing the elasticity and flexibility of the final coating [136].

Other excipients, which are commonly used for the preparation of aqueous or organic coatings, are anti-tacking agents, which are supposed to prevent sticking of tablets to the coating equipment or to other tablets. For a colouring of the coating, pigments may also be added. Furthermore, the processing of an aqueous coating dispersion sometimes needs stabilizers, e.g. emulsifiers [139].

For all types of excipients, there is a wide selection of different substances available. The choice of the right excipients and their concentration not only depends on the applied polymer, but also on the intended functionality of the coating, as excipients may also impact the properties of the film coating [140]. Despite the effect on the mechanical properties, especially the influence of the excipients on the permeability of the film coating needs to be considered. For functional coatings, it is intended to keep the permeability as low as possible, as a high permeability generally may alter the functionality of the coating. This is especially important for gastro-resistant and sustained release coatings, as the permeation of water may induce an earlier than intended drug release from the solid dosage form than intended.

For moisture protection of sensitive APIs, the coating should preferably be almost impermeable. In Fig. 5 the different factors, which influence the permeability of a film coating, are shown. Besides the type of anti-tacking agent, especially the choice of plasticizer has an influence on the permeability of the coating film. While hydrophilic plasticizers such as polyethylene glycol, are leachable and lead to an increased
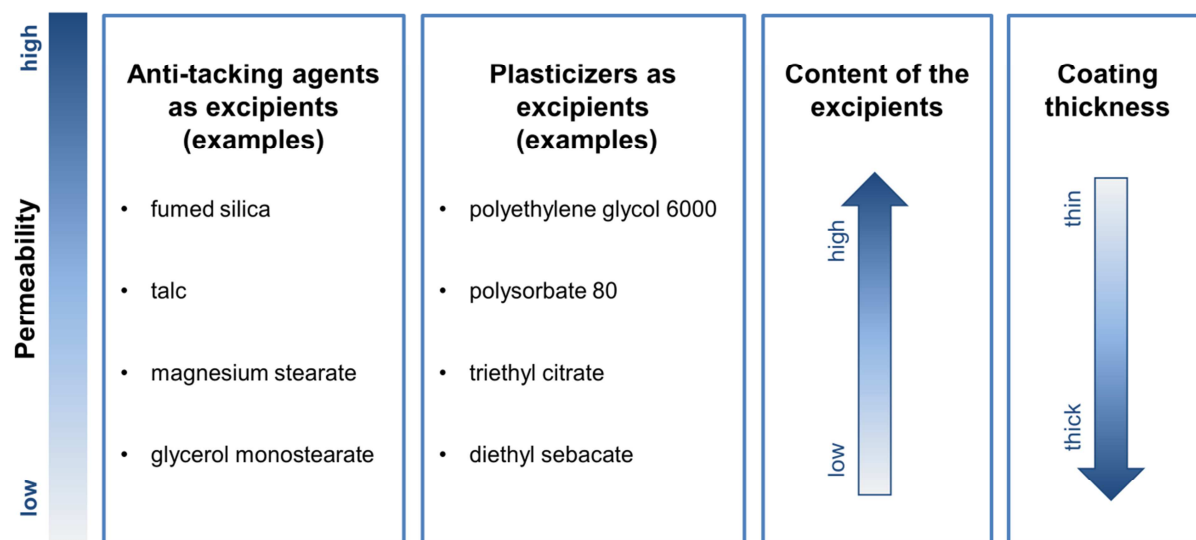
Fig. 5: Overview of the factors, which influence the permeability of a film coating.

permeability, leaching is less pronounced with lipophilic plasticizers such as triethyl citrate. Also the content of the excipients influences the permeability, as they are not covalently bound to the polymer molecules. Thus, excipients cause defects in the polymer structure, which in turn may alter the functionality of the coatings. In addition, the coating thickness is a critical factor concerning the coating permeability [139].
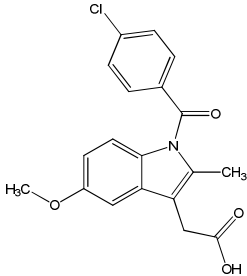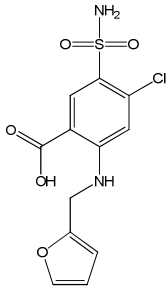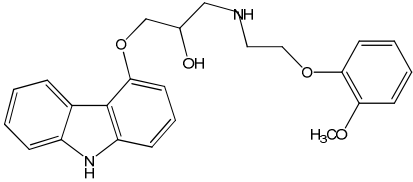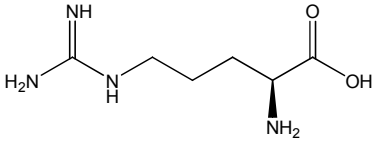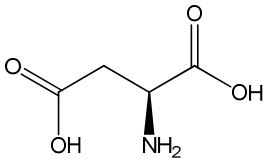
Thus, there are many aspects that have to be considered during development of pharmaceutical coatings. The right excipients enabling the coating process for an economic industrial production have to be selected. Simultaneously, the composition of the coating must guarantee a stable coated dosage form with a defined drug release behaviour. Apart from formulation considerations, the selection of the process conditions plays an important role [125] because they may affect the properties of the formulation and the API, especially if they are sensitive to moisture and heat.

1.5 Selected model drugs

An overview of the model drugs and coformers used in the present study is given in Table 3. Indomethacin (IND) is a nonsteroidal anti-inflammatory drug, which belongs to BCS class II. As it has often been used as model API for poorly water-soluble drugs, it is already well characterised and much knowledge is available regarding the stability and recrystallisation behaviour of its different polymorphs and its amorphous form [141–143]. So far, five different polymorphs have been identified for IND, of which the so-called γ-polymorph presents the most stable one [144]. IND has also been investigated as model drug in various CASs, including IND-API [37,38,41,65,66,81] as well as IND-amino acid systems [60,79,84,145]. As IND is an acidic drug with a pK_a of 4.5 (Table 3), salt formation has often been observed in combination with a basic coformer, such as arginine (ARG) or lysine [59,79]. Especially with the combination of IND and ARG much research has been conducted during the last years, as this system has been shown to be physically stable during storage under dry conditions and to improve the dissolution behaviour of IND [32,43,56,60,83,85,145]. Also, the first successful preparation of a CAS tablet formulation was realised with a co-amorphous IND-ARG system [99]. However, although it has been shown that the strong molecular interactions in the co-amorphous IND-ARG salt system lead to a high physical stability under dry conditions, there is no data available regarding the stability of this system under humid storage conditions. Furthermore, also the chemical stability of this system should be investigated, as it is known that IND may undergo basic hydrolysis in alkaline media [146]. Thus, a potential chemical degradation of IND during combined storage with the basic amino acid ARG needs to be excluded.

Table 3: Overview of the model drugs and coformers used in the present work.

Name	Structure	pK$_a$	M$_R$ [g/mol]	BCS class
Indomethacin (model drug)		pK$_a$ = 4.5	357.79	II
Furosemide (model drug)		pK$_a$ = 3.64	330.74	IV
Carvedilol (model drug)		pK$_a$ = 7.8	406.48	II
L-Arginine (coformer)		pK$_{a1}$ = 12.5 pK$_{a2}$ = 9.1	174.20	-
L-Aspartic acid (coformer)		pK$_a$ = 3.9	133.10	-

Furosemide (FUR) is a loop diuretic drug belonging to BCS class IV, thus showing poor solubility and permeability [147,148]. Solubility improvement is therefore crucial for an increase of the bioavailability of FUR [149]. It is also an acidic drug with a pK_a of 3.8 (Table 3) and similar to IND, the most stable CASs of FUR have been reported to be formed with a basic coformer leading to the formation of co-amorphous salts [32,58,60,79]. However, in comparison to IND, there is only few data available regarding co-amorphous systems containing FUR.

Carvedilol (CVD) is a non-cardioselective β-blocker and a weakly basic drug that belongs to BCS class II. Several approaches have been tried to improve its solubility, which were recently summarised in a publication [150]. Also, various co-amorphous CVD systems have already been investigated, including CVD-API [39], CVD-organic acid [45], and CVD-amino acid systems [79,117]. Although it has previously been shown that (dry) ball-milling of CVD with acidic amino acids does not lead to co-amorphous systems [79], Mishra et al. recently developed a suitable spray-drying process for the preparation of co-amorphous CVD-aspartic acid (ASP) and CVD-glutamic acid [151]. It is assumed that the pK_a difference between CVD with a pK_a of 7.8 [45] and ASP with a $pK_{a\ \beta\text{-COOH}}$ of 3.9 (Table 3) [152] enables the formation of a co-amorphous CVD-ASP salt, similar to the co-amorphous IND-ARG and FUR-ARG salts. As acidic amino acids are usually poor coformers for CASs, the co-amorphous CVD-ASP system is one of only a few co-amorphous salt systems comprising a basic drug and an acidic amino acid [79].

1.6 Objectives of this work

Because of the disadvantages of the existing formulation techniques for amorphous drugs, co-amorphous systems have recently gained considerable interest as alternative and promising formulation approach. Nevertheless, this relatively new approach needs further research, especially with regard to how these systems may be formulated and how co-amorphous systems behave during down-streaming into final dosage forms. In this context, the effect of moisture on the properties of co-amorphous systems has to be considered, which has only been investigated in a few studies so far. As it is a well-known problem that moisture can act as plasticizer and thereby enable recrystallisation of an amorphous system, it is also necessary to investigate the stability of co-amorphous systems under humid conditions, which may exist during production or storage. Therefore, co-amorphous formulations should actually be protected against moisture. In this regard, pharmaceutical coatings present a well-established technique to protect formulations against moisture. Nevertheless, there is little known on coating of co-amorphous formulations so far. Therefore, one aim of the present study was to investigate the effect of humid storage conditions on the solid-state properties of a co-amorphous system as well as to examine the effect of polymer coatings on the performance and stability of a co-amorphous tablet formulation.

However, in contrast to its negative effect on the storage stability of amorphous systems, water may be applied for the amorphisation of a crystalline formulation, as the immersion in aqueous media was previously shown to enable *in situ* amorphisation of various drug-polymer mixtures. If such an amorphisation may be induced in a controlled manner within the final dosage form immediately before intake by the patient, the *in situ*

amorphisation shows distinct advantages compared to the conventional amorphous formulation approaches, especially with regard to the long-term stability of the formulation. However, the applicability of an *in situ* amorphisation to co-amorphous systems has not yet been investigated and therefore, it was a further aim of the present study to examine, whether water is able to induce an *in situ* co-amorphisation of a crystalline API and a crystalline low molecular weight coformer. While the immersion of mixtures of a drug and a water insoluble polymer in aqueous media is rather simple, it is more complex for API-small molecule combinations, as the commonly used coformers are readily soluble in water. The immersion of such a non-modified formulation would lead to a rapid disintegration in the case of tablets. Thus, API and coformer would be spatially separated and a co-amorphisation of both small molecules prevented. Therefore, the present study intended to develop a special tablet coating, which is suited to allow the penetration of water into the formulation, while simultaneously assuring the integrity of the tablet, thus enabling the co-amorphisation of both substances during immersion in aqueous media. As the present study served as a proof-of-concept, the feasibility of an *in situ* co-amorphisation was investigated with two different types of poorly water-soluble drugs, namely acidic (indomethacin, furosemide) and basic (carvedilol) APIs.

2. Materials and Methods

2.1 Materials

2.1.1 Model drugs (APIs) and coformers

Indomethacin (IND) was purchased from Fagron (Barsbüttel, Germany), Tokyo Chemical Industry (Tokyo, Japan), and from Hawkins Pharmaceutical group (Minneapolis, USA). IND from all three suppliers had a purity of > 98 % and was present in the γ-form (γ-IND; confirmed by solid-state analysis, see section 2.2.9). Crystalline furosemide (FUR) was bought from Fagron (Barsbüttel, Germany) and crystalline carvedilol (CVD) from Tokyo Chemical Industry (Tokyo, Japan).

The coformer L-arginine (ARG) was purchased from Merck (Darmstadt, Germany) and citric acid (CA) as well as L-aspartic acid (ASP) were both purchased from Carl Roth (Karlsruhe, Germany).

2.1.2 Tableting excipients

For tableting, the excipients β-mannitol (Caelo, Hilden, Germany), croscarmellose sodium, magnesium stearate (both from Fagron, Barsbüttel, Germany), and fumed silica (Aerosil® 200; Evonik, Darmstadt, Germany) were used. Spray-dried mannitol (Pearlitol® 200 SD) was a gift from Roquette (Lestrem, France).

2.1.3 Coating excipients

Kollicoat® Protect was kindly supplied by BASF (Ludwigshafen, Germany) and dissolved in distilled water prior to coating. The coating dispersion Eudragit® L 30D-55 was a gift

from Evonik (Darmstadt, Germany) and mixed with additional purified water, talc (Fagron, Barsbüttel, Germany), polyethylene glycol 6000 (PEG 6000; Carl Roth, Karlsruhe, Germany), and silicone anti-foaming emulsion consisting of 30 % dimethicone in water (Carl Roth, Karlsruhe, Germany).

2.1.4 Chemical reagents

For spray-drying, acetone from Biesterfeld (Hamburg, Germany) and Ethanol from Merck (Darmstadt, Germany) were used. To prepare the spray-drying solutions both were each mixed with Milli-Q$^®$ water (Merck Millipore, Darmstadt, Germany).

For HPLC analysis, acetonitrile (HPLC grade) and acetic acid 100 % were obtained from VWR (Hanover, Germany). Phosphoric acid 85 % and potassium dihydrogen phosphate were both purchased from Carl Roth (Karlsruhe, Germany). Again, Milli-Q$^®$ water was used for preparation of the mobile phases. The degradation products 4-chlorobenzoic acid (CBA) and 5-methoxy-2-methyl-3-indolacetic acid (MMIA) were bought from Merck (Darmstadt, Germany) and Sigma-Aldrich (Steinheim, Germany), respectively.

Standard solutions (1.0 mol/l) of hydrochloric acid (HCl) and sodium hydroxide, as well as potassium dihydrogen phosphate were all purchased from Carl Roth (Karlsruhe, Germany) and used for the preparation of defined media for the immersion as well as the drug release studies.

2.1.5 Adjustment of different relative humidities

To generate different relative humidities (RHs), saturated solutions of potassium acetate (Merck, Darmstadt, Germany), magnesium nitrate hexahydrate (Carl Roth, Karlsruhe, Germany), and sodium chloride (VWR, Hanover, Germany), respectively, were used. The resulting RHs of 28 ± 5, 58 ± 5, and 75 ± 5 % were monitored with an Extech RHT10 data logger (Extech Instruments, Massachusetts, USA). Phosphorus pentoxide (Sicapent®) was bought from Merck (Darmstadt, Germany) to generate dry storage conditions (0 % RH).

2.2 Methods

2.2.1 Ball milling

Physical mixtures (PMs) of γ-IND and ARG were prepared by vibrational ball mixing (Mixer Mill MM200; Retsch, Haan, Germany). Briefly, γ-IND and ARG were used at an equimolar ratio (1 : 0.49 weight ratio) and premixed with a spatula. Subsequently, about 1 g of the blend were placed in 25 ml milling jars together with three stainless steel balls (Ø 3 mm) and mixed at 25 Hz for 30 s in the vibrational ball mill. The absence of amorphisation was confirmed by XRPD and DSC (see section 2.2.9).

The co-amorphous systems of IND and ARG (CoA IND-ARG) or FUR and ARG (CoA FUR-ARG), respectively, were also prepared by vibrational ball milling with the MixerMill MM301. Briefly, approximately 500 mg of an equimolar blend of the respective API and ARG were placed in 25 ml jars together with two stainless steel balls (Ø 9 mm) and milled at 25 Hz for 99 min, while placed in a cold room (6 °C). The co-amorphisation was confirmed by XRPD and FTIR spectroscopy (see section 2.2.9).

2.2.2 Spray-drying

Spray-drying was performed with a Mini Spray Dryer B-290, equipped with an Inert Loop B-295 (both from Büchi, Flawil, Switzerland).

For preparation of a spray-dried co-amorphous indomethacin-arginine system (SD CoA IND-ARG), the spray-drying approach developed by Jensen et al. was applied [32]. Briefly, γ-IND and ARG were mixed at an equimolar ratio and dissolved in acetone and water (70:30 v/v) to obtain a 4 % (w/v) solution. Subsequently, 500 ml of this solution

were spray-dried using the following process parameters: 90 °C inlet temperature, 58 °C outlet temperature, 5 ml/min feed flow rate, and 30 m^3/h drying air flow.

To prepare a spray-dried co-amorphous carvedilol-aspartic acid system (SD CoA CVD-ASP), a spray-drying solution was prepared by dissolving 1.327 g of an equimolar CVD-ASP powder blend in 600 ml of an ethanol-water mixture (70:30 v/v). Subsequently, the resulting solution was spray-dried using the following process parameters: 130 °C inlet temperature, 69 °C outlet temperature, 3 ml/min feed flow rate, and 35 m^3/h drying air flow.

2.2.3 Tablet preparation

Tableting was performed in single press mode on an instrumented rotary tablet press (Fette 102i; Fette Compacting, Schwarzenbek, Germany) at a rotor speed of 5 rpm. To prepare biconvex tablets that were suited for coating, round concave punches with a diameter of 8 mm were used. Filling of the die was performed manually and the tableting settings were adjusted to produce compacts with a mass of about 200 mg and with a sufficient tensile strength (> 1 MPa).

All prepared tablet formulations contained the API and the respective coformer in an equimolar ratio with a drug load of 25 %. For preparation of the powder blends, all ingredients except for the lubricant magnesium stearate were first passed through a sieve (mesh size 500 μm) and blended with a Turbula® T2F mixer (W.A. Bachofen, Basel, Switzerland) for 15 min. Subsequently, magnesium stearate was added and the mixtures were blended for additional 2 min. ARG and CA both needed to be ground with a mortar and pestle before sieving.

The compositions of the tablets containing SD CoA IND-ARG (SD-T) and for the crystalline reference formulation comprising a physical mixture of γ-IND and ARG (PM-T) are shown in Table 4. The batch size was 35 g for SD-T and 25 g for PM-T, respectively. SD-T was prepared with a compaction pressure of 63 MPa. In contrast, for PM-T a compaction pressure of 244 MPa was necessary to produce tablets with a sufficient tensile strength, which is likely to be caused by different compaction properties of the spray-dried and the crystalline material. Before coating and tablet characterisation, SD-T and PM-T were stored protected from light at 23 °C/0 % RH for 24 h.

Table 4: Compositions of the prepared spray-dried (SD-T) and physical mixture (PM-T) tablet formulations (% w/w).

	SD-T	PM-T
γ-Indomethacin	-	25.0
Arginine	-	12.2
SD CoA IND-ARG	37.2	-
β-mannitol	55.8	55.8
Croscarmellose sodium	5.0	5.0
Fumed silica	1.0	1.0
Magnesium stearate	1.0	1.0

For the tablet formulations containing either crystalline FUR and ARG (FA-T) or γ-IND + ARG (IA-T), or γ-IND + ARG + CA (IAC-T) in a molar 1:1 API:ARG (:0.3 CA) ratio, the batch size was always 25 g. Their compositions are shown in Table 5. Additionally, co-amorphous reference tablets were produced containing either CoA FUR-ARG or CoA IND-ARG (see section 2.2.1). The batch sizes were 2 g for these formulations. To produce tablets with a sufficient tensile strength, compaction pressures between 137 and 166 MPa were needed. Prior to tablet characterisation and coating, the tablet formulations were stored in an air-conditioned, light-protected room (21 °C/45 % RH) for at least 24 h.

Table 5: Compositions of the prepared FUR-ARG (FA-T), IND-ARG (IA-T), IND-ARG-CA (IAC-T), co-amorphous FUR-ARG (CoA FA-T), and co-amorphous IND-ARG (CoA IA-T) tablet formulations (% w/w).

	FA-T	IA-T	IAC-T	CoA FA-T	CoA IA-T
γ-Indomethacin	-	25.0	25.0	-	-
Furosemide	25.0	-	-	-	-
Arginine	13.2	12.2	12.2	-	-
Citric acid	-	-	4.0	-	-
CoA FUR-ARG	-	-	-	38.2	-
CoA IND-ARG	-	-	-	-	37.2
Pearlitol® 200 SD	54.8	55.8	51.8	55.8	54.8
Croscarmellose sodium	5.0	5.0	5.0	5.0	5.0
Fumed silica	1.0	1.0	1.0	1.0	1.0
Magnesium stearate	1.0	1.0	1.0	1.0	1.0

For the tablet formulations containing either an equimolar mixture of crystalline CVD and ASP (CA-T) or only CVD (C-T), the compositions are shown in Table 6. Compaction pressures between 74 and 84 MPa were needed to produce tablets with a sufficient tensile strength. Prior to tablet characterisation and coating, the tablet formulations were stored in an air-conditioned, light-protected room (21 °C/45 % RH) for at least 24 h.

Table 6: Composition of the prepared CAR-ASP (CA-T) and CAR (C-T) tablet formulations (% w/w).

	CA-T	C-T
Carvedilol	25.0	25.0
Aspartic acid	8.2	-
Pearlitol® 200 SD	59.8	68.0
Croscarmellose sodium	5.0	5.0
Fumed silica	1.0	1.0
Magnesium stearate	1.0	1.0

2.2.4 Tablet characterisation

Crushing force, tablet diameter, and tablet thickness of the prepared tablet formulations were determined (n = 5-10) with a multifunctional tablet tester (TBH 525; Erweka, Heusenstamm, Germany). With the obtained data, the tensile strengths of the biconvex tablets were calculated according to Pitt et al. [153] using the following Eq.:

$$\sigma_t = \frac{10\,P}{\pi \cdot D^2} \cdot \left(2.84 \cdot \frac{t}{D} - 0.126 \cdot \frac{t}{W} + 3.15 \cdot \frac{W}{D} + 0.01\right)^{-1} \qquad \text{(Eq. 2)}$$

where σ_t is the tablet tensile strength (N/m^2), P the crushing strength (N), D the diameter (m), t the tablet thickness (m), and W the tablet central cylinder thickness (m).

Friability was tested by determination of the weight loss (%) of 10 tablets after 100 rotations (25 rpm) in an Erweka friability tester (TA-10; Heusenstamm, Germany).

Investigations of the disintegration time of the prepared tablet formulations were performed according to the 2.9.1 Test A of the Ph. Eur. (ZT 320, Erweka, Heusenstamm, Germany). With SD-T/SD-CT and PM-T/PM-CT the test was performed with discs (n = 6) using purified water as medium. As sticking of the tablets to the discs was observed for all other tested tablet formulations (FA-T, IA-T, IAC-T, CA-T, and C-T), disintegration testing was carried out without discs with these formulations (n = 3). To compare the disintegration behaviours of the uncoated and the gastro-resistant coated tablets, disintegration testing was performed in 0.1 M HCl with these formulations.

With CA-T and C-T, the amount of CVD in the final tablet formulation was determined by HPLC (see section 2.2.11). About 10 mg of each sample were dissolved in 50.0 ml of

the mobile phase, sonicated for 15 min, and filtered (pore size: 0.22 µm) prior to quantification (n = 10).

2.2.5 Film coating and coating characterisation

Coating of the prepared tablet formulations was performed in a drum coater (Hüttlin Solidlab 1; Schopfheim, Germany) equipped with a 1.5 l drum. All tablet formulations were coated at different batches together with blue-coloured placebo tablets isolated with ethylcellulose (Ø 8 mm, 205 ± 2.4 mg, biconvex). The colouring of the placebos tablets allowed the separation of the tablets after coating.

The tablet formulations SD-T and PM-T were coated with an aqueous solution containing 15 % Kollicoat$^®$ Protect (w/w), which was prepared by dissolving Kollicoat$^®$ Protect in purified water using a magnetic stirrer. The coating conditions were as follows: inlet air temperature 55 °C, inlet air flow rate 47 - 50 m^3/h, atomising air pressure 0.2 bar, microclimate 0.1 bar, drum rotation speed 14-16 rpm, spray rate 2.5 g/min. A final drying step under the same conditions as those of the coating process followed for 5 min. Coating levels of 3.6 mg/cm^2 were applied to SD-T and 2.5 mg/cm^2 to PM-T. The coated SD-T formulation was named SD-CT and the coated PM-T formulation was referred to as PM-CT.

FA-T, IA-T, IAC-T, CA-T, and C-T were coated with a coating consisting of Eudragit$^®$ L. For preparation of the coating dispersion, the plasticizer PEG 6000 (20 % w/w referring to the dry polymer mass), the anti-tacking agent talc (50 % referring to the dry polymer mass), and a drop of silicone antifoaming emulsion were homogenised in purified water using an Ultra Turrax$^®$ (IKA, Staufen, Germany) for 10 min. Subsequently, this mixture

was slowly poured into Eudragit® L 30D-55, which was gently stirred. The coating dispersion was then passed through a 0.5 mm sieve and stirred continuously before and during the coating process. The resulting coating dispersion contained 41.5 % Eudragit® L 30D-55, 2.5 % PEG 6000, and 6.2 % talc (w/w).

The coating parameters were as follows: inlet air temperature 50 °C, inlet air flow rate 35 m^3/h, atomising air pressure 0.55 bar, microclimate 0.5 bar, drum rotation speed 25 rpm, spray rate 2.5 - 3.5 g/min. After the coating process, the coated tablets were cured at 40 °C in an oven over night. Polymer amounts of 2 - 3 mg/cm^2 were applied to the tablet formulations. The resulting coated tablet formulations were named as follows: FA-CT (coated FA-T), IA-CT (coated IA-T), IAC-CT (coated IAC-T), CA-CT (coated CA-T), C-CT (coated C-T).

Scanning electron microscopy (SEM) was used to study the morphology and thickness of the applied film coatings. The horizontally placed film coated tablets were vertically cut with a razor blade, fixed with the cross-section facing up and coated with a thin carbon layer. SEM pictures were taken with a Leo 1525 scanning electron microscope (Zeiss, Jena, Germany) with a working voltage of 5.00 kV.

2.2.6 Stability studies

2.2.6.1 Storage of physical mixtures

Approximately 200 mg of the crystalline PMs (of γ-IND and ARG) as well as of plain γ-IND or plain ARG were placed into open jars. The jars were stored in desiccators at different RHs (28 ± 5, 58 ± 5, and 75 ± 5 %) and the desiccators were placed in a closed dark chamber at 23 ± 2 °C (RT). Solid-state characterisation (FTIR, XRPD, DSC; see

section 2.2.9) and TGA (see section 2.2.8) of the PMs as well as of plain γ-IND and ARG were conducted after 1, 10, 21, and 101 d of storage, respectively.

2.2.6.2 Storage of tablets

A portion of each, SD-T, SD-CT, PM-T, and PM-CT, was stored at 23 °C/0 % RH (RT/0 %) in a desiccator and the solid-state properties of the formulations were analysed 0 d, 1 d, 32 d and 94 d after tableting or coating, respectively (see section 2.2.9). TGA was carried out after 0 d, 1 d, 32 d and 240 d of storage (see section 2.2.8).

The other portion of the formulations was stored in a desiccator at 23 °C/75 % RH (RT/75 %). Analysis of the solid-state properties of the formulations was performed after 0 d, 26 d and 91 d (see section 2.2.9). TGA was carried out after 0 d, 26 d and 240 d of storage (see section 2.2.8).

2.2.7 Immersion process of coated tablets

The tablets coated with Eudragit® L (see section 2.2.5) were immersed in 750 ml of 0.1 M HCl at 37 °C using a disintegration tester according to the Test A of the monograph 2.9.1 in the Ph. Eur. (ZT 320, Erweka, Heusenstamm, Germany) without discs.

FA-CT and IA-CT were immersed for 10, 20, 30, 60, and 120 min, respectively. The IAC-CT formulation was only immersed for 10, 20, 30, and 120 min, respectively, as the analytical results of the solid-state of the samples after different immersion times differed only negligibly. C-CT and CA-CT were immersed for 45 and 120 min, respectively.

After the respective immersion times, samples were carefully removed with a tweezer. As the applied analytical methods were not suitable for the analysis of moist samples,

the immersed coated tablets had to be dried prior to their physical characterisation. This subsequent drying step was conducted under the same conditions, which were used for curing of the coated tablets (40 °C in an oven overnight). After drying, the solid-state properties of the immersed coated tablets were analysed (see section 2.2.9).

In addition, drug release was investigated with the immersed and dried C-CT and CA-CT (see section 2.2.10). Additionally, for drug release testing in phosphate buffer pH 6.8 immersed CA-CT tablet samples (120 min) without subsequent drying were analysed.

2.2.8 Determination of the water content of the tablets and physical mixtures

To assess the water content of the samples, thermogravimetric analysis (TGA) was performed on a Pyris 1 TGA (Perkin Elmer, Waltham, USA). Measurements were performed in triplicate after storage at the respective storage conditions. In the case of the tablets and the hardened PMs, samples were carefully ground prior to the measurements. Approximately 10 mg of each sample were placed in a platinum pan and heated from 25 to 200 °C at a heating rate of 10 °C/min. The water content was determined as total weight loss in % (w/w) in the temperature range between 25 and 150 °C.

To assess, whether differences in the obtained results of TGA analysis were statistically significant, a single-factor ANOVA was performed. Values were determined to be significantly different, if the p-value was lower than 0.05 (95 % confidence level).

2.2.9 Solid-state characterisation of the tablets and physical mixtures

2.2.9.1 X-ray powder diffractometry (XRPD)

XRPD patterns were recorded in triplicate with a PANalytical X´Pert PRO X-ray diffractometer (Almelo, The Netherlands; Cu Kα anode; λ = 1.5406 Å; 45 kV; 40 mA). All tablets as well as hardened PMs were carefully ground with mortar and pestle prior to analysis and approximately 100 mg of each ground sample were measured at ambient conditions in reflection mode. Data was collected between 5 and 35 °2θ using a step size of 0.0131 °2θ and a scan speed of 0.045 °2θ min^{-1}. All diffractograms were baseline offset-corrected and normalised to unit area using The Unscrambler X software, ver. 10.3 (CAMO, Oslo, Norway).

2.2.9.2 Fourier-transform infrared spectroscopy (FTIR)

Infrared spectra were collected in triplicate over a range of 4000 to 400 cm^{-1} (32 scans, resolution of 4 cm^{-1}) using a Tensor 37 FTIR spectrometer (Bruker, Ettlingen, Germany), equipped with an attenuated total reflectance module (MIRacle; Piketech, Madison, USA) and a diamond crystal plate. In the case of the tablets and the hardened PMs, samples were carefully ground prior to the measurements. Before data analysis, baseline offset-correction and normalisation to unit area were performed for all spectra using The Unscrambler X software, ver. 10.3. Depending on the type of sample, different characteristic spectral regions were selected for the analysis of the solid-state properties.

The obtained data was further investigated using multivariate analysis and a principal component analysis (PCA) was performed with the baseline corrected and area normalised spectra using The Unscrambler X software, ver. 10.3.

2.2.9.3 Differential scanning calorimetry (DSC)

Conventional DSC (cDSC) was carried out to study the differently stored PMs as well as plain γ-IND and ARG. The experiments were carried out with a DSC 1 (Mettler Toledo, Columbus, USA) and about 6 mg of each sample were placed into an aluminium pan and sealed with a pinholed lid. Samples were heated from -20 to 220 °C (in case of the plain substances from -20 to 280 °C) at a linear heating rate of 10 °C/min. The melting temperatures (T_m) were determined as mean values of the peak temperatures of three independent samples using the STARe Software (Mettler Toledo, Columbus, USA). Determination of the peak temperatures instead of the onset temperatures was chosen, as the additionally appearing melting events in the thermograms of the PMs were very broad and with a gradual onset. Therefore, similar masses (5.6-6.2 mg) were used for all samples. Additionally, the enthalpies (ΔH) of the endothermic events (melting enthalpy ΔH_m) were calculated from the area under the curve of the total heat flow of three independent thermograms.

To assess, whether differences in the obtained results of DSC analysis were statistically significant, a single-factor ANOVA was performed. Values were determined to be significantly different, if the p-value was lower than 0.05 (95 % confidence level).

2.2.9.4 Modulated differential scanning calorimetry (mDSC)

The mDSC measurements performed with the PMs and the plain substances were carried out with the DSC 1. To determine the glass transition temperature (T_g) of co-amorphous IND-ARG, mDSC was performed using the modulation technique software TOPEM® (Mettler Toledo, Columbus, USA), which involves a stochastic temperature modulation [154]. Approximately 6 mg of each sample were placed into an aluminium

pan and sealed with a pinholed lid. Samples were heated from -20 to 180 °C at a linear heating rate of 2 °C/min, which was superimposed by stochastic temperature pulses (± 0.250 °C) with a frequency range between 15 and 30 s. All thermograms were again analysed with the STARe Software and the T_g was calculated as the midpoint from onset and end temperature of three independent thermograms of the reversing heat flow signal.

As the mDSC measurements of the DSC 1 were not sensitive enough to detect the glass transitions in the thermograms of the prepared co-amorphous tablet formulations, the mDSC measurements of all tablet samples were carried out with a Discovery DSC (TA instruments, New Castle, USA) under a nitrogen gas flow of 50 ml/min. Approximately 6 mg of each ground sample were placed into an aluminium Tzero pan [155] and sealed with a pinholed lid. After an isothermal step of 5 min at -10 °C, samples were heated up to 180 °C with a heating rate of 2 °C/min, amplitude of 0.212 °C, and a period of 40 s. The T_gs were calculated as the midpoint between onset and offset temperature of the reversing heat flow signal of three replicates using the Trios software, ver. 4.0.1 (TA Instruments, New Castle, USA). Melting points were recorded as the onset temperatures of the endothermic event of the total heat flow signal again using the Trios software.

2.2.9.5 Dynamic mechanical analysis (DMA)

Dynamic mechanical analysis (DMA) experiments were performed in duplicate using a DMA Q800 (TA instruments, New Castle, USA). The tablets were carefully ground prior to analysis and each powdered sample (approximately 100 mg) was evenly spread on the bottom of a stainless-steel powder pocket, which was loaded into a 35 mm dual

cantilever clamp. Using a constant heating rate of 3 °C/min, samples were heated up from RT to 160 °C. During heating, samples were deformed in an oscillatory manner at a constant amplitude of 20 µm (frequency of 1 Hz).

2.2.10 Drug release from the tablets

The drug release profiles from SD-T, SD-CT, PM-T, and PM-CT were measured in triplicate. After at least 26 d of storage at the respective storage conditions drug release was investigated with an USP apparatus 2 (Distek Premiere 5100; Distek, New Jersey, USA) at 50 rpm and 37 °C in 900 ml phosphate buffer pH 4.5 (100 mM KH_2PO_4). At preselected time points, samples were taken by a peristaltic pump (Pumpdrive 5001; Heidolph, Schwabach, Germany), simultaneously filtered (pore size 1 µm) and replaced by the corresponding volume of preheated dissolution medium. The saturation level of γ-IND was analysed by adding γ-IND in excess to 50 ml of buffer, stirring at 37 °C for 5 h and subsequent filtration. All samples were diluted with acetonitrile and the content of IND was determined by HPLC (see section 2.2.11).

To detect possible differences between the resulting drug release profiles of the coated and uncoated formulations, a single-factor ANOVA was performed for every single time point of drug release. Concentration values were considered as significantly different, if the p-value was smaller than 0.05 (95 % confidence level).

From the resulting drug release profiles, for each formulation a theoretical value, F_{abs} (Eq. 3), was calculated, which compares the obtained areas under the drug release curves (AUC) with a hypothetical AUC ($AUC_{100\ \%}$), assuming that the contained IND remains dissolved over the whole 4 h of drug release.

$$F_{abs} = AUC/ AUC_{100\%} \tag{Eq. 3}$$

Consequently, the hypothetical $AUC_{100\%}$ is the product of the average weight of each SD-T and PM-T (w), the drug load and the duration of drug release testing:

$$AUC_{100\%} = w \cdot 0.25\% \cdot 240\ min \tag{Eq. 4}$$

A change of F_{abs} by application of a coating may also be calculated as F_{abs} change referring to the amount of polymer applied to the tablet surface:

$$\Delta F_{abs}/\text{polymer level}\ \left(\frac{\%}{mg/cm^2}\right) = \frac{F_{abs\ (coated)} - F_{abs\ (uncoated)}}{\text{coating level } (mg/cm^2)} \tag{Eq. 5}$$

To investigate whether the prepared CA-CT and C-CT formulations were indeed gastro-resistant, the drug release behaviours were measured in triplicate in 900 ml of 0.1 M HCl (37 °C, paddle speed 50 rpm) using an USP apparatus 2 (Distek Premiere 5100; Distek, New Jersey, USA). Samples of the drug release medium were taken after 120 min to quantify the amount of CVD by HPLC according to the Ph. Eur. (see section 2.2.11).

In addition, the drug release behaviours of untreated CA-T and C-T as well as of CA-CT after immersion for 120 min were investigated in triplicate in 900 ml of phosphate buffer pH 6.8 (37 °C, paddle speed 50 rpm). Drug release analysis was performed for 120 min and 6 ml samples were taken at predetermined time points (1, 3, 7, 11, 15, 20, 30, 45, 60, 90, and 120 min) without replacement. For quantification of CVD in both media, 5.0 ml of the filtered drug release medium (pore size 1 µm) were taken and diluted with acetonitrile. The amount of dissolved CVD was subsequently quantified by HPLC (see section 2.2.11).

2.2.11 High performance liquid chromatography (HPLC)

HPLC was carried out for the quantification of the dissolved API during drug release testing as well as for the detection of degradation products during stability testing. All studies were performed with a VWR Hitachi Chromaster 5000 (Radnor, USA).

2.2.11.1 API Quantification

For quantification of IND during drug release, the applied HPLC method was modified from Lenz et al. [99], using a LiChrospher® 100 RP 18e column (125 x 4 mm, 5 µm; Merck Millipore, Darmstadt, Germany). The flow rate of the mobile phase (acetonitrile and diluted phosphoric acid pH 2.0 in a ratio of 60:40 v/v) was 2.0 ml/min and the injection volume 20 µl. IND was eluted at 1.7 min and detected at a wavelength of 202 nm. The absorbance was linear in a concentration range between 0.21 and 63.9 mg/l ($R^2 = 0.999$).

For the quantification of CVD, the used HPLC method was adopted from the CVD monograph of the Ph. Eur. 9.2. Briefly, the LiChrospher® 100 RP 18e column (125 x 4 mm, 5 µm) was used with a mobile phase consisting of 35 % v/v acetonitrile and 65 % v/v aqueous potassium phosphate buffer (pH adjusted to 2.0 with phosphoric acid). The analysis was performed by isocratic elution with a flow rate of 1.0 ml/min and an injection volume of 20 µl. CVD was eluted at 4.6 min and the UV detection was performed at 240 nm. The absorbance was linear in a concentration range between 0.18 and 31.5 mg/l ($R^2 = 0.999$).

2.2.11.2 Detection of degradation products

It is well known that IND undergoes basic hydrolysis in alkaline aqueous solution, leading to the degradation products 4-chlorobenzoic acid (CBA) and 5-methoxy-2-methyl-3-indolacetic acid (MMIA) [146]. As these degradation products may either arise during storage of IND at high RHs or during immersion of IND tablet formulations in aqueous media, HPLC was conducted with these samples to detect a possible degradation. In case of the differently stored PMs, IND and CBA were also quantified.

The applied HPLC method was adopted from the IND monograph of the Ph. Eur. 9.0 with some modifications. Briefly, a 300 x 4 mm column (Knauer, Berlin, Germany) was used, which contained a Nucleosil 100 C_6H_5 phase (particle size 7 μm, 40 °C; Macherey-Nagel, Düren, Germany). In accordance with the Ph. Eur., a gradient method was used, where the mobile phase A consisted of acetic acid and water (10 g/l mixture) and phase B of acetonitrile. The gradient was set according to the indomethacin monograph and the flow rate was 1.0 ml/min. A sample volume of 20 μl was injected and UV detection of IND and CBA was performed at a wavelength of 254 nm. The elution of IND occurred at 16.4 min, while the basic hydrolysis products MMIA and CBA eluted at 4.9 and 5.7 min, respectively. The elution times were validated by analysis of plain solutions of CBA, MMIA, and IND, respectively.

For analysis of the immersed IA-CT and IAC-CT, tablets were ground and dissolved in a mixture of acetonitrile and water (60:40, v/v). Prior to injection, the resulting sample solution was sonicated for 15 min and filtered (pore size: 0.11 μm).

For quantification of CBA in the differently stored PMs, about 5 mg of each sample were dissolved in 10.0 ml of the mixture of acetonitrile and water (60:40, v/v). This solution was further diluted (1:10) to determine the concentration of IND. In the respective

solutions quantification of CBA and IND was linear in a concentration range between 0.15 - 20.5 mg/l and 4.9 - 60.7 mg/l, respectively (both $R^2 = 0.999$). The concentrations of IND and the degradation product CBA were calculated as molar percentages (%) of the theoretically present amount of IND.

For stability analysis of tablets containing FUR, the used HPLC method was adopted from Youm et al. [156]. Briefly, the LiChrospher[®] 100 RP 18e column (125 x 4 mm, 5 µm) was used with a mobile phase of 30 % v/v acetonitrile and 70 % v/v 10 mM potassium phosphate buffer pH 3.85. The flow rate was 1.0 ml/min and the sample volume injected was 10 µl. Elution of FUR occurred at 5.8 min and was detected at 233 nm. Prior to analysis, about 10 mg of each ground tablet were dissolved in 100.0 ml of the mobile phase, sonicated for 15 min, and filtered (pore size: 0.22 µm).

3. Results and Discussion

3.1 The effect of a film coating on the solid-state properties and the drug release behaviour of co-amorphous indomethacin-arginine tablets after storage

3.1.1 Development of the prepared tablet formulations and tablet characterisation

Recently, Lenz et al. have developed the first stable co-amorphous tablet formulation, containing co-amorphous spray-dried indomethacin-arginine. The formulation led to tablets with satisfactory properties regarding disintegration time and uniformity of dosage forms and the tablets were stable during the tableting process as well as upon storage for at least ten months at 0 % RH/23 °C or 0 % RH/40 °C [99]. Thus, in the first study of this thesis, this co-amorphous tablet formulation (SD-T), with its corresponding crystalline formulation (PM-T) serving as reference, was prepared to investigate the effect of a polymer coating on the performance of a co-amorphous tablet formulation.

The prepared tablet formulations contained fumed silica to improve the flowabilities of the powder blends, croscarmellose sodium as superdisintegrant, and magnesium stearate as internal lubricant. The filler mannitol was chosen because of its low hygroscopic nature, fast disintegration, and low interaction potential.

To investigate the effect of a coating on the solid-state properties and the drug release behaviour of the prepared formulations, a transparent, immediate release coating was used in the present study. As it was intended to evaluate and to compare how water affects the formulations during storage and during the coating process, water was used as solvent for spray coating. The selected model coating was Kollicoat® Protect, which is a mixture of a polyvinyl alcohol-polyethylene glycol copolymer (55-65 %, w/w), polyvinyl alcohol (35-45 %, w/w) and fumed silica (0.1-0.3 %, w/w) (Fig. 6) [134]. It is used as

aqueous polymer solution without the need for external plasticization and forms transparent, readily water-soluble films. In addition, Kollicoat® Protect may be used as a water vapour protective coating by adding a high content of solids and thus, it might be a well suited polymer for the protection of co-amorphous formulations.
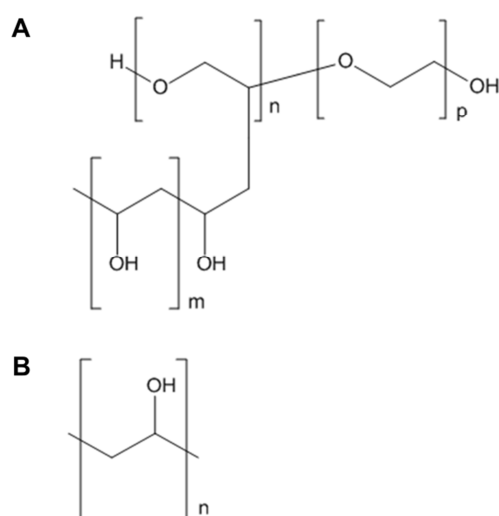
Fig. 6: Chemical structures of the main components of Kollicoat® Protect: (A) Polyvinyl alcohol-polyethylene glycol copolymer (55-65 %), (B) polyvinyl alcohol (35-45 %).

However, upon the addition of solids the transparency of the coating may be lost and thus a potential colour change of the initially yellow colour of the investigated co-amorphous formulations to the white colour of crystalline systems might not be detectable. Moreover, solids in the coating may potentially influence the drug release behaviour. Therefore, as the present study focused on the analysis of the coating process and the effect of the plain polymer on the solid-state properties and the drug release behaviour of the prepared formulations, no pigments were added. The process

conditions were chosen based on the technical information of Kollicoat® Protect, whereby preferably mild conditions (see section 2.2.5) were selected [134].

The characterisation of the prepared uncoated tablets showed a tensile strength of 1.97 ± 0.40 MPa for SD-T (tablet weight of 172 ± 7 mg) and 0.68 ± 0.10 MPa for PM-T (tablet weight of 204 ± 4 mg). These different tensile strengths of the formulations may be related to the different compaction properties of the spray-dried and the crystalline material in SD-T and PM-T, respectively. Because of the poor compaction behaviour of PM-T, it was not able to produce tablets with a sufficient tensile strength of > 1 MPa. Thus, both formulations also showed a different behaviour with regard to friability testing, where the weight loss of SD-T was only 0.1 %, while for PM-T a value of 0.5 % was obtained. However, both formulations did not exceed the suggested maximum loss (1 %) of the Ph. Eur. / USP. Additionally, the requirements of Ph. Eur. and USP regarding the disintegration time were fulfilled by both formulations. It was observed that the different tensile strengths also led to different disintegration behaviours. While PM-T disintegrated quickly by breaking into small particles (1.1 ± 0.2 min), SD-T disintegrated by erosion, which resulted in a slower disintegration time of 4.4 ± 0.3 min. As expected, application of the immediate release coating caused an only slightly delayed disintegration of both formulations (SD-CT: 4.8 ± 0.3 min; PM-CT: 1.9 ± 0.4 min).

### 3.1.2 Visual inspection and water content of the prepared formulations

It is widely known that γ-IND changes its colour from white to yellow during amorphisation [90,100]. Indeed, directly after tablet preparation SD-T were yellow, whereas PM-T were white (Fig. 7A and B). After the coating process, SD-CT still showed the same yellow colour as the uncoated tablets, while PM-CT revealed a slightly yellow surface (Fig. 7C and D). By vertically dividing PM-CT, it was observed that this colour change happened only at the surface, whereas the inside of the tablet halves remained completely white (Fig. 7E).
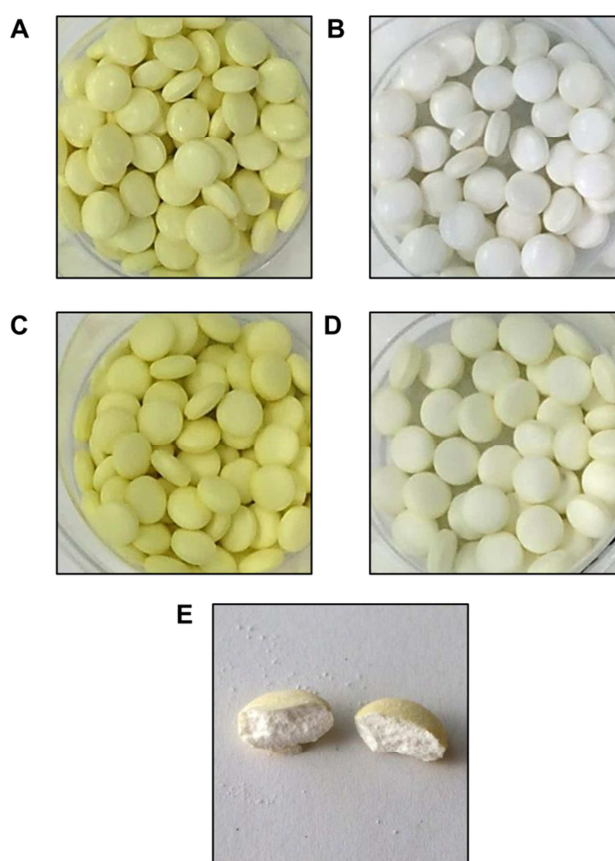
Fig. 7: Images of all formulations immediately after tableting and coating. (A) SD-T (B) PM-T (C) SD-CT (D) PM-CT (E) cross section of a PM-CT tablet.

After storage at RT/0 % for up to 94 d, there was no detectable change of the colour or mechanical behaviour of the prepared formulations. However, after storage at RT/75 % for 26 d it was observed that PM-T (PMT-RT/75 %) as well as PM-CT (PMCT-RT/75 %) were now completely yellow (Fig. 8B and D). With regards to their mechanical stability, PMT-RT/75 % were soft and slightly disintegrated, while PMCT-RT/75 % maintained their initial shape. Considering the yellow colour of amorphous IND it was likely that PMT and PMCT underwent amorphisation during storage at RT/75 %.

After 26 d of storage at RT/75 %, SD-T (SDT-RT/75 %) and SD-CT (SDCT-RT/75 %) were still yellow but their colour slightly darkened (Fig. 8A and C). Additionally, both tablet formulations were more tightly packed and therefore harder after storage. Both, colour darkening and tablet hardening, have also been observed previously with amorphous sodium indomethacin upon storage at 56 % and 83 % RH, respectively [157]. Upon further storage at RT/75 % for 91 d the colour change increased slightly for both, SDT-RT/75 % and SDCT-RT/75 % as well as PMT-RT/75 % and PMCT-RT/75 %.
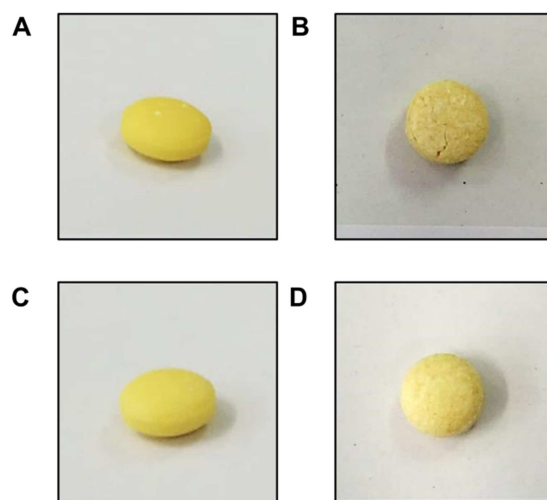
Fig. 8. Images of all formulations after storage at RT/75 % for 26 d. (A) SD-T (B) PM-T (C) SD-CT (D) PM-CT.

TGA results are shown in Table 7. Samples stored at RT/0 % contained only low amounts of water (0.4-2.0 %), whereas samples stored at RT/75 % exhibited a slightly higher weight loss during TGA (3.4-4.2 %). Overall, this water content of up to 4.2 % was still in an acceptable range for tablets, which was probably a result of the low hygroscopic nature of mannitol [158]. While PM-T and PM-CT stored at RT/0 % (PMT-RT/0 %, PMCT-RT/0 %) contained less water than the corresponding SD formulations (SDT-RT/0 %, SDCT-RT/0 %), PMT-RT/75 % and PMCT-RT/75 % showed an even slightly higher water content compared to their co-amorphous counterparts after storage for 240 d. Considering the generally more hygroscopic nature of amorphous materials relative to the crystalline form, this high water content might also be an indicator of the possible amorphisation of PMT-RT/75 % and PMCT-RT/75 % during storage.

Table 7: TGA results of the investigated samples. Water content (means in % w/w ± SD) after storage for the different time periods at 0 % and 75 % RH, respectively.

|	RT/0 %			
storage time periods	SD-T	SDC-T	PM-T	PM-CT
0 d	1.9 ± 0.1	1.7 ± 0.1	0.7 ± 0.1	0.6 ± 0.1
1 d	1.5 ± 0.1	1.5 ± 0.1	0.5 ± 0.1	0.7 ± 0.1
32 d | 26 d	1.4 ± 0.2	2.0 ± 0.3	0.9 ± 0.5	0.7 ± 0.2
240 d	1.2 ± 0.1	1.4 ± 0.1	0.5 ± 0.1	0.4 ± 0.1
	RT/75 %			
storage time periods	SD-T	SD-CT	PM-T	PM-CT
0 d	1.9 ± 0.1	1.7 ± 0.1	0.7 ± 0.1	0.6 ± 0.1
1 d	n.d.	n.d.	n.d.	n.d.
32 d | 26 d	3.6 ± 0.1	3.4 ± 0.3	3.5 ± 0.1	3.5 ± 0.1
240 d	3.6 ± 0.1	3.5 ± 0.7	4.2 ± 0.1	4.1 ± 0.5

* n.d. = no data

3.1.3 Solid-state characterisation of the prepared formulations

   3.1.3.1 XRPD

XRPD is a valuable technique to distinguish between crystalline and amorphous phases, as diffractograms of crystalline phases reveal distinct and specific peaks, while those of amorphous samples show only the so-called "halo" [17]. Because the investigated powder blends contained crystalline β-mannitol, their diffractograms were dominated by the reflections of β-mannitol. For an interpretation of possible solid-state changes of IND and ARG, the characteristic reflections of γ-IND and crystalline ARG in the diffractograms of the crystalline PM formulations had to be selected first. Reflections of γ-IND were determined at 11.7, 17.1, 24.1 and 27.6 °2θ, while a characteristic reflection of crystalline ARG in the powder blend could only be observed at 18.4 °2θ. Unprocessed Kollicoat® Protect revealed only a broad halo with a peak maximum at 19.6 °2θ, which could not be observed in the diffractograms of the coated formulations because of the comparatively low concentration of the polymer.

Fig. 9A shows the diffractograms of all co-amorphous formulations after storage at RT/0 % for 94 d as well as after storage at RT/75 % for 91 d, respectively. It can be seen that all diffractograms corresponded to those of the spray-dried co-amorphous powder blend (SD-PB) and no reflections of crystalline γ-IND or ARG were detectable. Thus, there was no difference between coated and uncoated tablets. Water, heat, as well as mechanical stress during the coating process did not induce recrystallisation of SD CoA IND-ARG and the samples were stable for at least 94 d of storage. Additionally, there was no evidence for recrystallisation during storage at RT/75 % for up to 91 d, which demonstrates the high physical stability of the prepared co-amorphous formulations, even if stored at humid conditions.
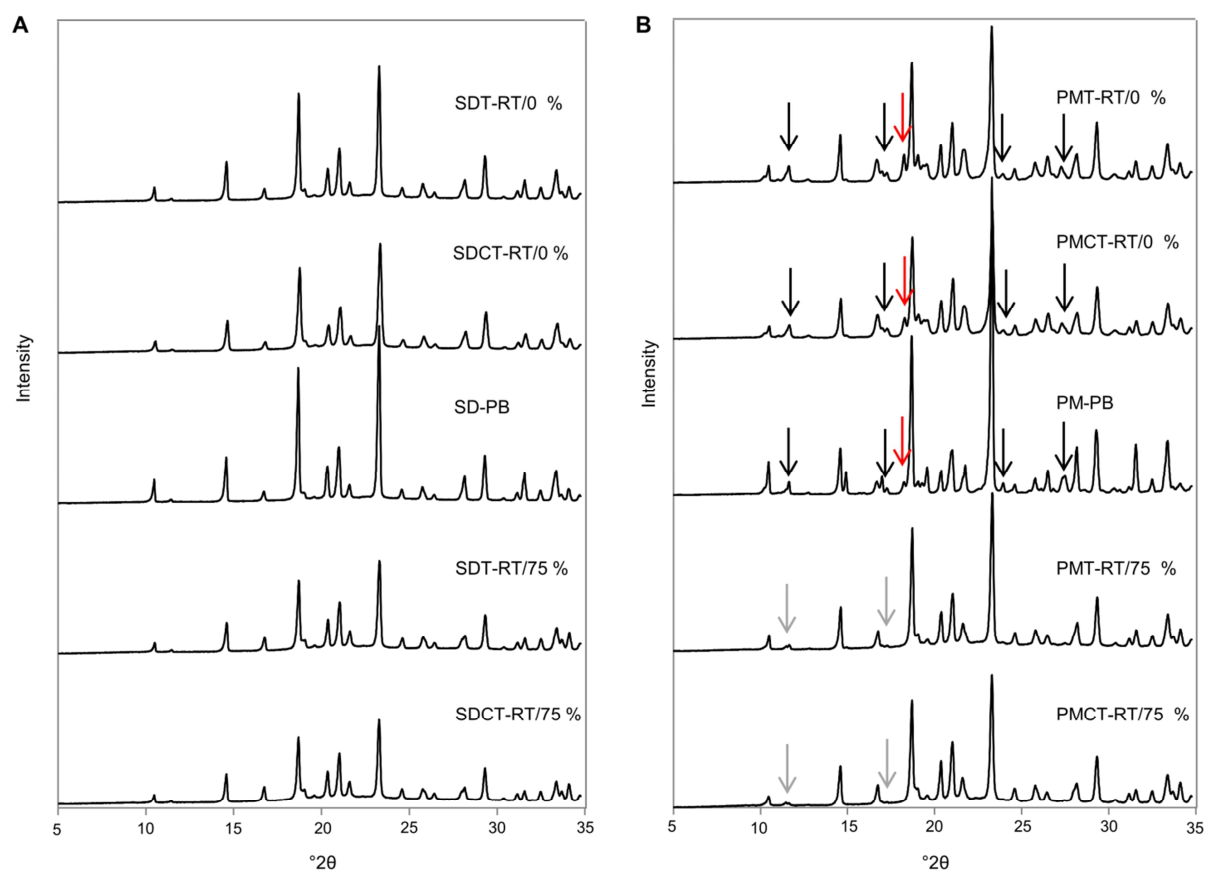
Fig. 9: (A) XRPD diffractograms of the freshly prepared co-amorphous powder blend (SD-PB) as well as co-amorphous tablets (SD-T) and coated tablets (SD-CT), after 94 d of storage at RT/0 % and 91 d at RT/75 %, respectively. (B) XRPD diffractograms of the freshly prepared crystalline powder blend (PM-PB) as well as crystalline tablets (PM-T) and coated tablets (PM-CT), after storage at the same conditions as above. Reflections of crystalline γ-IND and ARG are indicated by black (less pronounced in grey) and red arrows, respectively.

The corresponding diffractograms of the PM formulations are shown in Fig. 9B. As expected, all samples that were stored at RT/0 % revealed the characteristic reflections of crystalline γ-IND and ARG. However, samples stored at RT/75 % for 91 d showed distinct changes in the diffractograms, as all reflections of crystalline γ-IND and ARG

were less pronounced (11.7 and 17.1 °2θ) or completely vanished (18.4, 24.1, and 27.6 °2θ), which is illustrated in Fig. 9B by arrows. Thus, the diffractograms were similar to those of the SD formulations (Fig. 9A).

Moreover, with PMT-RT/75 % and PMCT-RT/75 %, the formation of a halo could be observed (shown for PM-CT in Fig. 10), which was indicated by a vertical shift of the diffractograms. For both formulations, less pronounced reflections and the formation of a halo could already be observed after 26 d of storage at RT/75 % (data not shown). Together with the observed colour change of the PM formulations upon storage at RT/75 % this data strongly indicated an *in situ* amorphisation of IND and ARG.
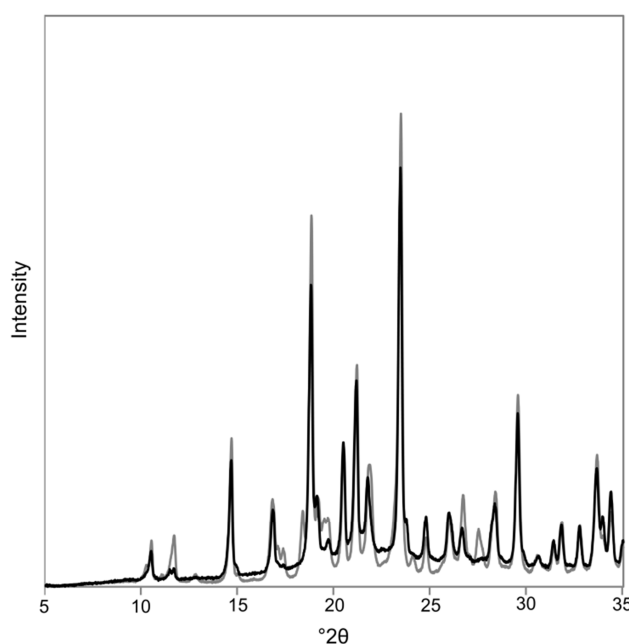

Fig. 10: Comparison of XRPD diffractograms of tablets containing crystalline IND-ARG after storage at RT/0 % for 94 d (grey diffractogram) and at RT/75 % for 91 d (black diffractogram).

3.1.3.2 FTIR spectroscopy

FTIR spectroscopy is an analytical technique, which allows the detection of molecular interactions. Especially for the analysis of co-amorphous IND-ARG FTIR spectroscopy is a very useful tool, as it cannot only distinguish between different IND polymorphs, but also detect the co-amorphisation of IND-ARG resulting from molecular interactions in this system [56]. In Fig. 11 the FTIR spectra of γ-IND, the co-amorphous (SD-PB) as well as the crystalline powder blend (PM-PB) are compared in the region from 1100 to 1800 cm^{-1}, because this is the most characteristic region for SD CoA IND-ARG, as previously reported [32].
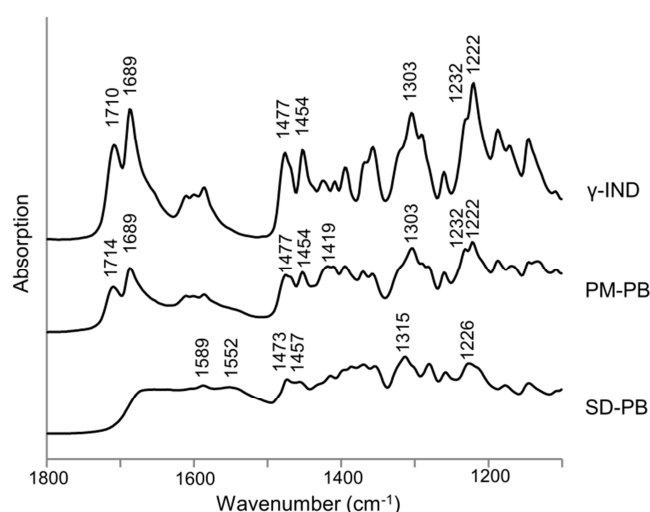

Fig. 11: FTIR spectra of powder blends of co-amorphous (SD-PB) and of crystalline IND-ARG (PM-PB) as well as of γ-IND as reference.

It can be observed that the spectrum of PM-PB was dominated by γ-IND, while the band at 1710 cm^{-1} was slightly shifted to 1714 cm^{-1}. Other differences between the spectra of PM-PB and γ-IND primarily resulted from the tableting excipient mannitol, which

revealed IR bands in the region between 1100 and 1450 cm^{-1}. In contrast, SD-PB showed a different spectrum. Löbmann et al. [56] have previously investigated the changes in the FTIR spectra as a result of co-amorphisation of IND-ARG. The most distinct change is the disappearance of the bands of γ-IND at 1710 and 1689 cm^{-1} with a simultaneous formation of a broad plateau between 1680 and 1500 cm^{-1} with a small peak at 1589 cm^{-1}, which both also were observed in SD-PB (Fig. 11). This change of the SD-PB spectrum is probably a consequence of salt formation of the co-amorphous IND-ARG, as the vanished bands at 1710 and 1689 cm^{-1} are characteristic for free carboxylic acid vibrations of γ-IND [99]. In addition, the shoulder at 1552 cm^{-1}, which is related to the COO^{-} stretching vibration of γ-IND, was found in the spectrum of SD-PB [32]. A further difference between PM-PB and SD-PB –due to amorphisation of γ-IND– was a band shift from 1303 to 1315 cm^{-1} and the replacement of the bands at 1232 and 1222 cm^{-1} by a band at 1226 cm^{-1}. Despite these distinct differences, the region between 1500 and 1350 cm^{-1} also varied between SD-PB and PM-PB. While PM-PB showed the characteristic bands of γ-IND at 1477 and 1454 cm^{-1}, in the spectra of SD-PB both bands were less pronounced and slightly shifted to 1473 and 1457 cm^{-1}, respectively. In contrast to SD-PB, PM-PB also revealed a band at a wavelength of 1419 cm^{-1}, which is related to crystalline ARG. Because of the comparatively low intensity of the ARG absorption this was the only band of crystalline ARG that was detected in PM-PB in the analysed region. Also, in the spectra of the coated tablets (Fig. 12) no bands of Kollicoat$^{®}$ Protect were detectable.
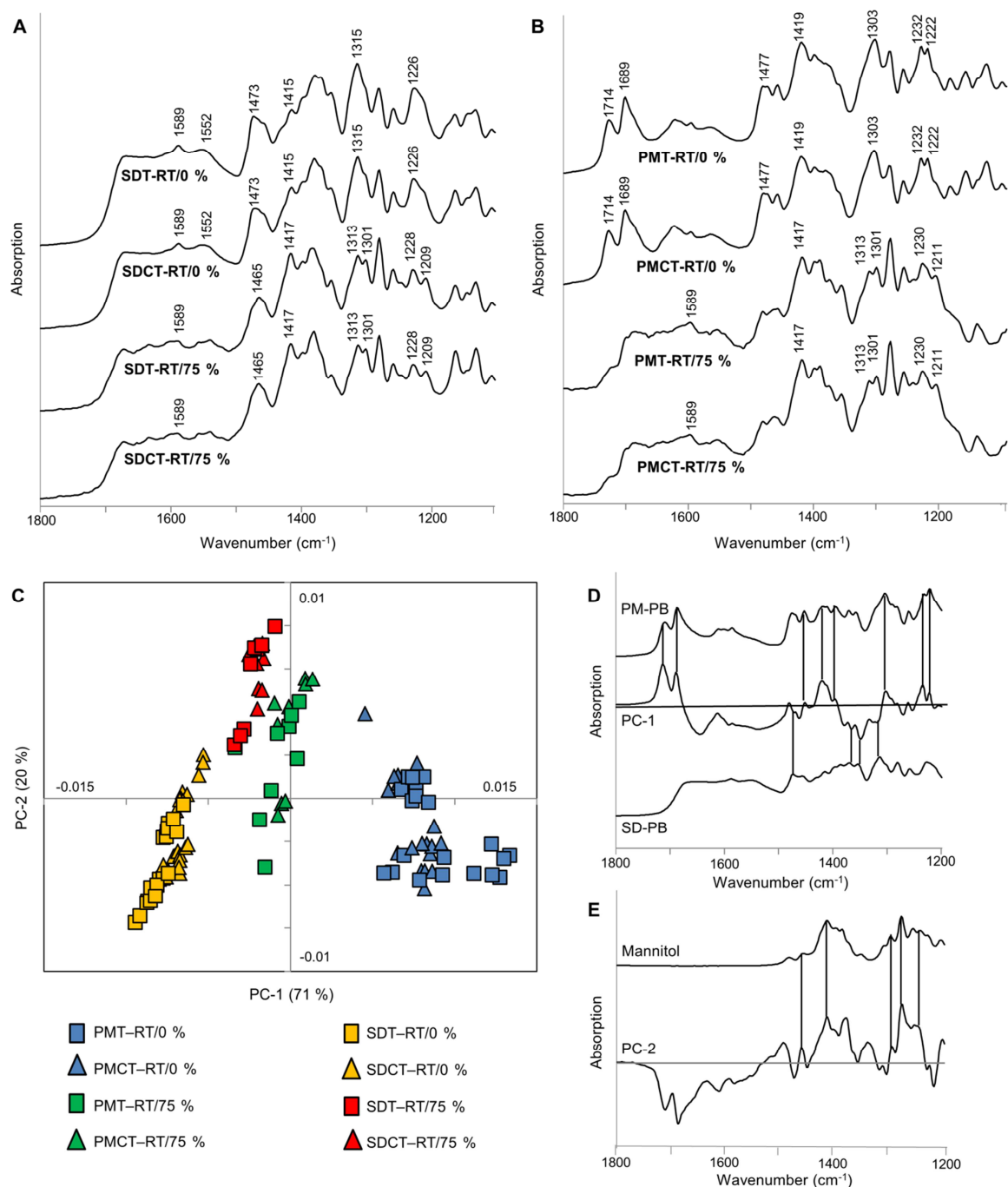
Fig. 12: FTIR spectra and PCA of the FTIR spectra (1800-1200 cm^{-1}). (A) FTIR spectra of the SD formulations after storage at RT/0 % for 94 d and RT/75 % for 91 d. (B) FTIR spectra of the PM formulations after storage at RT/0 % for 94 d and RT/75 % for 91 d. (C) Scores plot of all prepared formulations after 0, 32 and 94 d of storage at RT/0 % as well as after 26 and 91 d of storage at RT/75 %. (D) Loadings plot of PC-1 as well as reference spectra of PM-PB and SD-PB. (E) Loadings plot of PC-2 as well as a reference spectrum of mannitol.

FTIR spectra of the SD formulations are displayed in Fig. 12A. It can be observed that after coating of SD-T no changes in the resulting FTIR spectra of the SD-CT were detectable, which confirmed the results of the XRPD data indicating that the coating process did not induce a recrystallisation of co-amorphous IND-ARG. Principal component analysis (PCA) of the FTIR spectra also verified this observation, as coated and uncoated SD formulations clustered in the same region. The scores plot of the PCA is shown in Fig. 12C, in which co-amorphous formulations (immediately after production and after 32 d and 94 d of storage at RT/0 %, respectively) clustered in the negative part of principal component 1 (PC-1), while crystalline formulations under the same conditions clustered in the positive part. The loadings plot of PC-1 (Fig. 12D) clearly showed that the positive part of the plot described the characteristic bands of PM-PB and the negative part the bands of SD-PB.

The change of the PM formulations after storage at RT/75 % for 91 d is shown in Fig. 12B. As expected from the XRPD data, the bands of crystalline γ-IND at 1710 and 1689 cm^{-1}, that were observed at the storage condition of RT/0 %, almost disappeared and the characteristic plateau of SD CoA IND-ARG between 1680 and 1500 cm^{-1} as well as the small peak at 1589 cm^{-1} appeared in the spectra. This change was already observed after 26 d of storage at RT/75 % and is shown in the scores plot of the PCA, where both PMT–RT/75 % and PMCT–RT/75 % moved from the positive part into the negative part of PC-1 (Fig. 12C). Hence, this data indicated not only amorphisation, but more specifically co-amorphisation of the initially crystalline IND-ARG.

Also, other changes of the spectra of PMT-RT/75 % and PMCT-RT/75 % compared to PMT-RT/0 % and PMCT-RT/0 % were observed such as shifted bands between 1211

and 1419 cm^{-1} and an additional band at 1313 cm^{-1} (Fig. 12B). Similar bands were observed with SDT-RT/75 % and SDCT-RT/75 % (Fig. 12A). These changes also appeared in the scores plot of the PCA, where the formulations that were stored at RT/75 % moved into the positive part of the principal component 2 (PC-2) (Fig. 12C). The comparison of the loadings plot of PC-2 with the spectrum of plain mannitol (Fig. 12E) indicated that the change of the sample spectra upon storage at RT/75 % was the result of a comparably higher absorption of mannitol. It was assumed that adsorbed water reduced the intensity of co-amorphous and crystalline IND-ARG IR absorption, which led to a comparatively higher mannitol IR absorption of samples, that were stored at RT/75 % than of the corresponding samples stored at RT/0 %. This would also explain the observation that SDT-RT/75 % and SDCT-RT/75 % moved slightly closer to the positive part of PC-1 in the scores plot of the PCA (Fig. 12C), as the bands of SD IND-ARG were marginally less pronounced because of the adsorbed water. In any case, the characteristic SD IND-ARG plateau between 1750 and 1500 cm^{-1} could still be observed in the spectra of SDT-RT/75 % and SDCT-RT/75 % and there was no band of γ-IND detectable (Fig. 12A). Considering the fact that even the initial crystalline formulations (PM-T and PM-CT) turned into co-amorphous systems upon storage at RT/75 %, it is likely that the co-amorphous formulations were physically stable. Thus, together with the visual appearance and XRPD data, it may be summarised that the SD formulations did not recrystallise but only changed their mechanical behaviour upon storage at RT/75 %.

3.1.4 Drug release behaviour of the prepared formulations

Despite the characterisation of the solid-state properties it is also necessary to examine the *in vitro* drug release behaviour of the different formulations, as this property is a valuable precursor of any bioavailability study. Especially amorphous systems may show a non-expected drug release behaviour because of a phase transition from the initial amorphous form into other solid-state forms during dissolution [159]. This can either be caused by a solid-to-solid transition at the surface of the tablet, which in turn leads to a much lower supersaturation than expected, or by a recrystallisation from the supersaturated solution, both of which reducing the bioavailability of the API [160,161].

Drug release profiles in phosphate buffer pH 4.5 of all differently stored formulations are shown in Fig. 13A-D. The behaviour of SDT-RT/0 % and PMT-RT/0 % (Fig. 13A and C) corresponded to the observations by Lenz et al., as both formulations showed a supersaturation of IND (SDT-RT/0 %: c_{max} 14.9 mg/900 ml; PMT-RT/0 %: c_{max} 16.9 mg/900 ml compared to the saturation level of γ-IND: 5.6 mg/900 ml) with a following decrease of the IND concentration as a result of recrystallisation of γ-IND from the supersaturated solution. The unexpected supersaturation of the PM formulations can be related to an *in situ* co-amorphisation of γ-IND and ARG after contact with the dissolution medium, which was confirmed by a colour change from white to yellow, that has already been observed by Lenz et al. [99]. Additionally, it was noticed that PMT-RT/0 % reached the maximum supersaturation level earlier than SDT-RT/0 % (SDT-RT/0 %: t_{max} 40 min; PMT-RT/0 %: t_{max} 10 min) and that its recrystallisation also occurred faster. This behaviour was related to the different properties of both tablet formulations, as the faster disintegration of PMT-RT/0 % led to a higher c_{max} and a lower

t_{max} compared to SDT-RT/0 % (see section 3.1.1). As both formulations included only mannitol as filler without binder, the PMT formulation showed a lower tensile strength because of the poor compaction behaviour of the crystalline material, leading to more friable and rapidly disintegrating tablets.
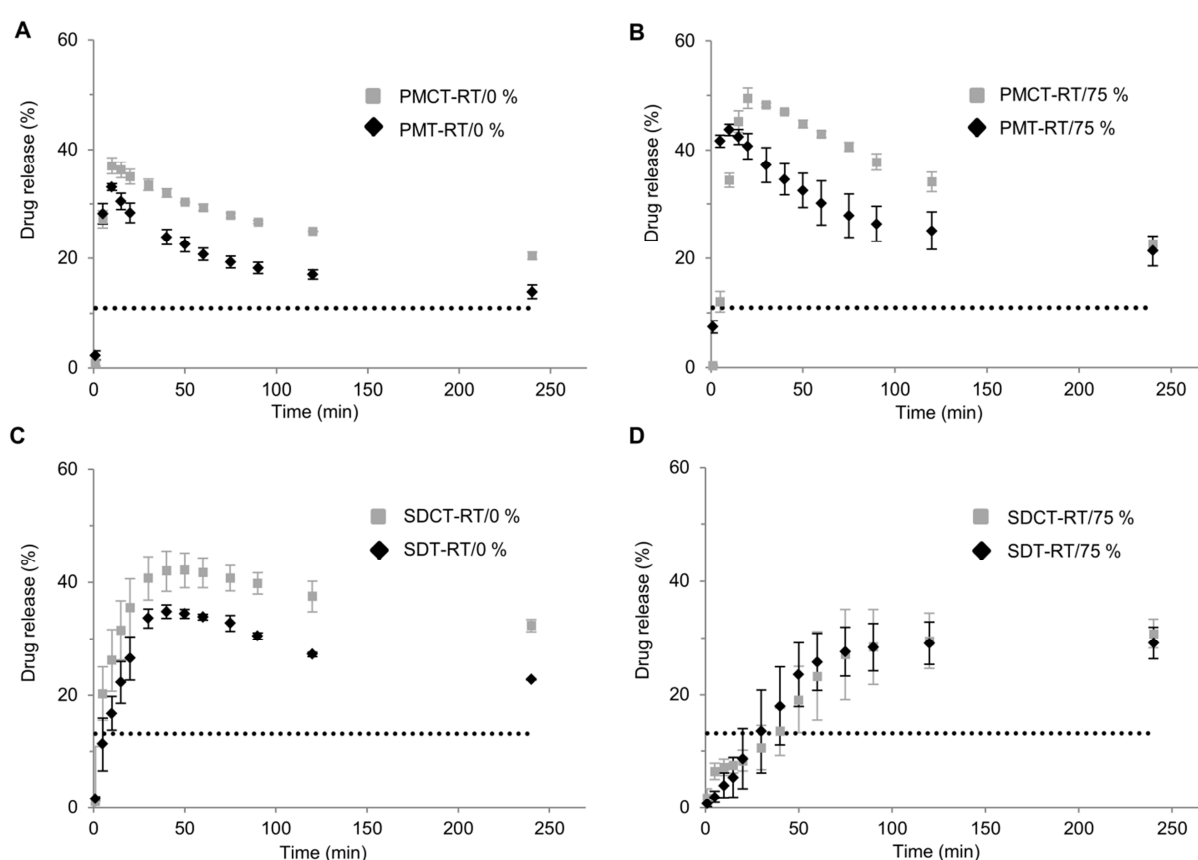
Fig. 13. Drug release at 37 °C. (A,B) Drug release from PM-T and PM-CT after storage at RT/0 % and RT/75 %, respectively. (C,D) Drug release from SD-T and SD-CT after storage at RT/0 % and RT/75 %, respectively. Means ± SD, n = 3. Dotted lines indicate the γ-IND saturation level (5.6 mg/900 ml).

Although such a fast disintegration is usually beneficial for drug release, in this case it was unfavorable, because the resulting high supersaturation level of PMT-RT/0 % led to a faster recrystallisation of the drug from the supersaturated solution. In contrast, the harder spray-dried SD-T formulation disintegrated slowly by erosion, which resulted in a longer time period needed to reach c_{max} and a slower onset of drug crystallisation.

To enhance the bioavailability of the prepared formulations, it would be advantageous to prevent or decrease both above mentioned recrystallisation routes, which should result in a higher c_{max} and a slower or ideally no decrease of the maximum IND concentration. Interestingly, in this study the presence of a coating polymer improved the drug release behaviour of PMC-TRT/0 %, PMCT-RT/75 %, and SDCT-RT/0 %, compared to the respective uncoated formulations. The results of this observation are shown in Fig. 13A-C, as the coated tablet formulations reached higher c_{max} values (Table 8) combined with a slower IND recrystallisation, which was indicated by a lower decrease of the drug release curve and a higher IND concentration after 4 h of drug release testing (c_{4h} of PMT-RT/0 %: 7.1 mg/900 ml; c_{4h} of PMCT-RT/0 %: 10.4 mg/900 ml; c_{4h} of PMT-RT/75 %: 11.5 mg/900 ml; c_{4h} of PMCT-RT/75 %: 10.9 mg/900 ml; c_{4h} of SDT-RT/0 %: 9.8 mg/900 ml; c_{4h} of SDCT-RT/0 %: 13.9 mg/900 ml). ANOVA showed that with PMCT-RT/0 %, PMCT-RT/75 %, and SDCT-RT/0 % the majority of the data points was significantly different from the respective uncoated formulations (not significantly different: PMCT-RT/0 %: 1 and 5 min; PMCT-RT/75 %: 15 and 240 min; SDCT-RT/0 %: 1-40 min).

Table 8: Comparison of drug release data of the investigated tablet formulations.

	c_{max}	c_{max}	t_{max}	AUC	F_{abs}	ΔF_{abs}	ΔF_{abs} /polymer level
	(% IND)	(mg/900 ml)	(min)	(% · min)	(%)	(%)	(%/mg · cm^{-2})
PMT-RT/0 %	33.1	16.9	10	4459	18.6		
PMCT-RT/0 %	37.1	18.9	10	6198	25.8	7.2	2.88
PMT-RT/75 %	43.7	22.3	10	6535	27.2		
PMCT-RT/75 %	49.4	25.2	20	8139	33.9	6.7	2.68
SDT-RT/0 %	34.8	14.9	40	6489	27.0		
SDCT-RT/0 %	42.1	18.0	50	8676	36.2	9.2	2.49
SDT-RT/75 %	29.2	12.5	240	5980	24.9		
SDCT-RT/75 %	30.8	13.2	240	6001	25.0	0.1	0.03

As Table 8 shows, the AUC and thus, the F_{abs} values improved for the coated tablets in the case of PMCT-RT/0 %, PMCT-RT/75 %, and SDCT-RT/0 %, as the F_{abs} value was at least 6.7 % higher than the F_{abs} of the corresponding uncoated formulation. Hence, the application of the coating allowed a 9.2 % higher availability of IND during drug release from SDCT-RT/0 % compared to SDT-RT/0 %, which means an improvement of 34 %. Altogether, the improvement of the F_{abs} value per mg/cm^2 applied polymer was between 2.49 and 2.88 % for PMCT-RT/0 %, PMCT-RT/75 %, and SDCT-RT/0 %, respectively (Table 8). Therefore, this coating is -despite the low amount of applied polymer compared to polymer based glass solutions- potentially suited to improve the bioavailability of co-amorphous IND-ARG formulations.

As the dissolution profiles are the result of a combination of several factors, it is difficult to interpret all underlying processes, which occur during drug release. However, concerning the improvement of drug release by Kollicoat® Protect the mechanism is probably similar to that of polymers in ASDs.

It is known that the dissolution profiles of ASDs can be superior compared to those of plain amorphous drugs [162,163]. These underlying processes are complex and the resulting drug release profiles highly depend on the type of polymer and the drug itself [160–162,164]. However, previous studies have shown that the beneficial effect of the polymers during drug dissolution does not necessarily depend on their presence in the formulation in form of a glass solution with the drug [160,165]. The superior concentration-time profiles of ASDs compared to those of the plain amorphous drug can on the one hand be related to an increased equilibrium solubility of the drug by interaction with the polymer [162,163]. In the present study, the coating of Kollicoat® Protect was also able to increase the level of IND supersaturation during drug release from the prepared formulations. In this context, the close contact of the polymer with the tablet surface might play an important role, as the low concentration of polymer compared to ASDs was sufficient to achieve this effect. On the other hand, polymers in polymer-based glass solutions may show an inhibiting effect on drug recrystallisation from a supersaturated solution [162,163]. In the present study, Kollicoat® Protect also revealed such a stabilising effect on the supersaturated drug solutions, because the decrease of the dissolved amount of IND after reaching c_{max} was -despite a higher c_{max}- lower or similar for all coated tablets compared to the uncoated formulations.

Kollicoat® IR (polyvinyl alcohol-polyethylene glycol copolymer), the polymer on which the composition of Kollicoat® Protect is based, has already been shown to be a valuable

excipient in ASDs containing amorphous itraconazole [166]. In general, drug release from tablets or coated tablets is different from drug release from matrix systems such as polymer-based glass solutions. However, the mechanisms by which Kollicoat® Protect improved the drug release of the co-amorphous system in the present study might at least partly be similar to that of Kollicoat® IR in the study by Janssens et al. [166]. In this study, Kollicoat® IR had led to a very high dissolution rate of itraconazole and maintained drug supersaturation for up to 4 h of dissolution testing, which had been related to its high aqueous solubility and low viscosity. However, the study by Janssens et al. also revealed problems with regard to the preparation of the Kollicoat® IR-based glass solutions, as the crystallinity of the polymer increased during hot melt extrusion, which might affect the stability of these extrudates. In addition, drug release from these glass solutions was significantly improved only to itraconazole loadings up to 25 %. Both problems are typically associated with polymer-based glass solutions [28]. Thus, the use of polymers as tablet coatings, for example Kollicoat® Protect, would be a superior approach, if they could lead to the same stabilising effect during drug release as the glass solutions. In the present study, it could be shown for the first time that coatings can have a beneficial effect on co-amorphous formulations during drug release. Further studies are needed to investigate whether higher coating levels or other polymers may also affect recrystallisation inhibition.

As Fig. 13D shows, storage of SD formulations at RT/75 % led to a distinct change of the drug release profiles of both coated and uncoated tablets, which were characterised by the formation of a plateau. This behaviour may be explained by the fact that tablets were tightly packed after storage at RT/75 %, which resulted in poor disintegration, leading to a slow dissolution. Thus, the insufficient disintegration did not allow a

pronounced supersaturation, as the hard tablets showed a retarding effect. Therefore, a definite improvement of the concentration vs. time profile by application of the investigated coating was not detected. According to the ANOVA, the data of all time points was not statistically different from each other (except for the value at 5 min). This lack of sufficient disintegration and therefore poor dissolution is a well-known problem related to amorphous formulations [28]. As this behaviour was only observed with the SD formulations stored at RT/75 %, further studies are needed to investigate whether this change of the disintegration and dissolution behaviour could be prevented, for example by application of a coating consisting of Kollicoat® Protect with high solid contents, which would generate a moisture protective coating.

The concentration vs. time profiles of the PM formulations after storage at RT/75 % are shown in Fig. 13B. It can clearly be observed that both formulations reached a higher c_{max} (PMT-RT/75 %: 22.3 mg/900 ml; PMCT-RT/75 %: 25.2 mg/900 ml) and also a higher F_{abs} than the respective formulations, which were stored at RT/0 % (Fig. 13A, Table 8). The F_{abs} values of PMT-RT/75 % (27.2 %) and PMCT-RT/75 % (33.8 %) were even comparable to those of SDT-RT/0 % (27.0 %) and SDCT-RT/0 % (36.2 %) (Table 8). This observation corresponded to the results of the solid-state analysis of the investigated formulations, which revealed an *in situ* amorphisation of the PM formulations during storage at RT/75 %. Although PM formulations underwent an *in situ* amorphisation upon contact with the dissolution media, this amorphisation was not complete, as shown by a lower F_{abs} of PMT-RT/0 % and PMCT-RT/0 % compared to the SD formulations (Table 8). Consequently, the *in situ* amorphisation of PM samples stored at RT/75 % led to a higher co-amorphous content and therefore to both, a higher maximum concentration of dissolved IND and a higher F_{abs} value. This novel way of *in*

situ amorphisation of IND-ARG is promising, as the costly and time consuming process of spray drying might be substituted by storage of crystalline physical mixture formulations at humid conditions. Moreover, it was observed that SD formulations hardened upon storage at RT/75 % and thus revealed a poor disintegration behaviour. As the PM samples did not show an altered disintegration behaviour upon storage at the same conditions, the use of *in situ* amorphisation might also be advantageous for the mechanical stability of this system.

3.1.5 Conclusion

In the present study it could be shown for the first time that coating of a co-amorphous formulation is possible without inducing recrystallisation, with the coated formulations being stable for at least three months. In addition, a high physical stability of the prepared co-amorphous IND-ARG formulations was observed, as during storage at RT/75 % the co-amorphous formulations remained stable. Moreover, the initially crystalline formulations turned into co-amorphous systems and humid storage conditions can even be applied for *in situ* co-amorphisation of this system. A second study of this thesis will therefore further investigate this process of *in situ* co-amorphisation during storage at humid conditions.

Nevertheless, moisture protective coatings may be useful for this and other highly stable co-amorphous formulations, as a change of the mechanical and disintegration behaviour of the co-amorphous formulations was observed after storage at high humidity, which is a well-known problem of amorphous formulations.

Additionally, it was shown that the applied polymer Kollicoat® Protect improved the drug release behaviour of the prepared formulations because the coated formulations revealed a higher c_{max} and an increased AUC compared to the uncoated formulations. Therefore, this study showed that not only polymers used in polymer-based glass solutions or added directly to the dissolution media, but also small amounts of polymers, applied as coatings, can have a beneficial effect on the drug release from co-amorphous formulations. Future studies will need to investigate whether higher levels of Kollicoat® Protect, or other water-soluble coating polymers, may improve the drug release behaviour of co-amorphous systems even more.

3.2 Investigations on the feasibility of humid storage conditions to induce *in situ* co-amorphisation of indomethacin and arginine

3.2.1 Characterisation of plain IND and ARG

To get a deeper insight into the observed *in situ* co-amorphisation of IND and ARG upon storage of crystalline tablets at humid conditions (see section 3.1), in the present study physical mixtures of γ-IND and ARG were stored at different storage conditions for specific time periods (see section 2.2.6.2). However, to evaluate changes of a physical mixture upon storage at defined conditions, also possible changes of the plain substances upon storage need to be investigated. In the present study, the plain drug γ-IND and the amino acid ARG were therefore stored separately at the respective storage conditions (see section 2.2.6.2) and subsequently analysed.

For the γ-IND samples, no changes were detected upon storage at 28, 58, and 75 % RH. FTIR spectra of all differently stored γ-IND samples looked identical, revealing the typical bands of γ-IND (data not shown). Also the diffractograms of these samples were similar, as were the DSC thermograms, which only showed the endothermic melting event of γ-IND at 161.9 ± 0.2 °C (Fig. 14). TGA analysis revealed the non-hygroscopic nature of the crystalline drug, as it contained only about 0.1 % of water, even if stored at 58 and 75 % RH, respectively (data not shown). According to the ANOVA, the data of all three storage conditions were not significantly different ($p > 0.05$). Taken together, this data indicated that humidity did not affect the properties of γ-IND, if it was stored on its own.
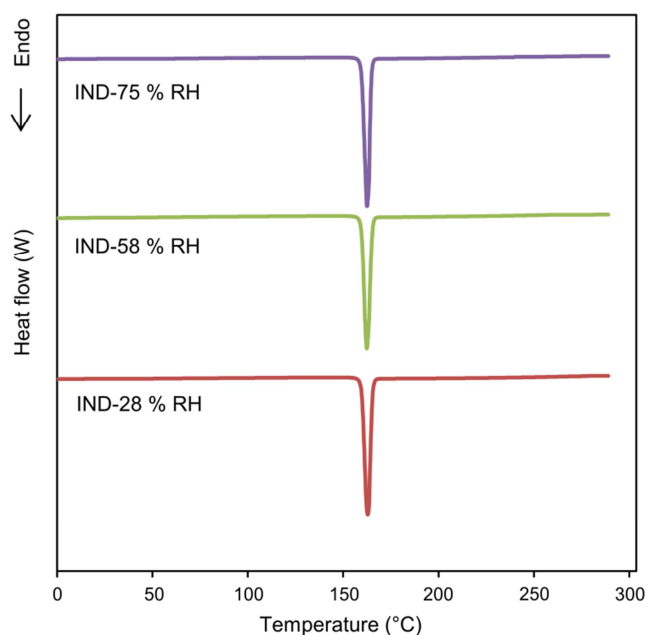
**Fig. 14:** cDSC thermograms of γ-IND after storage at 28 % (IND-28 % RH), 58 % RH (IND-58 % RH), and 75 % RH (IND-75 % RH), respectively.

In contrast to IND, the analysis of ARG revealed distinct differences between the applied storage conditions. The respective diffractograms are shown in Fig. 15. It was observed that the differently stored ARG diffractograms did not correspond to that of the starting material. Furthermore, ARG, which was stored at 28 % RH (ARG-28 % RH), exhibited other reflections than ARG, which was stored at 58 % RH (ARG-58 % RH) and 75 % RH (ARG-75 % RH), respectively. The characteristic reflections of each sample are depicted in Fig. 15. According to the literature [167], the diffractograms of ARG-58 % RH and ARG-75 % RH can be related to ARG dihydrate, while the diffractogram of ARG-28 % RH is assigned to ARG anhydrate. The diffractogram of bulk ARG looked similar to that of ARG-28 % RH, although the intensity of the characteristic peak of ARG anhydrate at 18.4 °2θ was less pronounced in bulk ARG, while the diffraction at 19.5 °2θ was more

intense compared to ARG-28 % RH (Fig. 15). This difference in the diffraction intensities

might be related to a preferred orientation of the crystals.
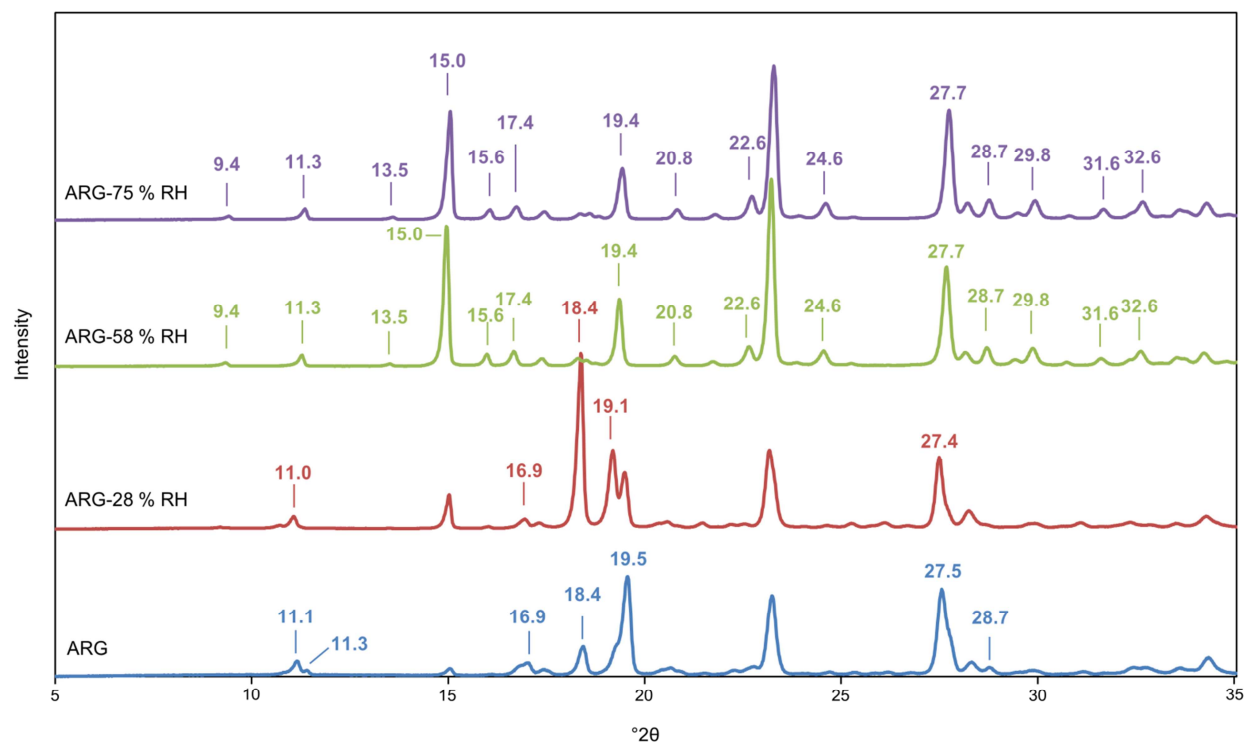
Fig. 15: XRPD diffractograms of unstored bulk ARG as well as of ARG after 10 d of storage at 28 % RH (ARG-28 % RH), 58 % RH (ARG-58 % RH), and 75 % RH (ARG-75 % RH), respectively. Characteristic reflections are marked.

Similar to the diffractograms, the weight losses in the TGA thermograms of ARG-28 % RH, ARG-58 % RH, and ARG-75 % RH were all significantly ($p < 0.05$) different (Table 9, Fig. 16). Compared to ARG-28 % RH, both ARG-58 % RH and ARG-75 % RH contained much more water and revealed a strong dehydration event at about 100 °C. In agreement with the XRPD data, the weight loss of ARG-58 % RH and ARG-75 % of 16.4 to 16.8 % after storage for at least 10 d (Table 9) corresponded to about two molecules of water (theoretical value 17.1 %), confirming the formation of ARG dihydrate upon storage at 58 and 75 % RH.

In all cDSC thermograms an endothermic event at 100 °C was observed, because of dehydration of ARG. In addition, melting of ARG (onset at about 218 °C; melting accompanied by ARG degradation) was detected (Fig. 17).

Table 9: TGA results of the investigated ARG and PM samples. Water content after storage at 28, 58, and 75 % RH, respectively, for the different storage time periods (means in % w/w ± SD, n = 3).

| storage time	28 % RH		58 % RH		75 % RH	
	ARG	PM	ARG	PM	ARG	PM
0 d	6.5 ± 0.08	3.0 ± 0.08	6.5 ± 0.08	3.0 ± 0.08	6.5 ± 0.08	3.0 ± 0.08
1 d	4.1 ± 0.03	1.0 ± 0.05	11.2 ± 0.02	6.2 ± 0.26	15.6 ± 0.17	7.5 ± 0.13
10 d	0.9 ± 0.00	0.5 ± 0.04	16.7 ± 0.01	5.8 ± 0.06	16.7 ± 0.01	8.4 ± 0.11
21 d	0.9 ± 0.06	0.1 ± 0.01	16.5 ± 0.01	5.8 ± 0.18	16.8 ± 0.01	8.1 ± 0.11
101 d	0.2 ± 0.02	0.1 ± 0.02	16.4 ± 0.03	6.5 ± 0.18	16.6 ± 0.01	8.6 ± 0.86
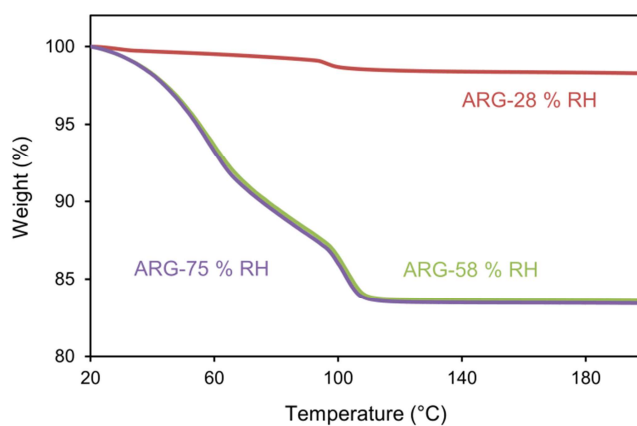
Fig. 16: TGA results of ARG after storage at 28 % RH (ARG-28 % RH), 58 % RH (ARG-58 % RH), and 75 % RH (ARG-75 % RH), respectively.
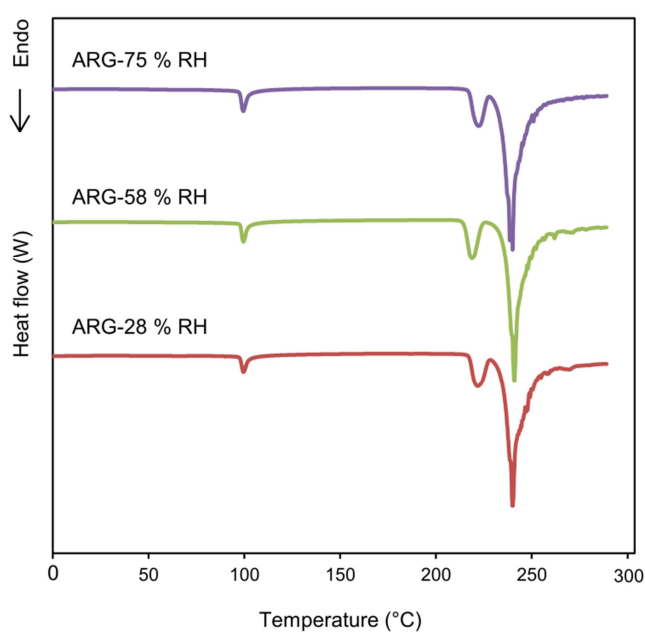
Fig. 17: cDSC thermograms of ARG after storage at 28 % (ARG-28 % RH), 58 % RH (ARG-58 % RH), and 75 % RH (ARG-75 % RH), respectively.

FTIR spectra of ARG-28 % RH differed from those of ARG-58 % RH and ARG-75 % RH (Fig. 18). On the one hand, these differences in the spectra are related to a change in the region of the guanidyl group of ARG, with a band shift at 1679 [168] and 1602 cm^{-1}, as well as an additional band at 1641 cm^{-1} [168]. On the other hand, the band at 1550 cm^{-1} of ARG-28 % RH shifted slightly to 1556 cm^{-1} in ARG-58 % RH and ARG-75 % RH and became more pronounced. This shift indicates a change in the amide II (CN stretch) vibration of ARG. Additionally, the bands at 1720 and 1259 cm^{-1}, exhibited by ARG-28 % RH, which are assigned to the free carboxylic acid group, could not be found in ARG samples stored at 58 and 75 % RH (Fig. 18) [169,170]. Taken together, the data indicate the formation of ARG dihydrate when stored at 58 and 75 % RH leading to distinct changes in the FTIR spectra in the region of the carboxylic acid and guanidyl group.
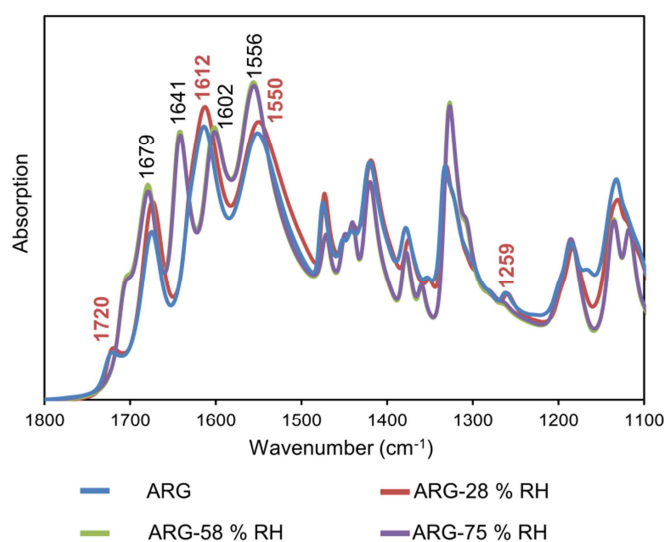

Fig. 18: FTIR spectra of unstored bulk ARG as well as of ARG after 10 d of storage at 28 % RH (ARG-28 % RH), 58 % RH (ARG-58 % RH), and 75 % RH (ARG-75 % RH), respectively.

3.2.2 Characterisation of the physical mixtures

   *3.2.2.1 Visual inspection and water content of the differently stored mixtures*

In a previous study of this thesis, a colour change of the crystalline IND-ARG tablets from white to yellow was observed upon exposure to 75 % RH over 26 d (see section 3.1.2) [171]. In the present study, a distinct change of the colour of the plain PMs was also observed, however already after 1 d of storage at 75 % RH. PM samples, which were stored at 28 % RH (PM-28 % RH) and 58 % RH (PM-58 % RH), maintained the white appearance of the fresh PM. In contrast, PMs, which were stored at 75 % RH (PM-75 % RH) turned yellow within 1 d and their colour intensified over time (Fig. 19). From a light yellow (1 d) over a bright yellow (10 d) and a light orange (21 d), the colour turned to almost dark orange/brown (101 d). In addition to the colour change, the PM-75 % RH samples initially became more and more sticky and then hardened upon storage. As it is well known that the amorphous form of IND is yellow [90,100], this colour change indicated an amorphisation of IND upon storage at 75 % RH.

| 0 d | 1 d | 10 d | 21 d | 101 d |
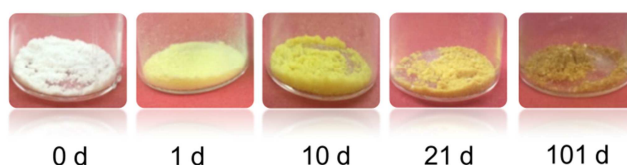
Fig. 19: Images of the PM of IND and ARG after storage at 75 % RH for 0, 1, 10, 21, and 101 d.

The results of the TGA analysis are shown in Fig. 20. ANOVA showed that the weight losses of the PMs stored at the different storage conditions were significantly different at each storage time period ($p < 0.05$). As expected, PM-28 % RH contained only a very small amount of water (Table 9). In accordance with ARG-58 % RH, PM-58 % RH contained ARG as dihydrate, shown by the strong dehydration event at about 100 °C as well as by the calculation from the weight loss during TGA. This weight loss amounted to 6.52 % (Table 9), compared to the theoretical value of 6.34 % water content in ARG dihydrate within the PM. In contrast, PM-75 % RH showed a more pronounced weight loss than PM-58 % RH and the distinct dehydration event at about 100 °C was not observed, both observations indicating that ARG was not completely present as a dihydrate. However, based on the fact that plain ARG forms a dihydrate during storage at 75 % RH (see section 3.2.1), the TGA data strongly indicates that ARG was involved in another reaction when stored together with γ-IND.
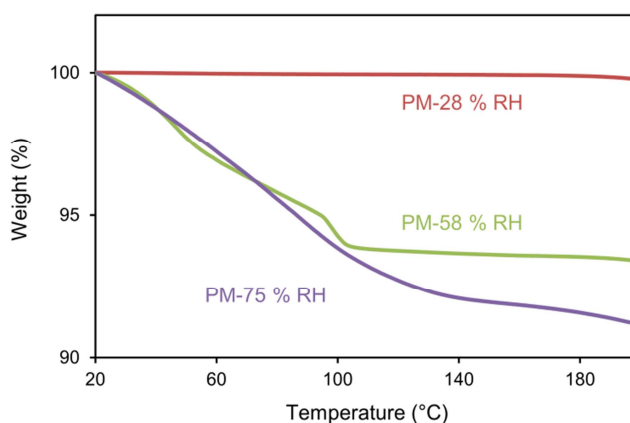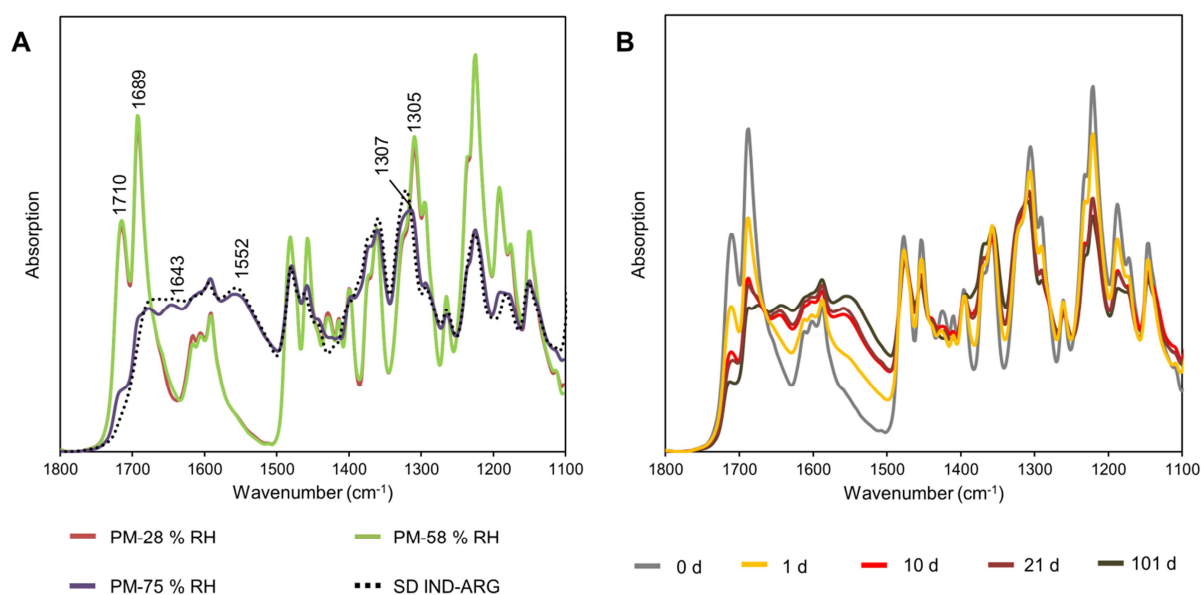

Fig. 20: TGA results of the PM of IND and ARG after storage at 28 % (PM-28 % RH), 58 % RH (PM-58 % RH), and 75 % RH (PM-75 % RH), respectively.

3.2.2.2 Solid-state properties of the differently stored mixtures

To detect a possible co-amorphisation of IND and ARG, FTIR analysis was conducted. Fig. 21A shows the FTIR spectra of the PMs after storage for 101 d at the different storage conditions. The spectra of PM-28 % RH and PM-58 % RH corresponded to that of the unstored PM, which resembles the spectrum of plain γ-IND, indicating that the FTIR spectra of the PMs were dominated by γ-IND as a result of the comparatively low absorption of ARG. In contrast, the spectrum of PM-75 % RH differed markedly from the other spectra and resembled the spectrum of the spray-dried co-amorphous reference SD CoA IND-ARG. The characteristic bands of γ-IND at 1710 and 1689 cm^{-1} could not be found in the spectrum of PM-75 % RH while the formation of a broad plateau with a shoulder at 1552 cm^{-1} was observed, indicating co-amorphous salt formation of IND and ARG, in accordance with a previous publication [56]. However, the additional small band at 1643 cm^{-1} of PM-75 % RH is not related to the co-amorphisation of IND-ARG. As a similar band at 1641 cm^{-1} was also observed in the spectrum of plain ARG-75 % RH (Fig 18), this band might also result from ARG dihydrate. In Fig. 21B the temporal progress of the co-amorphisation process upon exposure to 75 % RH is displayed. It may be noticed that the intensity of the γ-IND bands at 1710 and 1689 cm^{-1} already decreased after 1 d of storage. After 10 d of storage both bands further decreased in intensity and the shoulder at 1552 cm^{-1} started to appear indicating co-amorphous salt formation. The spectrum after 10 d of storage did not differ very much from that after 21 d, while after 101 d of storage, the characteristic γ-IND bands almost completely disappeared and the shoulder at 1552 cm^{-1} became very distinct.
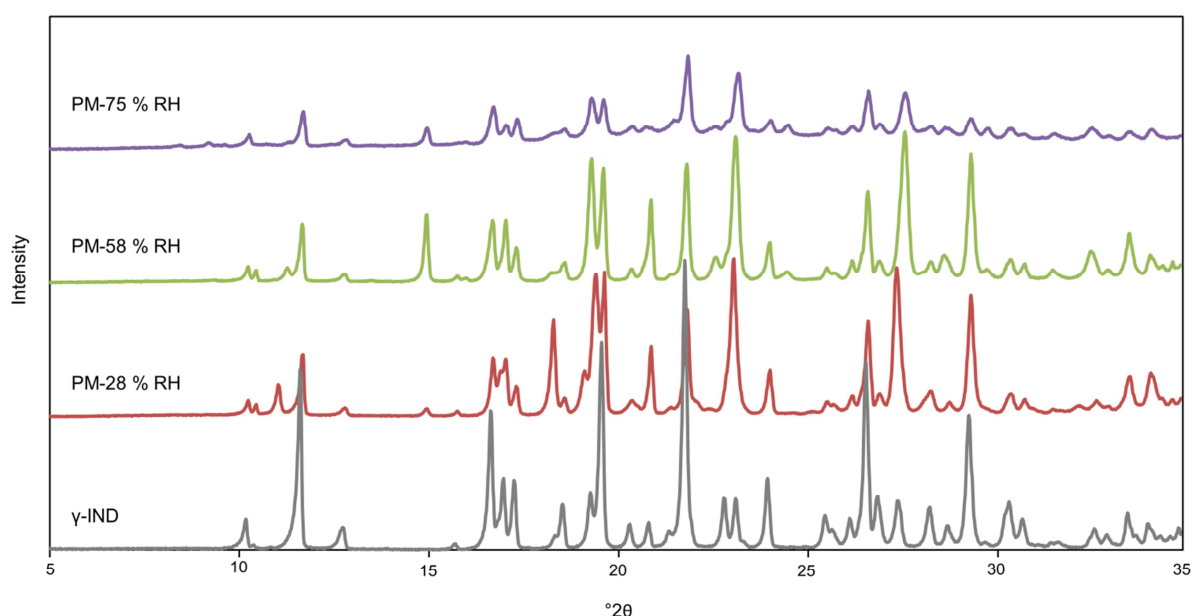
Fig. 21: (A) FTIR spectra of the PM of IND and ARG after 101 d of storage at 28 % RH (PM-28 % RH), 58 % RH (PM-58 % RH), and 75 % RH (PM-75 % RH), respectively, as well as of a co-amorphous spray-dried IND-ARG reference (SD IND-ARG). (B) FTIR spectra of the PM of IND and ARG after storage at 75 % RH for 0, 1, 10 d, 21, and 101 d.

For further characterisation of the differently stored PMs, XRPD analysis was carried out. The diffractograms of the PMs are shown in Fig. 22, together with the diffractogram of plain γ-IND as reference. It may be observed that the diffractograms of PM-28 % RH and PM-58 % RH showed partly different reflections. As the characteristic γ-IND reflections were present in both, PM-28 % RH and PM-58 % RH, differences in the diffractograms between these two storage conditions resulted from ARG, which was present as ARG anhydrate and dihydrate in PM-28 % RH and PM-58 % RH, respectively. If exposed to 28 % RH, the PMs showed the characteristic reflections of ARG anhydrate at 11.0, 18.4, 19.1, and 27.4 °2θ (Fig. 22, refer also to Fig. 15, ARG-

28 % RH). In contrast, in PM-58% RH reflections of ARG dihydrate at 11.3, 15.0, 19.4, 22.6, 24.6, 28.7, and 31.6 °2θ could be detected (Fig. 22, refer also to Fig. 15, ARG-58 % RH and ARG-75 % RH). The ARG dihydrate reflections were also observed in PM-75 % RH, but were markedly less pronounced. Additionally, the intensities of the γ-IND reflections were decreased compared to the diffractograms of the other PMs (Fig. 22). Thus, XRPD analysis confirmed the FTIR results, suggesting amorphisation of ARG and IND in the PMs upon exposure to 75 % RH.

Fig. 22: XRPD diffractograms of the PM of IND and ARG after 10 d of storage at 28 % RH (PM-75 % RH), 58 % RH (PM-58 % RH), and 75 % RH (PM-75 % RH), respectively, as well as of the γ-IND reference.

In Fig. 23 the diffractograms of PM-75 % RH after the selected days of storage are compared to a diffractogram of PM stored at 58 % RH for 10 d. Overall, it may be noticed that the peak intensities decreased over time, while the baseline slightly shifted upwards, indicating the formation of a so-called amorphous "halo" [17]. As the peak height of the reflections as well as the area under the baseline provide information on the amorphous content of a sample [112], the XRPD data suggested that the amorphous content in PM-75 % RH increased with storage time, which is in accordance with the FTIR data. Nevertheless, even after 101 d of storage still reflections of γ-IND and ARG were detectable. Thus, the XRPD data indicated that even though the amorphisation started rapidly upon exposure to 75 % RH, it was not completed within the 101 d of storage.
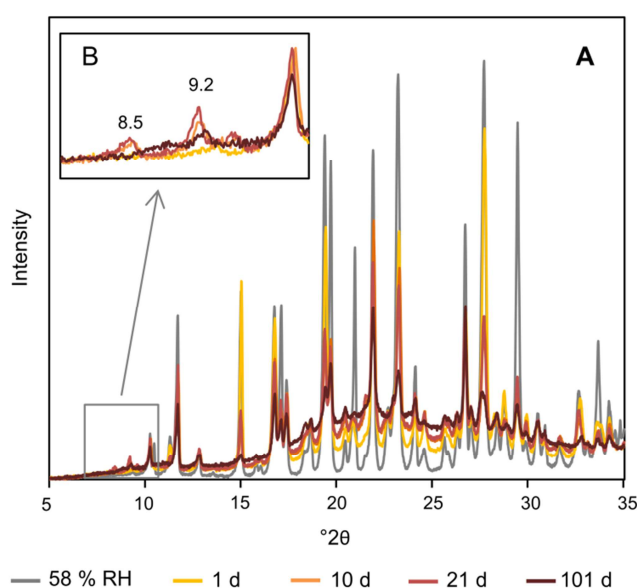
Fig. 23: Comparison of XRPD diffractograms of the crystalline PM of IND and ARG after storage at 75 % RH for 1, 10, 21, and 101 d as well as after storage at 58 % RH for 10 d (58 % RH) between (A) 5 and 35 °2θ and between (B) 7 and 11 °2θ.

Additionally, it was found that the diffractograms of PM-75 % RH after 10 and 21 d of storage revealed additional reflections at 8.5 and 9.2 °2θ (Fig. 23B), which were neither related to a hydrate of ARG nor to any known polymorph of IND [144]. Hence, DSC studies were carried out to further evaluate these PMs.

Exemplary thermograms of the cDSC measurements on PMs after storage at the different storage conditions are depicted in Fig. 24.
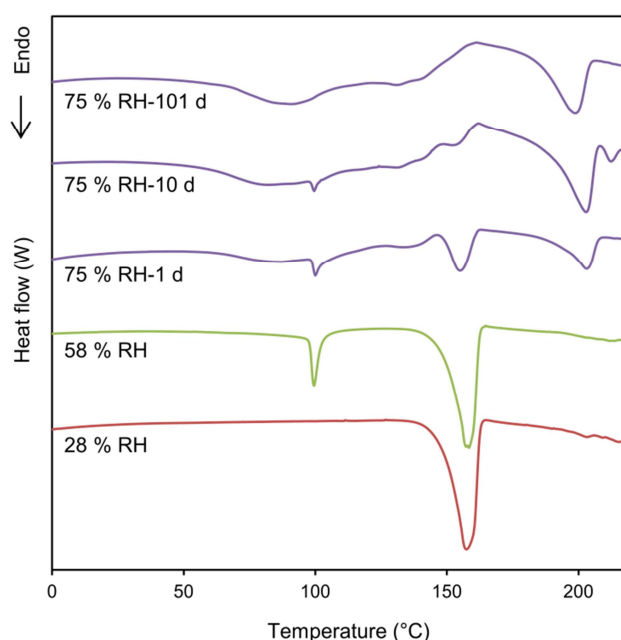
Fig. 24: cDSC thermograms of the PM after storage at 28 % RH, 58 % RH, and 75 % RH for 1, 10, and 101 d, respectively.

Regardless of the storage time, the thermograms of PM-28 % RH and PM-58 % RH, respectively, were superimposed and all showed an endothermic melting event for γ-IND at 158 ± 0.4 °C with a ΔH_m of 56.8 ± 2.7 J/g (Fig. 24), but no glass transition in the mDSC thermograms (data not shown). The only difference between these two storage

conditions was an endothermic event at about 100 °C with PM-58 % RH, which was related to dehydration of ARG dihydrate.

The results of the DSC analysis for the PM-75 % RH are summarised in Table 10. After 1 d of storage at 75 % RH, PMs also revealed dehydration of ARG dihydrate at 100 °C and the endothermic melting of γ-IND at 155.1 ± 0.2 °C. However, with a ΔH_m of 14.7 ± 1.5 J/g, the enthalpy of fusion of this melting event was significantly ($p < 0.05$) lower compared to PM-28 % RH and PM-58 % RH and a second broad endothermic event was detected at 203.9 ± 0.6 °C with ΔH of 21.2 ± 1.6 J/g (Fig. 24, Table 10). Additionally, in the mDSC thermograms a single high temperature T_g was found at 119.2 ± 1.9 °C (Table 10), confirming the co-amorphisation of IND and ARG as an amorphous salt. This T_g was slightly higher than the T_g of the SD CoA IND-ARG reference (113.8 ± 0.2 °C) as well as the literature values for co-amorphous IND-ARG, which have been reported to be located between 111.7 °C and 117.5 °C [32,32,67,83,85,99].

Table 10: Results of the DSC analysis for PMs stored at 75 % RH after different storage time periods (means ± SD, n = 3).

storage time	Glass transition (mDSC)	IND melting event (cDSC)		Additional endothermic event (cDSC)	
	T_g (°C)	T_m (°C)	ΔH_m (J/ g)	T_m (°C)	ΔH_m (J/g)
1 d	119.2 ± 1.9	155.1 ± 0.2	14.7 ± 1.5	203.9 ± 0.6	21.2 ± 1.6
10 d	120.5 ± 0.1	153.5 ± 0.1	6.8 ± 0.7	202.4 ± 1.0	44.0 ± 2.3
21 d	120.2 ± 0.5	-	-	203.2 ± 0.7	52.2 ± 4.2
101 d	116.9 ± 0.6	-	-	198.5 ± 0.3	41.5 ± 4.4

After 10 d of exposure to 75 % RH, this T_g was still observed at 120.5 ± 0.1 °C (Table 10). The endothermic melting of γ-IND was almost undetectable in these samples, while the enthalpy of the additional endothermic event (endotherm 1) at 202.4 ± 1.0 °C increased significantly ($p < 0.05$) to 44.0 ± 2.3 J/g, compared to the PM after 1 d of storage at 75 % RH. Moreover, these thermograms revealed another small endothermic event (endotherm 2) at about 212 °C (Fig. 24).

The thermograms of the samples stored for 21 d were essentially similar to those after 10 d (no significant difference, $p < 0.05$). The T_g was detected at 120.2 ± 0.5 °C, endotherm 1 at 203.2 ± 0.7 °C with a ΔH of 52.2 ± 4.2 J/g, and endotherm 2 at about 212 °C (Table 2).

At 101 d of storage at 75 % RH however, the endotherm 2 was not observed any longer. Moreover, dehydration of ARG and melting of γ-IND were not detected either (Fig. 24). Endotherm 1 shifted to 198.5 ± 0.3 °C during this time period, while the T_g of co-amorphous IND-ARG was still present in the mDSC thermograms, but slightly shifted to 116.9 ± 0.6 °C (Table 10). Thus, DSC analysis confirmed the results of the FTIR and XRPD analyses, indicating that co-amorphisation of IND and ARG already started after one day of storage at 75 % RH. Moreover, cDSC indicated the formation of a new solid form, which showed a melting event at about 203 °C. As this additional endothermic event could not be related to a polymorph or pseudopolymorph of IND or ARG or a basic hydrolysis product of IND, it was hypothesised that this event might be attributed to the melting of a crystalline salt of IND and ARG. As this endothermic event occurred in a high temperature range, it is obvious that it represented the melting of a salt, comparable to the high melting point of sodium-IND at 247 °C [172]. Surprisingly, despite the formation of this salt, the peak positions in the diffractograms of the PMs

(Fig. 22) did hardly change during storage at 75 % RH, while the peak intensities changed considerably. This surprising finding requires further investigation, especially on the crystallographic structure of this salt. However, because of the fact that FTIR data revealed salt formation of IND and ARG and due to the high temperature of the melting event detected in the cDSC thermograms, it seems obvious that a crystalline salt has formed during storage at 75 % RH.

In summary, solid-state analysis indicated the simultaneous formation of the co-amorphous as well as a crystalline IND-ARG salt during storage at 75 % RH, which began immediately after exposure to this RH and continued for the whole 101 d of storage. This change of the solid-state appeared to be linked to the presence of ARG, as solid-state analysis of plain γ-IND showed no alteration of the solid-state upon storage at all investigated conditions. The formation of ARG dihydrate probably played an important role in the initiation of the interaction between IND and ARG, as FTIR data revealed that incorporation of two water molecules into ARG led to a change in the spatial arrangement of the guanidyl and carboxylic group of ARG, which may have initiated the salt formation. Nevertheless, dihydrate formation alone was not sufficient to induce this change, as PMs stored at 58 % RH were stable, although ARG dihydrate formation was also observed upon exposure to 58 % RH. Hence, the high RH of 75 % RH seemed to be crucial for enabling these physical changes. It is assumed that next to the incorporation of water molecules into the crystal lattice of ARG, the additional water, which is adsorbed to the solid surface – especially at the points of physical contact between IND and ARG – also played an important role for facilitating the observed instability [73].

3.2.3 Chemical stability of IND and its physical mixtures

In previous studies the basic hydrolysis of IND, which is known to lead to the degradation products CBA and MMIA was investigated [146,173]. As ARG is a strong base (pK_{a1}: 12.5, pK_{a2}: 9.1, see Table 3), it was hypothesised that it may induce basic hydrolysis of IND in the presence of water vapour. Additionally, the observed colour darkening of the PMs upon storage at 75 % RH (see section 3.2.2.1) may potentially result from chemical changes in these samples. To clarify this assumption, HPLC analysis was carried out. Chromatograms of unstored PMs as well as of PMs after storage at 28 and 58 % RH for 101 d showed only one peak for IND and no additional peaks from any of its degradation products (exemplary data shown for 58 % RH in Fig. 25). In contrast, degradation was observed, if PMs were stored at 75 % RH (Fig. 25). In Table 11 the contents of IND and the degradation product CBA, both quantified by HPLC and displayed as molar percentages, in the PMs after the selected days of storage at 75 % RH are shown. It was observed that the degradation process started immediately after exposure to 75 % RH and continued for the whole 101 d of storage. However, if plain IND was stored at 75 % RH, no degradation was observed, as no peak of any hydrolysis product could be observed in the diffractograms (data not shown).
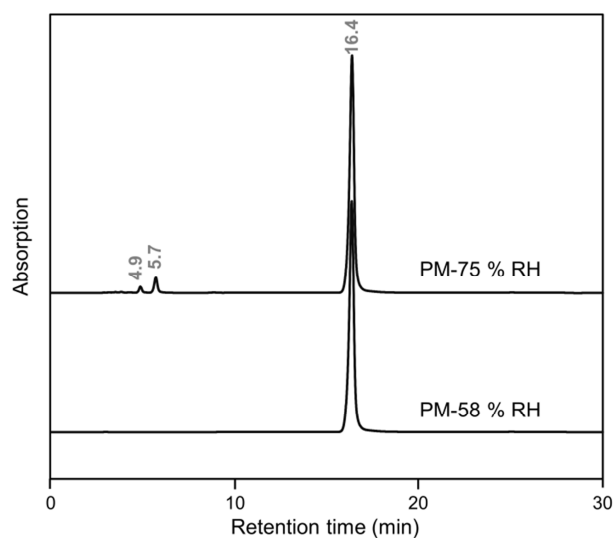
Fig. 25: Chromatograms of the crystalline PM after storage for 101 d at 75 % RH (PM-75 % RH) and 58 % RH (PM-58 % RH, respectively. Elution peaks are superscripted with the respective elution times.

Table 11: Content of IND and CBA in the PMs after the selected days of storage at 75 % RH, referring to the theoretically present amount of IND (means in molar % ± SD, n = 3).

storage time	IND (%)	CBA (%)
0 d	98.54 ± 1.96	-
1 d	95.08 ± 2.39	0.14 ± 0.02
10 d	94.21 ± 0.98	1.11 ± 0.03
21 d	94.56 ± 2.13	2.59 ± 0.03
101 d	81.93 ± 1.37	12.24 ± 0.48

Thus, it may be concluded that the physical and chemical changes of the PMs occurred nearly simultaneously and the RH of 75 % as well as the presence of ARG were crucial factors for both instabilities. It appears plausible that these two processes are accompanied by each other, as amorphous phases generally show a higher molecular mobility and water absorption compared to crystalline systems, both physicochemical properties enabling hydrolysis and other instabilities [73]. Thus, degradation of IND may not only have increased because of the longer storage period, but also because of the increasing amorphous fraction in PM-75 % RH, which facilitated a more pronounced hydrolysis of IND. Thus, after 101 d of storage, only 81.9 % of the theoretical amount of IND was still present in the respective samples.

3.2.4 Conclusion

The aim of the present study was to identify the conditions required to induce *in situ* co-amorphisation of IND and ARG as well as to investigate the chemical stability of IND during combined storage with ARG. Relatively humid storage conditions (75 % RH) were successfully identified as a requirement for the interaction between IND and ARG, because less humid storage conditions of 28 % and 58 % RH neither induced solid-state nor chemical changes of γ-IND. As it was revealed that the solid-state transformation of γ-IND was accompanied by basic hydrolysis of IND, it may be stated that the combined storage with ARG at 75 % RH negatively affects the chemical stability of IND. The present study demonstrated that these instabilities appeared to be linked to the dihydrate formation ability and water binding capacity of ARG, if stored at 75 % RH. Furthermore, it was shown that both, solid-state changes, as well as basic hydrolysis, started immediately after exposure to 75 % RH and continued for at least 101 d of storage. Therefore, the effect of ARG on the solid-state and chemical stability of IND must be considered. This holds especially true for manufacturing processes, which involve the use of water or water vapour.

Previously, the concept of intended *in situ* amorphisation was introduced by Priemel et al. [87,90,91]. This means that a formulation is amorphised directly prior to administration, thereby circumventing physical stability problems of the amorphous form during processing and storage. In this respect, the *in situ* co-amorphisation observed in the present study might be utilised for a controlled *in situ* co-amorphisation of IND and ARG in the final dosage form, the process being induced by ARG and water. To implement this concept, the process of co-amorphisation has to be performed in a

controlled way, without inducing chemical degradation of the drug. As in the present study after 10 d of storage at 75 % RH already a high fraction of IND and ARG was co-amorphous, even though the IND content was still 94.21 %, it might be possible to achieve co-amorphisation with little or no degradation. Hence, the third study of this thesis will deal with the development of a final dosage form, which may allow a controlled *in situ* co-amorphisation of IND and ARG.

3.3 Development of a film coated tablet formulation to allow a controlled *in situ* co-amorphisation of arginine and indomethacin or furosemide during immersion in an aqueous medium

3.3.1 Tablet formulation development and tablet characterisation

In previous studies of this thesis, co-amorphisation of crystalline IND and ARG was observed within tablets or physical mixtures during storage at high humidity (75 % RH) and during drug dissolution (see sections 3.1 and 3.2) [171]. Therefore, the present study intended to use this previously observed co-amorphisation of IND and ARG by contact with water for a controlled *in situ* amorphisation of IND. In addition, the possible transfer of the co-amorphisation concept to another acidic API (FUR) was investigated. The acidic API FUR was chosen, as it has been previously shown to form a co-amorphous salt with ARG, similar to IND (see section 1.5).

The commonly applied single doses of the APIs FUR and IND are 40 and 50 mg, respectively [174,175]. However, for comparative purposes, an API content of 50 mg was chosen for all investigated tablet formulations. In addition to the two tablet formulations containing FUR (FA-T) or γ-IND (IA-T), a third tablet formulation was prepared, which contained γ-IND with citric acid (IAC-T) as additive (molar ratio of 1:0.3). This formulation was prepared, as the previous study (see section 3.2.3) showed that ARG (pK_{a1}: 9.1; pK_{a2}: 12.5) and water (moisture) may induce base-catalysed hydrolysis of γ-IND. It was assumed that the additive CA (pK_{a1}: 3.1; pK_{a2}: 4.8; pK_{a3}: 6.4) might be able to prevent this hydrolysis by the formation of a controlled micro-pH environment.

The results of the characterisation of the prepared tablet formulations are shown in Table 12. The compaction pressures were selected such that tablets suitable for drum coating were obtained. According to Table 12, all three uncoated tablet formulations

showed sufficiently high tensile strengths, very low friabilities, and disintegrated quickly in 0.1 M HCl.

Table 12: Characterisation of the uncoated tablet formulations. Means ± SD, n = 3 (disintegration time), n = 10 (weight, tensile strength), n = 45 (compaction pressure).

	Compaction pressure (MPa)	Tablet weight (mg)	Tensile strength (MPa)	Friability (%)	Disintegration time (min)
FA-T	137 ± 21	206.5 ± 5.5	2.0 ± 0.4	0.04	2.7 ± 0.8
IA-T	163 ± 13	203.5 ± 2.2	1.4 ± 0.2	0.00	2.9 ± 0.3
IAC-T	166 ± 15	201.9 ± 4.0	1.9 ± 0.2	0.00	6.0 ± 0.6

It was assumed that a controlled *in situ* co-amorphisation might be achieved by the preparation of a conventional tablet formulation, containing API and coformer in crystalline form, which is surrounded by a gastro-resistant, but water-permeable coating. Thus, during immersion in an acidic medium, the medium may permeate through the coating and enable a co-amorphisation of the API with ARG within the tablet.

For this purpose, a special coating formulation was developed. For gastro-resistant coatings complete impermeability in the stomach is usually desired to avoid swelling and therefore disintegration of the tablet. Thus, the addition of plasticizers, which barely increase the permeability of a film coating, is recommended, e.g. triethyl citrate, which is often used together with Eudragit® L 30D-55 [139]. However, as the present study intended to obtain a permeable coating, PEG 6000 was chosen as plasticizer, as it is very hydrophilic and dissolves rapidly in water, thus leading to an enhanced permeability of the coating (see section 1.4.3) [176]. Typically used amounts of plasticizers are 10-

20 % w/w (referring to the dry polymer mass) [177]. In the present study, an addition of 20 % w/w of PEG 6000 was chosen, as preliminary studies showed that an amount of 10 % resulted in poorly flexible films, which ruptured during immersion in 0.1 M HCl. Another aspect of the coating, which determines its permeability, is the coating thickness (see section 1.4.3). Commonly applied amounts of polymers for enteric coatings of spherical tablets are 4-6 mg/cm^2 [139]. For an impermeable coating, a minimum coating thickness of 40-50 µm is usually required [139]. To maintain the permeability of the enteric coating employed in the present study, polymer amounts of about 2-3 mg/cm^2 (coating thicknesses of about 20-30 µm) were applied. In Table 13 characteristics of the prepared coatings are presented and SEM images are displayed in Fig. 26. It can be observed that all three formulations were coated by a thin and uniform coating with a mean coating thickness of about 25 µm.

Table 13: Characterisation of the prepared coatings.

	FA-CT	IA-CT	IAC-CT
Total weight gain (%)	4.0	2.7	3.2
Polymer weight gain (%) without excipients	2.4	1.6	1.9
Polymer per surface (mg cm^{-1})	3.2	2.1	2.5
Mean coating thickness (µm)	27.2	24.9	25.4
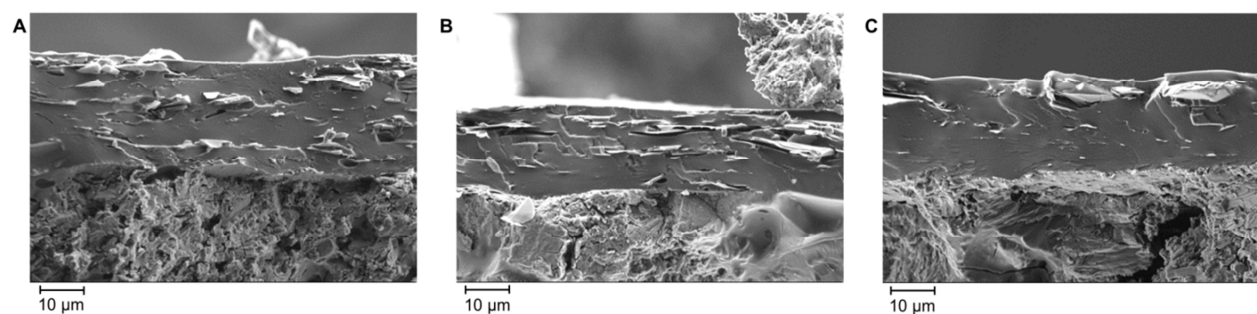
Fig. 26: SEM images of the cross sections of the prepared tablet coatings. (A) FA-CT (B) IA-CT (C) IAC-CT**.**

3.3.2 Immersion of the coated tablets in an acidic medium

None of the three coated tablet formulations disintegrated during immersion in 0.1 M HCl for up to 120 min. It was observed that all tablets were slightly deformed and increased in size, indicating the penetration of water into the tablets. Additionally, IA-CT turned yellow during the first 10-30 min of immersion. After 60 and 120 min of immersion, the intensity of this colour decreased. As it is known that the amorphous form of IND is yellow [100], this change in colour indicated an amorphisation of IND within the tablets.

3.3.3 Characterisation of the immersed coated tablets

   3.3.3.1 XRPD and HPLC analysis

To detect a possible amorphisation of the APIs within the tablets during immersion in 0.1 M HCl, tablet samples were analysed by XRPD (Fig. 27). In the diffractograms of the co-amorphous formulations, only the reflections of Pearlitol®, the diffractogram of which corresponded to that of α-mannitol [158], were observed. In contrast, the crystalline formulations also showed reflections of the APIs and ARG. Characteristic reflections of crystalline FUR in FA-T and FA-CT were determined at 6.1, 12.1, 14.2, 18.1, 24.8, and 27.6 °2θ, and a reflection of crystalline ARG was observed at 15.0 °2θ (Fig. 27A). For IA-T and IA-CT, characteristic reflections of γ-IND and crystalline ARG were determined at 10.2, 11.6, 12.7, 24.0, 26.7 and 15.0 and 18.4 °2θ, respectively (Fig. 27B). The only difference between the diffractograms of the uncoated and coated tablets were two additional reflections of talc at 9.5 and 28.6 °2θ. Due to the low concentration of CA, the diffractogram of IAC-CT corresponded to that of IA-CT.
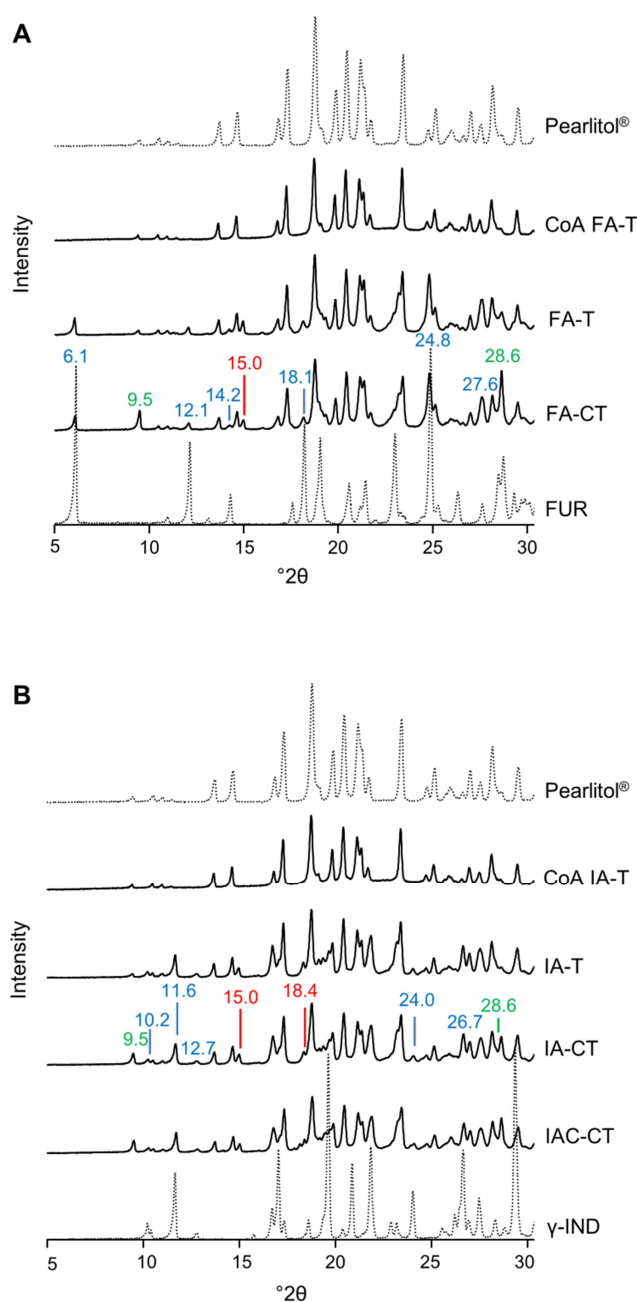
Fig. 27: XRPD diffractograms of the prepared FUR (A) and IND (B) tablet formulations. The diffractograms of the co-amorphous tablets (CoA FA-T, CoA IA-T), the crystalline tablets (FA-T, IA-T), and the coated crystalline tablets (FA-CT, IA-CT, IAC-CT) are displayed together with the diffractograms of Pearlitol®, FUR, and γ-IND. Characteristic reflections of the APIs, ARG, and talc in the diffractograms of the respective coated formulations are superscribed in blue, red and green, respectively.

In Fig. 28A the diffractograms of FA-CT samples after different time periods of immersion in 0.1 M HCl are shown as well as of untreated FA-CT (0 min) for comparison. To better display the time-dependent change of the characteristic FUR and ARG reflections, the diffractogram region between 18.6 and 23.7 °2θ was disregarded, as it only contained unspecific reflections of mannitol. It was observed, that already after 10 min of immersion the characteristic reflections of FUR became less intense and the characteristic reflection of ARG at 15 °2θ vanished. For better visualisation, Fig. 28B shows the diffractograms of FA-CT after immersion for 20 min and of FA-CT (0 min) as comparison. In addition to the decreased reflection intensities also a slight vertical shift of the baseline was observed, both indicating amorphisation of FUR and ARG within the tablets. Other reflections not belonging to FUR and ARG became less (13.7, 17.3, 19.9, 25.2, 27.0 °2θ) or more (10.5, 11.5, 14.7, 18.8, 23.5, 25.9, 26.6, 29.6 °2θ) intense in the diffractograms of FA-CT after 20 min of immersion, which was related to a transformation of Pearlitol® from α- to β-mannitol [158,178]. In the diffractograms of the samples immersed for 30 min, the intensity of the FUR and ARG reflections as well as the baseline shift were unchanged compared to the 10 and 20 min samples, while the transformation of mannitol continued. Thus, after 30 min, reflections of α-mannitol were no longer detectable in the diffractograms of these samples. After longer immersion time periods (60 and 120 min), the reflection of ARG still remained undetectable. In contrast, it was observed that the characteristic reflections of FUR became more pronounced again (Fig. 28B), indicating a recrystallisation of FUR.
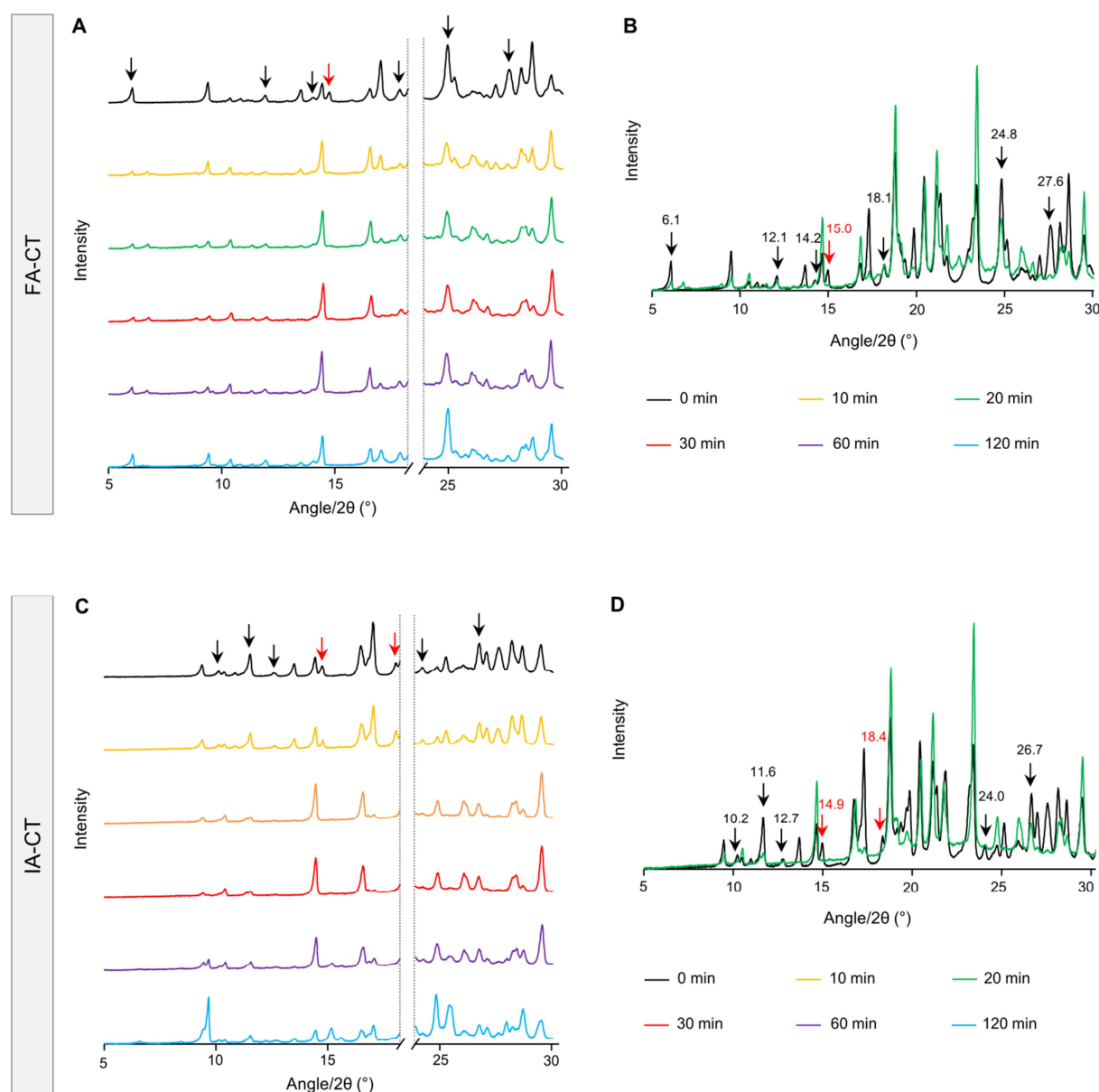
Fig. 28: Diffractograms of the coated tablets after different time periods of immersion in 0.1 M HCl. (A) All XRPD diffractograms of FA-CT from 5-18.5 and 23.8-30 °2θ. (B) XRPD diffractograms (5-30 °2θ) of FA-CT after immersion for 0 and 20 min, respectively. Characteristic reflections of FUR and ARG in the diffractogram of FA-CT (0 min) are indicated by black and red arrows, respectively. (C) All XRPD diffractograms of IA-CT from 5-18.5 and 23.8-30 °2θ. (D) XRPD diffractograms (5-30 °2θ) of IA-CT after immersion for 0 and 20 min, respectively. Characteristic reflections of γ-IND and ARG in the diffractogram of IA-CT (0 min) are indicated by black and red arrows, respectively.

To confirm that these reflections indeed resulted from FUR and not from any degradation product of FUR, HPLC was carried out with the FA-CT samples immersed for 120 min. As expected, the chromatograms only revealed one peak at the expected elution time of FUR (data not shown).

A similar behaviour during immersion in 0.1 M HCl was observed with IA-CT (Fig. 28C). A vertical baseline shift and a decrease of the intensities of the characteristic γ-IND and ARG reflections were already observed after 10 min of immersion. In contrast to the FA-CT formulations, these changes were more pronounced after 20 min of immersion, and the ARG reflections vanished. Again, for better detection of these transformations, the diffractograms of IA-CT after immersion for 20 min are depicted in Fig. 28D together with a diffractogram of untreated IA-CT (0 min). As for the FA-CT formulations, other changes in the diffractograms of the immersed IA-CT samples for up to 30 min were related to a transformation of mannitol from the α- to the β-modification. In addition, the diffractograms of IA-CT after 60 min and 120 min of immersion showed decreased mannitol reflections (α- and β-mannitol), as mannitol probably permeated through the coating during immersion. The diffractograms after 60 and 120 min of immersion revealed additional reflections, which were in part attributed to reflections of the degradation products CBA and MMIA of IND. Such a chemical degradation of IND appears to be obvious, as it is known that IND undergoes base catalysed hydrolysis in alkaline media and the tablets contained the basic component ARG (pK_{a1} = 12.5, pK_{a2} = 9.1) [146]. HPLC analysis was performed to confirm this hypothesis. As the chromatograms revealed peaks at the respective elution times of CBA and MMIA, HPLC analysis confirmed their presence in the IA-CT (120 min) samples. Apparently, the basic

amino acid ARG induced basic hydrolysis of IND inside the coated tablets during immersion in 0.1 M HCl. Interestingly, the acidic immersion medium (pH 1.2) was not able to prevent this chemical degradation.

As mentioned in section 3.3.1, it was assumed that the generation of a micro-pH environment might be able to prevent such a base catalysed hydrolysis of IND. To investigate this assumption, the IAC-CT formulation was prepared and immersed in 0.1 M HCl. The respective diffractograms are displayed in Fig. 29. The reflections of γ-IND did not decrease after immersion in 0.1 M HCl. The reflections of γ-IND were even increased after 120 min of immersion, while the reflection intensities of mannitol (α- and β-mannitol) were significantly reduced. Additionally, reflections of ARG were undetectable after 10 min. Therefore, it appears that ARG as well as portions of mannitol permeated through the coating during longer immersion time periods than 30 min, because both substances are soluble in 0.1 M HCl. As this observation led to a comparably higher concentration of γ-IND in the immersed as well as dried samples, the characteristic reflections of γ-IND became more pronounced. The addition of CA prevented the chemical degradation of IND as no reflections of the IND degradation products were detected in the diffractograms of the IAC-CT samples. Furthermore, HPLC chromatograms of these samples showed neither bands for CBA nor for MMIA. However, the prevention of the chemical degradation by CA also led to an inhibition of the amorphisation of IND within the tablet, which may be explained by an interaction of ARG with CA. Thereby, no ARG or only a reduced amount of it was available for the co-amorphisation with IND.
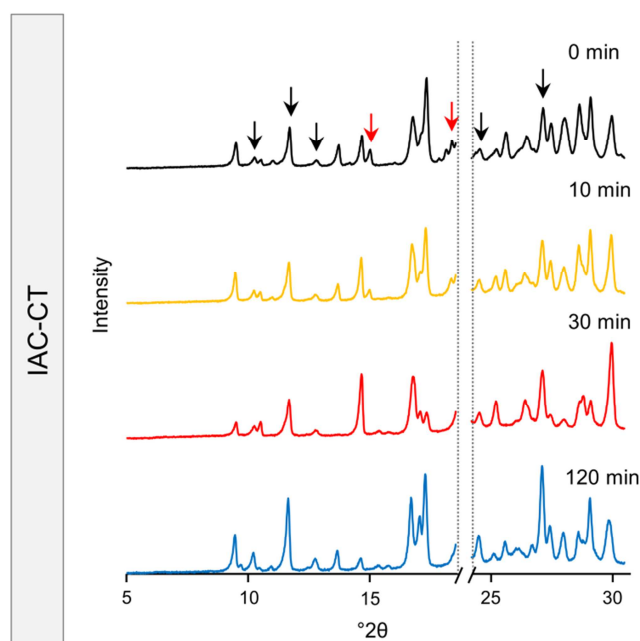
Fig. 29: XRPD diffractograms of IAC-CT after different time periods of immersion in 0.1 M HCl. Characteristic reflections of IND and ARG in the diffractogram of untreated IAC-CT are indicated by black and red arrows, respectively.

3.3.3.2 Detection of co-amorphisation by mDSC

The results of the XRPD study showed a simultaneous amorphisation of the APIs and ARG within the coated FA-CT and IA-CT tablets during immersion for up to 30 min. However, XRPD data is unable to detect whether the API and ARG exist as a co-amorphous system or rather as a physical mixture of amorphous drug and amorphous amino acid. Therefore, samples were thermally characterised using mDSC.

For mDSC analysis the samples with the highest amorphous content were chosen, which were the 20 min immersed samples of FA-CT and IA-CT, respectively. For comparison, with IAC-CT, the 20 min immersed samples were chosen.

Unfortunately, it was impossible to detect the T_g of CoA FUR-ARG in the prepared FUR formulations, not even in the CoA FA-T reference tablets. This observation may be explained by the low concentration of FUR and ARG in the tableting mixtures, as FUR and ARG together accounted for only 38.2 % of the tablet mass (see Table 5). In addition, the detection of the T_g may be difficult, because of the close appearance of two thermal events in the respective thermograms. The T_g of CoA FUR-ARG was reported to appear at 127.0 ± 0.5 °C [58]. In the present study, melting of mannitol led to an endothermic event in the reversing heat flow signal with a peak at 159.6 ± 0.1 °C and an onset temperature of 146.7 ± 1.3 °C. As glass transitions tend to spread over a temperature range of 10-30 °C, it was impossible to separate these two thermal events.

The reversing heat flow signals of the IA-CT and IAC-CT formulations as well as of the CoA IA-T reference are depicted in Fig. 30. While there was no T_g detectable in the thermogram of untreated IA-CT, the CoA reference tablet revealed one single T_g at 117.9 ± 4 °C. This high T_g was in accordance with the literature values for co-amorphous IND-ARG [32,85,99], and can be explained by strong ionic interactions between IND and ARG. Overall, this T_g was not very pronounced, which may again be related to the low concentrations of API and ARG in the tableting mixtures, and thus, low levels of possible co-amorphous content. A similar T_g was also detected in the reversing heat flow signal of the thermograms of the 20 min immersed IA-CT formulation (T_g: 104.4 ± 2.1 °C, Fig. 30). It has previously been shown that an alteration in the molar ratio of IND and ARG leads to decreased T_g values of CoA IND-ARG compared to those of the equimolar ratio [67]. Therefore, the slight decrease of the T_g compared to CoA IA-T might be explained by a non-equimolar interaction between IND and ARG during immersion in 0.1 M HCl, which may be caused by the spatial separation of IND and ARG or because

of a slight permeation of ARG through the coating. However, with 104.4 °C, the T_g of the immersed samples was still distinctly higher than the theoretical values of different IND-ARG mixtures calculated from the Gordon-Taylor equation [67], indicating strong molecular interactions. Thus, mDSC indicated that amorphous IND and ARG formed a co-amorphous salt during immersion in 0.1 M HCl. In contrast, the observed T_g was not detected in the reversing heat flow signal of IAC-CT (Fig. 30), which was in accordance with the XRPD data, confirming that the presence of CA inhibited co-amorphisation between IND and ARG.
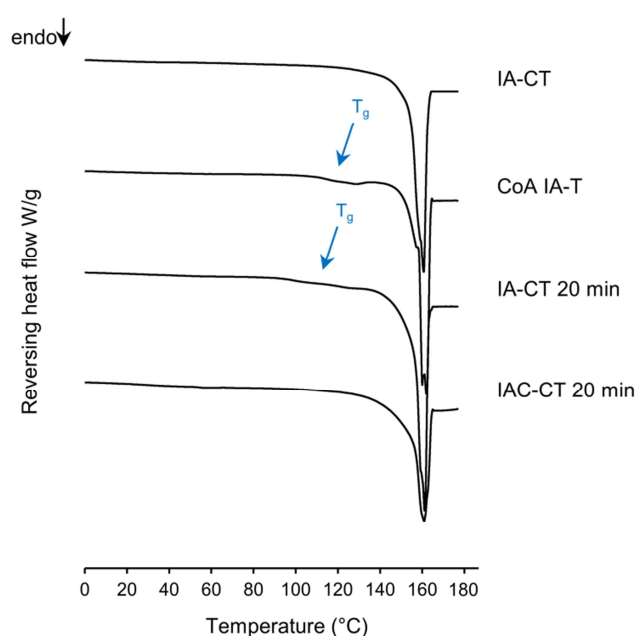
Fig. 30: Reversing heat flow signals of mDSC of IA-CT, the co-amorphous IND-ARG tablet (CoA IA-T), as well as of IA-CT and IAC-CT after 20 min of immersion in 0.1 M HCl, respectively. The glass transition (T_g) of co-amorphous IND-ARG is indicated by blue arrows.

3.3.3.3 FTIR spectroscopy

3.3.3.3.1 Investigation of the progress of co-amorphisation over time

As already stated, the interpretation of the XRPD data was rather complex because of the transformation of the excipient mannitol, which possessed distinct reflections in the diffractograms of the samples. Therefore, FTIR together with PCA was carried out to further analyse the time-dependent change of the samples during immersion in 0.1 M HCl. In the analysed wavenumber region of 1800-1500 cm^{-1} mannitol shows almost no absorption [178] and will thus not interfere with the interpretation of the changes in the API spectra. Additionally, this region is characteristic for both, CoA FUR-ARG and CoA IND-ARG, as the molecular interactions between API and ARG are observed in this region [56,58,67].

In Fig. 31A the spectra of the FA-CT formulations after different time periods of immersion are displayed and compared with the spectra of the untreated FA-CT (0 min) and a CoA FA-T reference tablet. The untreated FA-CT showed the characteristic bands of crystalline FUR: one band at 1672 cm^{-1}, which results from the free carboxylic acid group, a small band at 1591 cm^{-1}, and a band at 1562 cm^{-1}. In contrast, in the spectrum of CoA FA-T, the two bands at 1672 and 1562 cm^{-1} were transformed into shoulders, and the band at 1591 cm^{-1} was shifted to 1602 cm^{-1} and became more pronounced. These changes in the spectra were related to a salt formation between FUR and ARG upon co-amorphisation, as previously reported [58,67]. In Fig. 31A it may also be observed that during the first 30 min of immersion in 0.1 M HCl the characteristic bands of crystalline FUR decreased significantly and the band at 1591 cm^{-1} shifted slightly.
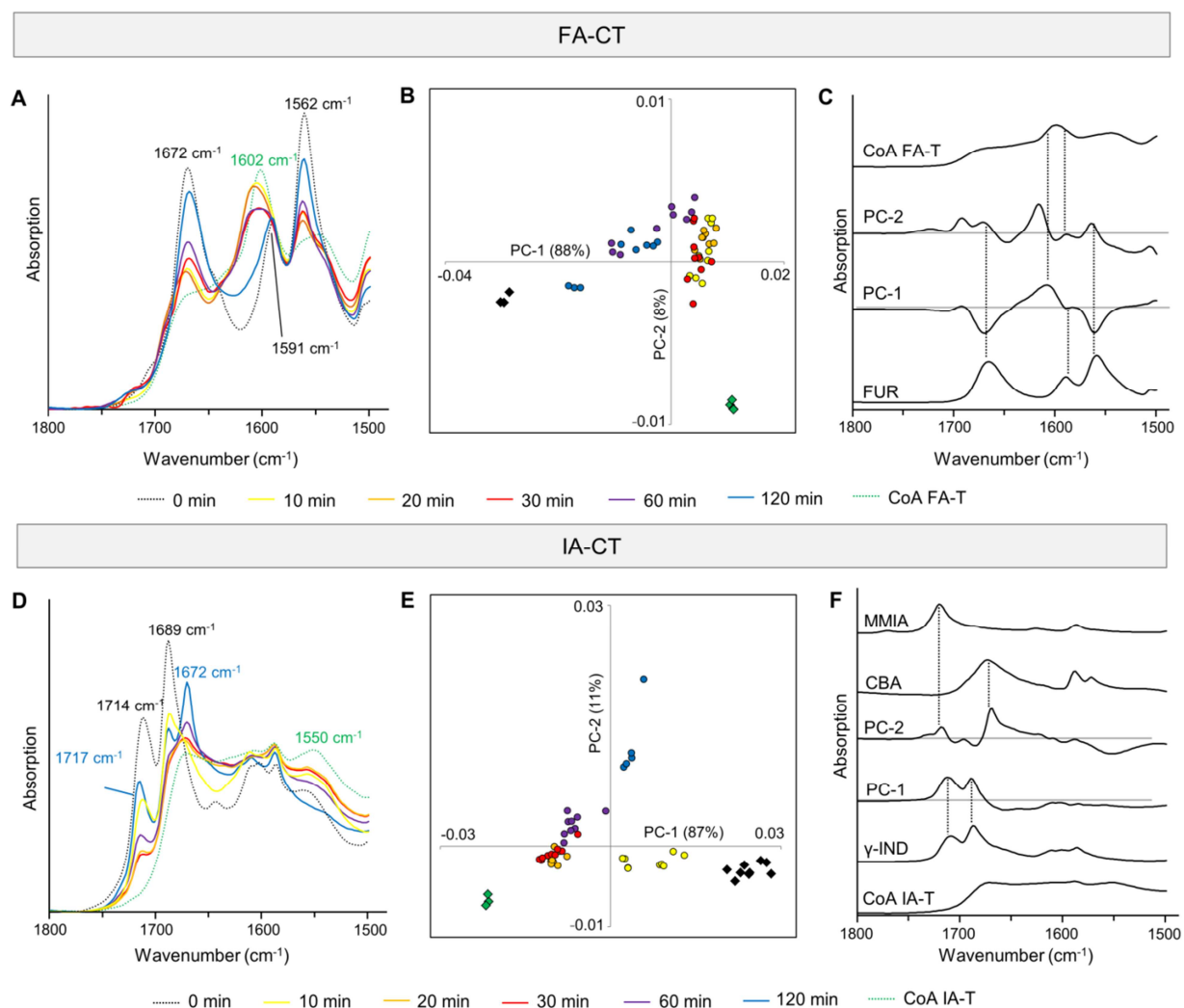
Fig. 31: FTIR spectra and the PCA thereof. (A) FTIR spectra and (B) Scores plot of the FA-CT formulation after different times of immersion in 0.1 M HCl. (C) Loadings plots of PC-1 and PC-2 as well as reference spectra of CoA FA-T and plain FUR. (D) FTIR spectra and (E) Scores plot of the IA-CT formulation after different times of immersion in 0.1 M HCl. (F) Loadings plots of PC-1 and PC-2 as well as reference spectra of the two degradation products MMIA, CBA, and plain γ-IND.

To analyse the time-dependent co-amorphisation within the tablets during immersion, a PCA of the FTIR spectra was performed. A model with 2 principal components explained 96 % of the variation. The respective scores plot is shown in Fig. 31B, where untreated crystalline FA-CT showed negative PC-1 score values, while the CoA FA-T references exhibited positive score values. The respective loadings plots (Fig. 31C) clearly shows that the negative part of PC-1 described the characteristic bands of crystalline FUR, while the positive part showed the shifted band at 1602 cm^{-1} of CoA FUR-ARG. Thus, in samples with low (negative) PC-1 scores, FUR was predominantly crystalline, while samples in the positive part of PC-1 showed the band of CoA FUR-ARG. As the samples immersed for up to 30 min clustered in the positive part of PC-1, the PCA revealed their co-amorphisation, which is in accordance with the XRPD data. The difference between these samples and the CoA FA-T samples was their position in the scores plot along PC-2 (Fig. 31B), where the CoA FA-T samples were found in the negative part. The respective loadings plot (Fig. 31C) also described the presence of crystalline FUR in the immersed samples as well as the difference in the position of the 1602 cm^{-1} band, which was slightly shifted to higher wavenumbers (20 and 30 min) or broadened (30 and 60 min) in the immersed samples (Fig. 31A). As FA-CT samples with immersion times of 60 and 120 min showed less positive or even negative PC-1 scores, the FTIR data indicated recrystallisation of FUR during longer immersion than 30 min (Fig. 31B).

For the IA-CT formulations, the FTIR spectra are shown in Fig. 31D. As for FA-CT, the untreated IA-CT formulation showed the characteristic bands of the crystalline API γ-IND. Löbmann et al. previously investigated the changes in the FTIR spectra upon co-

amorphisation of IND-ARG [56], which included the disappearance of the bands of γ-IND at 1714 and 1689 cm^{-1} and a simultaneous formation of a broad plateau between 1680 and 1500 cm^{-1} with a small peak at 1589 cm^{-1}. Both changes were also observed with CoA IA-T (Fig. 31D). As with CoA FUR-ARG, these changes are the consequence of a salt formation of CoA IND-ARG. During immersion in 0.1 M HCl, similar results were found as for the FUR formulations. The CoA IA-T and IA-CT formulations were also separated by PC-1, where positive values described the bands of crystalline γ-IND (Fig. 31E-F). Similar to FA-CT, the PCA of IA-CT showed a loss of crystallinity of IND within the tablets during the first 30 min of immersion. Longer immersion times led to a further movement of the score values of the samples, predominantly along PC-2 (Fig. 31E). In contrast to FA-CT, where PC-2 described the co-amorphous spectra, for IA-CT PC-2 described the appearance of new bands, which were attributed to the chemical degradation products of IND (Fig. 31F). These bands at 1717 cm^{-1} (MMIA) and 1672 cm^{-1} (CBA) were detected in the spectrum of IA-CT after immersion for 120 min (Fig. 31D). Thus, the results of the PCA were in accordance with the XRPD data, showing basic hydrolysis of IND within the tablets beginning at 60 min of immersion. This data was also in accordance with the visual observation that the yellow colouring of the immersed samples started to decline after longer immersion times than 60 min (see section 3.3.2).

In summary, the immersion in 0.1 M HCl led to a partial co-amorphisation of FUR with ARG or IND with ARG within the tablets during the first 30 min of immersion. With FA-CT formulations, the extent of co-amorphisation was similar for the 10, 20, and 30 min samples, while for the IA-CT samples after 20 and 30 min of immersion a higher co-

amorphous content was found than after 10 min. For both formulations, recrystallisation of the APIs was observed after longer immersion time periods than 60 min. With the IA-CT samples, the recrystallisation after 120 min of immersion was accompanied by a chemical degradation of IND.

3.3.3.3.2 Influence of the addition of citric acid on the co-amorphisation

For IAC-CT formulations, no distinct shifts of the γ-IND bands were detected during immersion in 0.1 M HCl (Fig. 32). Instead, after 120 min the bands of γ-IND were more pronounced than in the untreated samples. Similar to the interpretation of the XRPD diffractograms (see section 3.3.3.1), this observation may again be explained by the fact that the excipient mannitol was in part able to permeate through the film coating during immersion. Because of the resulting higher concentration of γ-IND, the γ-IND bands were intensified in the spectra of the 120 min immersed samples compared to the untreated IAC-CT (Fig. 32).
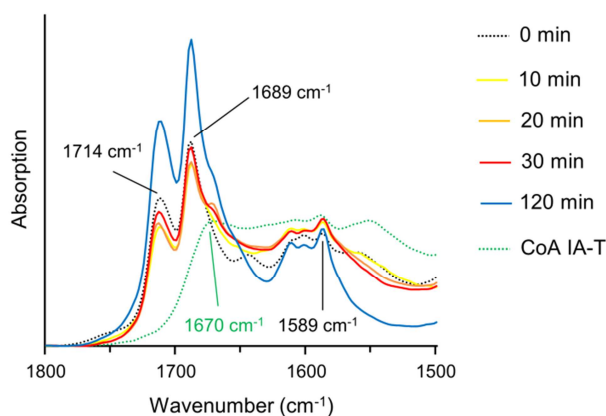
Fig. 32: FTIR spectra of the IAC-CT formulations after different time periods of immersion as well as of the CoA IA-T reference.

Taken together, the FTIR data was in accordance with the XRPD and mDSC results, showing that the addition of CA inhibited chemical degradation and co-amorphisation of IND with ARG. Thus, the addition of CA to generate a micro-pH environment to prevent chemical degradation of IND was not suitable to enable co-amorphisation of IND-ARG. The CA probably not only generated a micro-pH environment, but also interacted with ARG. Thus, ARG-IND and ARG-CA interactions might be competitive.

3.3.4 Conclusion

This study showed for the first time that an *in situ* co-amorphisation of acidic APIs with ARG during immersion in an acidic medium may be a suitable formulation approach for poorly water-soluble drugs, as the application of a gastro-resistant, but water-permeable coating has been shown to induce at least partial co-amorphisation of either FUR or γ-IND with ARG.

Furthermore, it was shown that during a prolonged immersion time period in an acidic medium, the basic amino acid ARG induced chemical degradation of IND. The addition of CA to a γ-IND+ARG tablet formulation was able to prevent this degradation, but also led to the suppression of the co-amorphisation process. It appeared that the chemical degradation and co-amorphisation of IND with ARG upon contact with water are processes, which may be difficult to separate. Thus, the presented concept of an *in situ* co-amorphisation of APIs with the basic amino acid ARG might be primarily suitable for those poorly water-soluble drugs, which are not susceptible to basic hydrolysis.

As the investigated *in situ* co-amorphisation approach might potentially be used for an amorphisation of crystalline APIs in the acidic gastric medium, in future studies the application of this concept *in vivo* should be investigated. Besides the more complex composition of the physiological gastric juice, especially the inter- and intraindividual variation of the gastric transit time for tablets needs to be considered, as in the present study a partial API recrystallisation after longer immersion times than 60 min was observed. Therefore, future studies will also have to deal with the development of a more suitable dosage form (e.g. a multiple unit pellet system).

3.4 Investigations on the applicability of *in situ* co-amorphisation in film coated tablets on the combination of carvedilol and aspartic acid

3.4.1 Tablet formulation development and tablet characterisation

In the previous study of this thesis a coated tablet formulation was developed, which enabled a controlled *in situ* co-amorphisation of acidic APIs with the coformer ARG (see section 3.3). As this study was the first showing a successful *in situ* co-amorphisation in a final dosage form, it remained unclear, whether this approach was applicable to different compounds or was limited to acidic APIs and basic coformers, or even solely to ARG based systems. Therefore, the aim of the present study was to assess the applicability of this *in situ* co-amorphisation approach on the combination of the basic drug CVD and the acidic amino acid ASP.

The results of the characterisation of the prepared uncoated tablets are summarised in Table 14. Because of the absence of ASP in the C-T formulations, the composition of this powder blend differed slightly from the CA-T formulation, which in consequence led to slightly different compaction behaviours. Thus, different compaction pressures were needed to produce tablets with similar weights and tensile strengths for both formulations (Table 14). Upon compaction, both CA-T and C-T had an acceptable friability and disintegrated rapidly in 0.1 M HCl. CVD contents of 25.2 ± 1.1 % and 25.6 ± 1.3 % were found for CA-T and C-T, respectively.

Table 14: Characterisation of the uncoated tablet formulations. Means ± SD, n = 3 (disintegration time), n = 10 (weight, tensile strength), n = 45 (compaction pressure).

	Compaction pressure (MPa)	Tablet weight (mg)	Tensile strength (N)	Friability (%)	Disintegration time (min)
CA-T	73.8 ± 9.4	196.6 ± 3.6	1.9 ± 0.3	0.19	0.3 ± 0.02
C-T	83.9 ± 8.5	196.7 ± 4.3	2.0 ± 0.2	0.17	0.3 ± 0.04

To maintain the permeability of the coating, 2-3 mg/cm^2 of the polymer were applied onto both uncoated formulations (see section 1.4.3 [179]). The total weight gains for CA-CT and C-CT were 3.2 % and 2.9 %, which corresponded to polymer amounts in the coating of 2.3 and 2.0 mg/cm^2, respectively. In accordance with these weight gains, SEM images showed that both formulations were surrounded by uniform coatings with coating thicknesses of about 20-25 µm (Fig. 33).
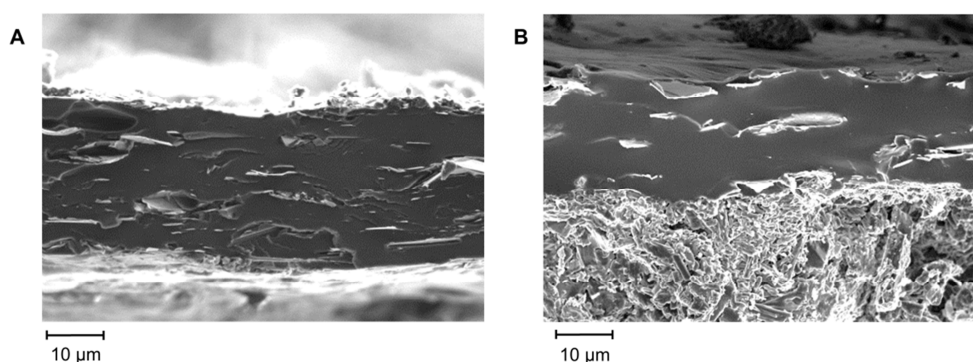
**Fig. 33:** SEM images of the cross sections of the applied tablet coatings. (A) CA-CT (B) C-CT.

During the immersion in 0.1 M HCl, both coated tablet formulations did not disintegrate. Permeation of medium through the coating was indicated by an increase of the tablet sizes accompanied by a deformation of the initial tablet shapes. While the formulation C-CT increased in size already during the first 10 min, permeation of water into the formulation CA-CT was visually observed only after about 20-30 min of immersion.

3.4.2 Solid-state analysis of the coated tablets after immersion

     3.4.2.1 XRPD

The diffractograms of the investigated tablet formulations are shown in Fig. 34 together with the reference diffractograms of crystalline CVD and ASP. All tablet formulations revealed the reflections of Pearlitol®, the diffractogram of which could be attributed to α-mannitol which is in accordance with the literature [158]. The only difference between the coated (CA-CT, C-CT) and the uncoated (CA-T, C-T) formulations was the presence of two additional reflections of talc at 9.5 and 28.6 °2θ in the diffractograms of CA-CT and C-CT, which was attributed to the coating material. Characteristic reflections of CVD were observed with all tablet formulations at 5.8, 13.0, 14.9, 15.2, and 24.4 °2θ. In contrast to C-T and C-CT, the diffractograms of CA-T and CA-CT also showed reflections of crystalline ASP (11.8, and 23.7 °2θ).
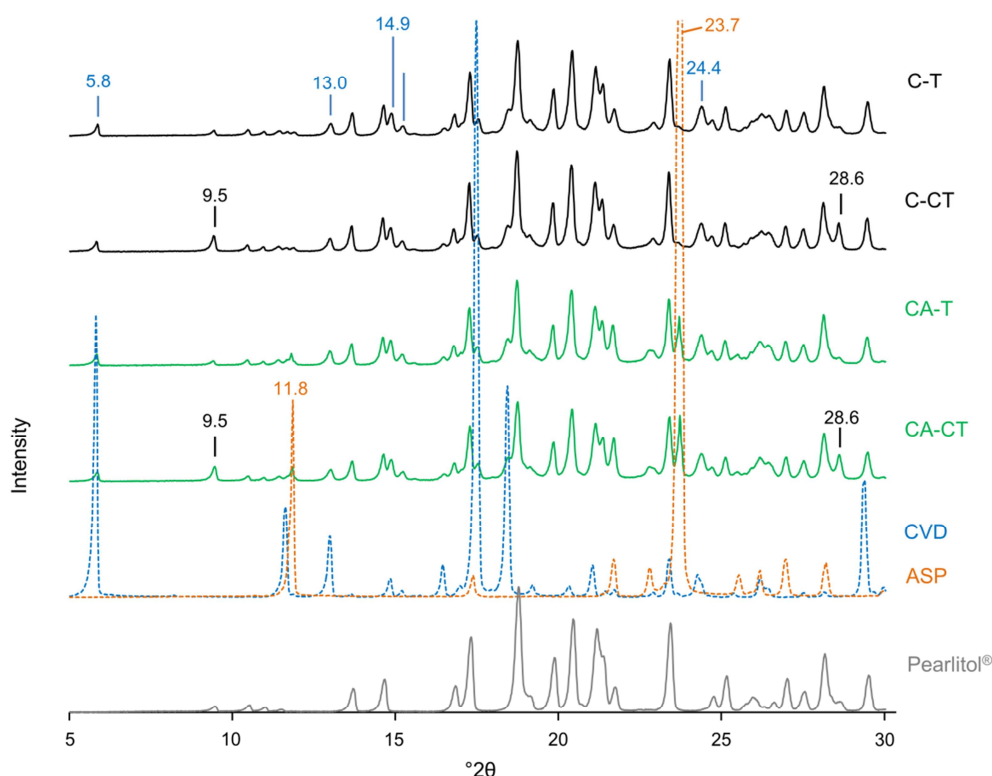
Fig. 34: XRPD diffractograms of the investigated tablet formulations in comparison to the diffractograms of the plain crystalline references CVD, ASP, and Pearlitol®. Characteristic reflections of CVD, ASP, and talc are indicated in blue, orange, and black, respectively.

To detect a possible amorphisation of CVD and ASP during immersion in 0.1 M HCl, the diffractograms of the immersed formulations were compared to those of untreated CA-CT and C-CT, respectively. For the formulations containg ASP this comparison is shown in Fig. 35A and B. It can be observed that the diffractograms after immersion for 45 and 120 min resembled each other and differed from that of untreated CA-CT. The baseline was slightly shifted, indicating the formation of a so-called "halo" (Fig. 35A). Furthermore, it was obvious that the most characteristic reflections of CVD disappeared

after immersion in 0.1 M HCl. In addition, the intensity of the two characteristic reflections of ASP at 11.8 and 23.7 °2θ were significantly decreased (Fig. 35B, for better visualisation the region between 16 and 23.5 °2θ was omitted). The remaining reflections in the diffractograms of immersed CA-CT were attributed to mannitol and talc. Taken together, both observations suggested the amorphisation of CVD and ASP in CA-CT during immersion in 0.1 M HCl. Other differences between the diffractograms of immersed and untreated CA-CT were related to a transformation of the excipient Pearlitol® from the α- to the β-modification of mannitol, as already reported in a previous study of this thesis (see section 3.3.3.1) [179].
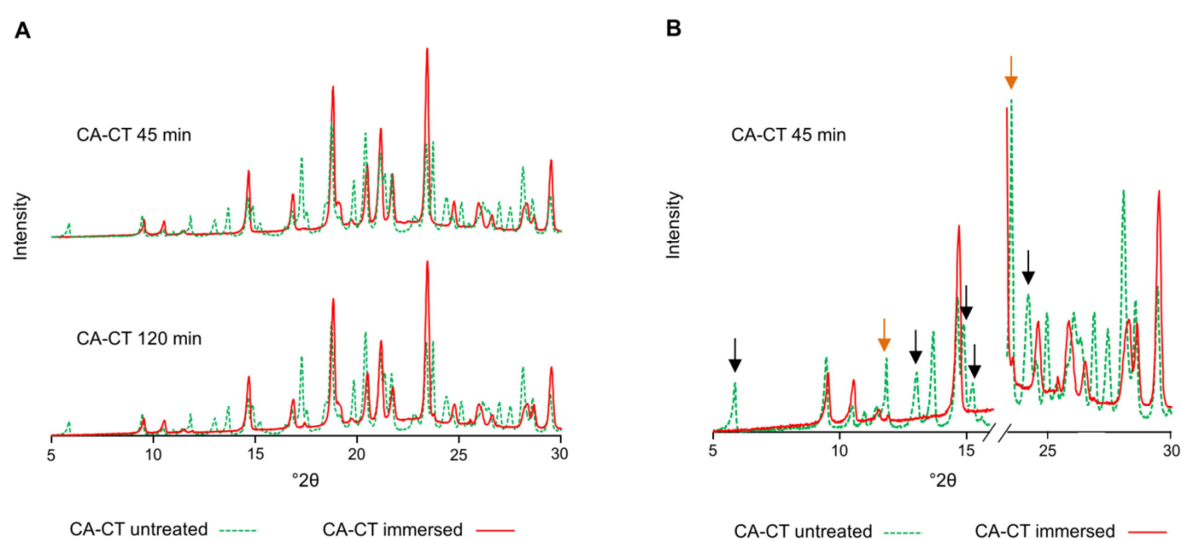
Fig. 35: XRPD diffractograms of CA-CT after immersion in 0.1 M HCl in comparison with a diffractogram of untreated CA-CT. (A) Diffractograms after 45 and 120 min of immersion, respectively. (B) Diffractograms after 45 min of immersion (the region between 16-23.5 °2θ is omitted). Characteristic reflections of CVD and ASP in untreated CA-CT are indicated by black and orange arrows, respectively.

This transformation of mannitol was also observed with the immersed C-CT samples (Fig. 36). However, in contrast to the immersed CA-CT formulations, the reflections of crystalline CVD were not altered after immersion in 0.1 M HCl and the baseline did not shift. Additionally, two new reflections (6.6 and 9.7 °2θ) appeared, which might be attributed to the formation of a CVD hydrochloride salt [180]. However, as an amorphisation of CVD was not observed, it seemed that an *in situ* amorphisation of CVD during immersion in 0.1 M HCl was only possible in the presence of ASP.
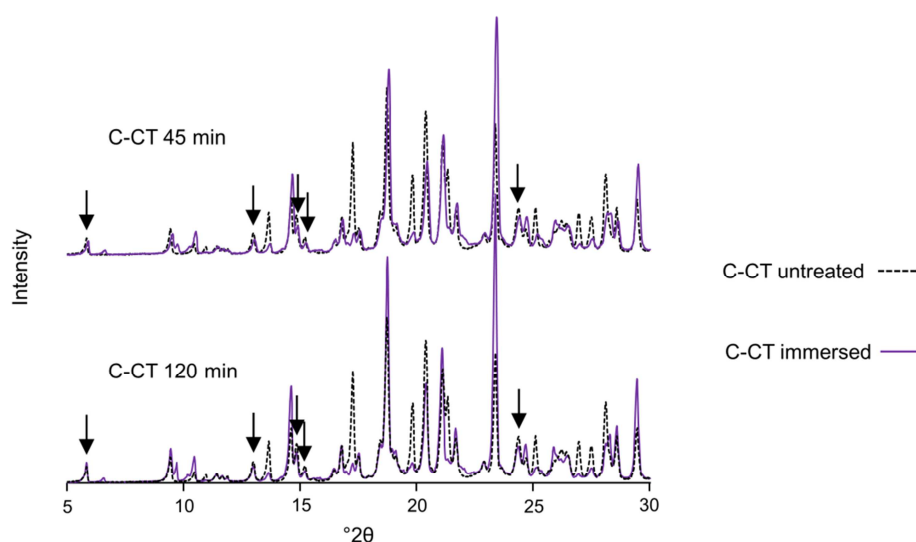

Fig. 36: XRPD diffractograms of C-CT after immersion in 0.1 M HCl for 45 and 120 min, respectively. For comparative purposes the diffractograms of untreated C-CT are shown. Characteristic reflections of CVD in C-CT are indicated by black arrows.

3.4.2.2 Thermal analysis

Although XRPD analysis is a useful technique to distinguish between crystalline and amorphous samples, it is less suited to differentiate between a co-amorphous system and a physical mixture of the two amorphous compounds. For this purpose, thermal analysis was used to determine the number of amorphous phases present in the samples.

As expected, all thermograms of the untreated formulations (CA-T, C-T, CA-CT, and C-CT) revealed a similar shape and showed only two endothermic events, which represented the melting of crystalline CVD (114.5 °C) and Pearlitol® (164.3 °C), respectively (Fig. 37, CA-CT).
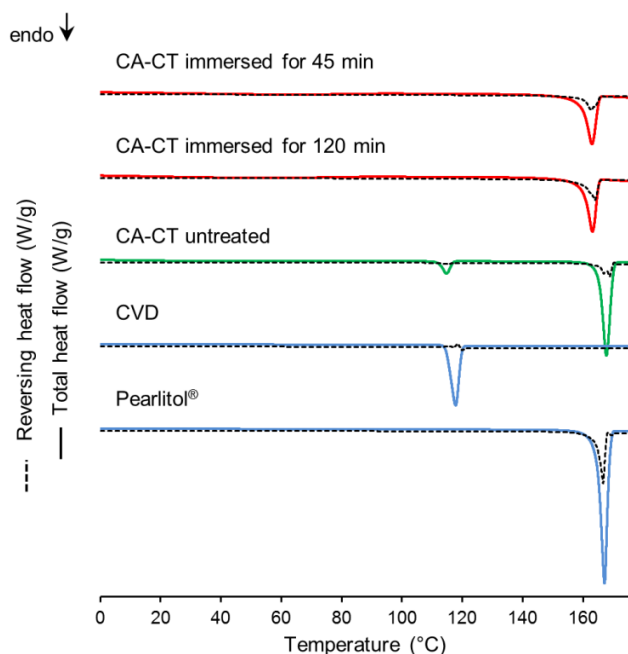
Fig. 37: Reversing heat flow and total heat flow signals of untreated CA-CT as well as of CA-CT after immersion in 0.1 M HCl for 45 and 120 min, respectively, in comparison with the signals of plain CVD and Pearlitol®.

The melting of ASP (270 °C) was not observed, as it occurs above the examined temperature region [181]. Additionally, the glass transition of Eudragit® L was not detected in the thermograms of the coated formulations because of the low amount of the applied polymer.

After immersion in 0.1 M HCl, the shape of the thermograms of CA-CT changed (Fig. 37). Melting of mannitol was still detected, although the onset of this endothermic event was slightly shifted to lower temperatures (159.8 ± 0.2 °C). Immersion of the samples in 0.1 M HCl for either 45 or 120 min also resulted in the disappeareance of the CVD melting event in the thermograms. In contrast, melting of CVD was still detected in the thermograms of the immersed coated tablets, which did not contain ASP (Fig. 38). Both findings were in accordance with the XRPD data (see section 3.4.2.1).
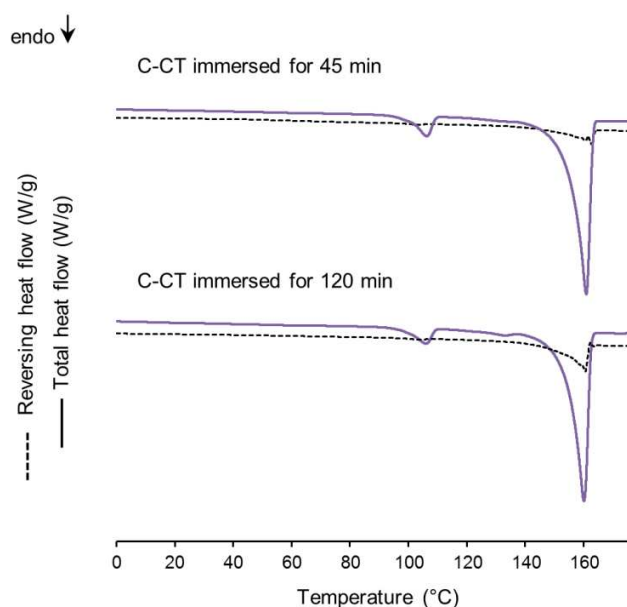
Fig. 38: Reversing heat flow and total heat flow signals of C-CT after immersion in 0.1 M HCl for 45 and 120 min, respectively.

However, no glass transition was found in the reversing heat flow signal of the immersed CA-CT samples (Fig. 37), although XRPD data indicated amorphisation of these samples. As expected, the prepared SD CoA CVD-ASP reference revealed a single T_g, which was found at 89.0 ± 0.1 °C. It is assumed that a T_g in the immersed CA-CT samples was not detected by DSC, because of the low amount of amorphous material compared to the high amount of crystalline mannitol. Therefore, DMA was carried out, as it is a highly sensitive technique for the detection of glass transitions in powdered samples [102,103,112]. Indeed, DMA responses of the immersed CA-CT samples differed from those of untreated CA-CT samples, as a distinct change in the tan δ signal between 80 and 110 °C was observed (Fig. 39, CA-CT immersed for 45 min).
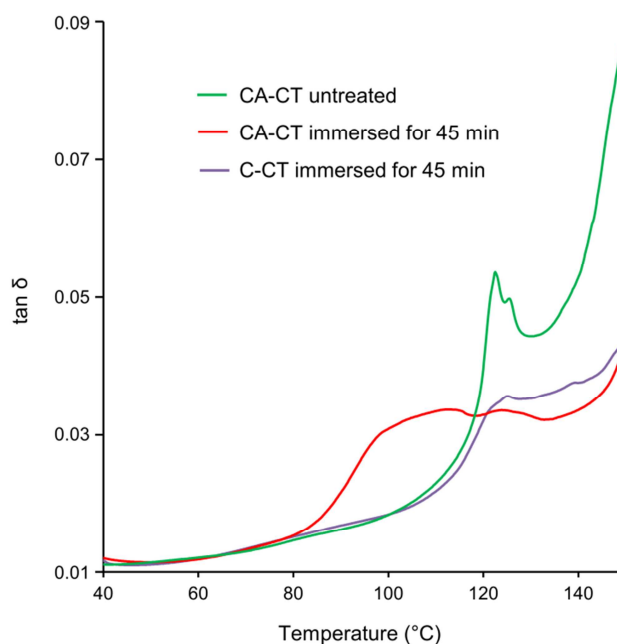
Fig. 39. tan δ signals of DMA measurements of CA-CT and C-CT after 45 min of immersion in 0.1 M HCl as well as of untreated CA-CT for comparison.

In contrast, neither any untreated formulation (CA-T, C-T, CA-CT, C-CT) nor the immersed C-CT formulations showed this increase of the tan δ signal (Fig. 39, CA-CT and C-CT immersed for 45 min). For these formulations, the tan δ signal started to change at slightly higher temperatures because of the melting of CVD.

In general, if DMA analysis is performed with a completely amorphous sample, the glass transition will appear as a sharp peak in the tan δ signal. However, if a physical mixture of an amorphous and a crystalline material is analysed, the intensity of this peak will decrease. Thereby, the glass transition becomes detectable only as a shoulder of the tan δ signal rather than a distinct peak [102]. As the amount of CVD and ASP, and therefore also the amount of amorphous material, was limited to 33.2 % w/w in the investigated formulation (Table 6), the absence of a sharp peak in the tan δ signal of immersed CA-CT samples appears comprehensible. The calculated tan δ_{max} value for the immersed CA-CT samples was 105.7 ± 3.8 °C, which is likely to correspond to the detected T_g of SD CoA CVD-ASP (89.0 ± 0.1 °C) in the DSC measurements, because a T_g obtained from DMA measurements is expected to be 10-20 °C above the T_g measured by DSC [117], resulting from the different measuring principles of these methods. The T_g of plain amorphous CVD is found at a low temperature of 38 °C [30]. Taken together, the detection of one single high-temperature T_g indicated the presence of a co-amorphous system in the immersed CA-CT samples. It was assumed that amorphous CVD and ASP interacted with each other, whereby the T_g of the system was increased compared to those of the plain amorphous drugs.

3.4.2.3 FTIR spectroscopy

To detect possible interactions between CVD and ASP in the immersed tablets, FTIR spectra were recorded. In Fig. 40A the spectra of SD CoA CVD-ASP, plain crystalline CVD, and an equimolar physical mixture (PM) of crystalline CVD-ASP are displayed. Also, a spectrum of untreated CA-CT was added to show the influence of the addition of mannitol on the characteristic bands of CVD in the spectra of the tablet formulations. It may be observed that the spectrum of the PM of CVD-ASP corresponded to the spectrum of crystalline CVD (Fig. 40A), probably because of the comparably low intensity of the ASP absorbance. Thus, possible interactions between CVD and ASP in the co-amorphous system could only be determined by analysis of the changes of the CVD bands. Indeed, by co-amorphisation distinct changes of the spectrum were observed, of which especially the disappereance of the NH stretching vibration of the secondary amine [182] of CVD at 3340 cm^{-1} was remarkable. It was postulated that the disappereance of this band in the spectrum of SD CoA CVD-ASP was the result of an interaction of the basic secondary amino group of CVD with the carboxylic acid group of ASP, leading to the formation of an amorphous salt. As mannitol also absorbs in the region between 3500-3000 cm^{-1} [178], the NH stretching vibration band at 3340 cm^{-1} was not clearly detectable in the spectrum of CA-CT. Therefore, a possible disappereance of this band after immersion in 0.1 M HCl could not be observed and thus, only the region between 1800 and 1000 cm^{-1} was selected to investigate a possible co-amorphisation of the immersed tablet formulations. In this region, characteristic changes by co-amorphisation of CVD with ASP were also detected and the interference with bands of mannitol was comparably low (Fig. 40B).
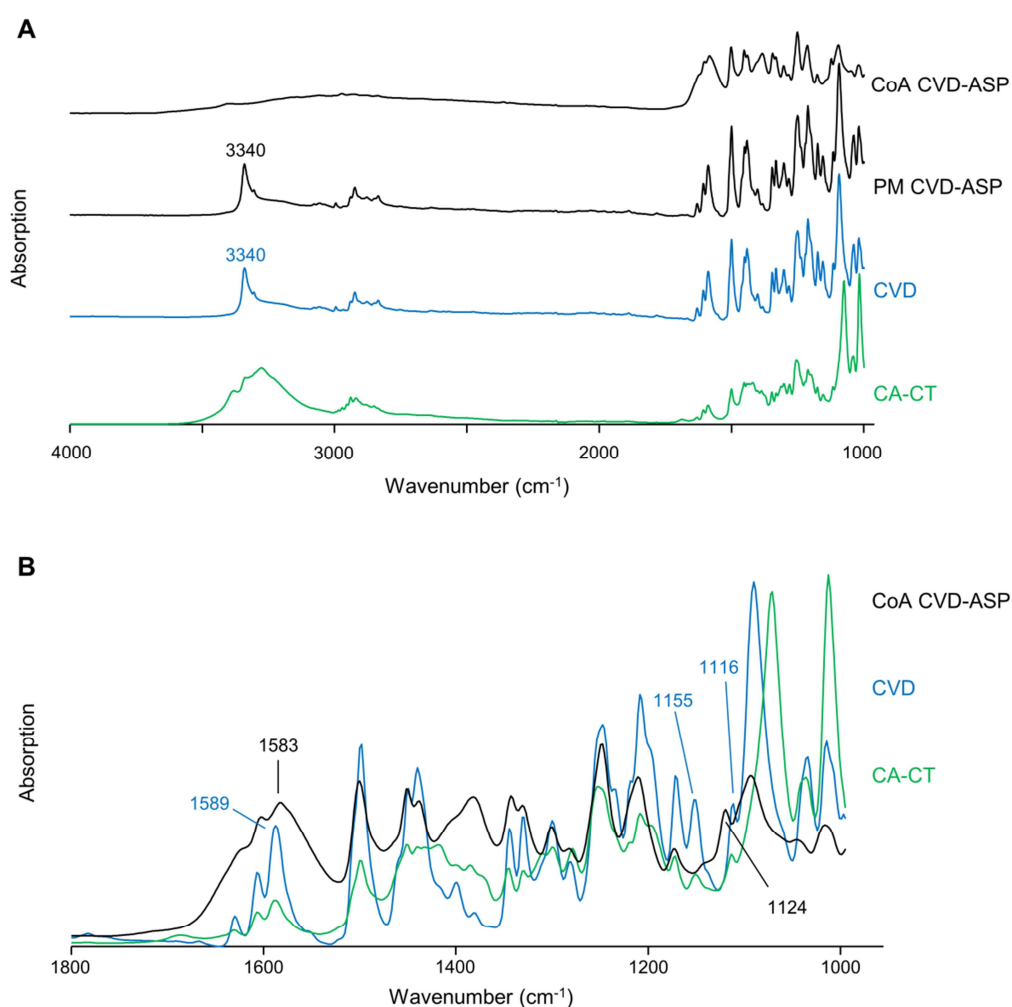
Fig. 40: FTIR spectra of selected untreated samples. (A) FTIR spectra of the spray-dried co-amorphous CVD-ASP reference (CoA CVD-ASP), plain CVD, the physical mixture of CVD and ASP (PM CVD-ASP), as well as the untreated CA-CT from 4000-1000 cm^{-1}. (B) FTIR spectra of CoA CVD-ASP, plain CVD, and untreated CA-CT, displayed only in the region from 1800-1000 cm^{-1}.

Between 1550 and 1650 cm^{-1}, peak broadening was observed for SD CoA CVD-ASP, which typically occurs during amorphisation of crystalline compounds [105]. Furthermore, the band of crystalline CVD at 1589 cm^{-1}, which was also found in the spectrum of CA-CT, shifted to 1583 cm^{-1} in the spectrum of SD CoA CVD-ASP. This band was assigned to the C=C stretching vibration of the phenyl ring of CVD [183]. Another distinct change by co-amorphisation of CVD with ASP occurred in the region between 1100 and 1200 cm^{-1}, where generally the bands corresponding to the CH in-plane bending vibrations of CVD are observed [183]. The bands of crystalline CVD at 1155 and 1116 cm^{-1}, also detected in CA-CT (Fig. 40B), disappeared in the spectrum of SD CoA CVD-ASP, while simultaneously a new band at 1124 cm^{-1} appeared.

To detect a possible co-amorphisation after immersion in 0.1 M HCl, the spectra of the immersed CA-CT were compared with the spectrum of untreated CA-CT. As the FTIR spectra of CA-CT immersed for either 45 or 120 min looked identical, only the spectrum of CA-CT immersed for 45 min is shown in Fig. 41. The immersed samples revealed the already mentioned distinct peak broadening between 1550 and 1650 cm^{-1} and a band shift from 1589 to 1585 cm^{-1}. Furthermore, the bands at 1155 and 1118 cm^{-1} disappeared and the band of SD CoA CVD-ASP at 1124 cm^{-1} appeared.

In contrast, these changes in the FTIR spectra were not observed with the immersed C-CT samples (Fig. 42). Similar to the XRPD data, changes in the FTIR spectra of the immersed C-CT samples resulted only from the transformation of mannitol.
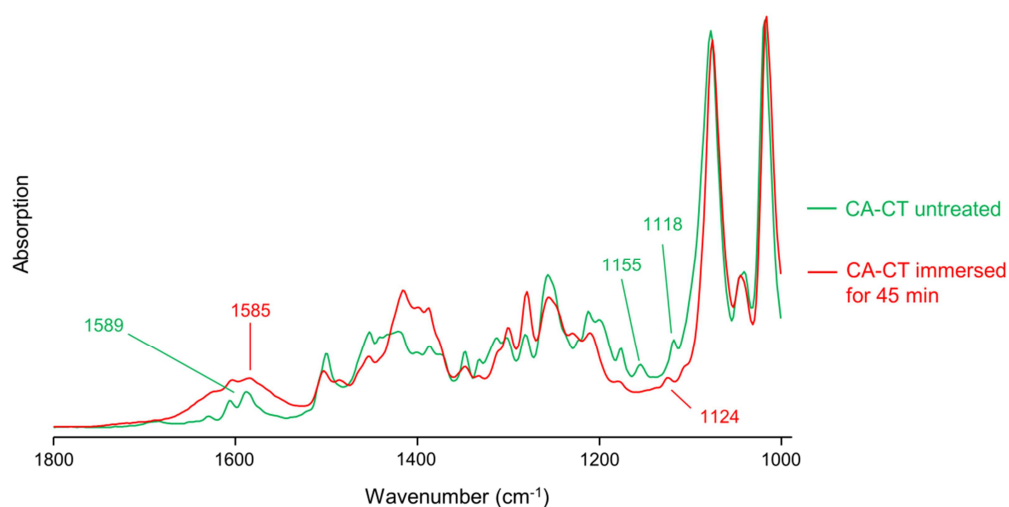
Fig. 41: FTIR spectrum (1800-1000 cm^{-1}) of CA-CT after immersion in 0.1 M HCl for 45 min in comparison with the spectrum of untreated CA-CT.
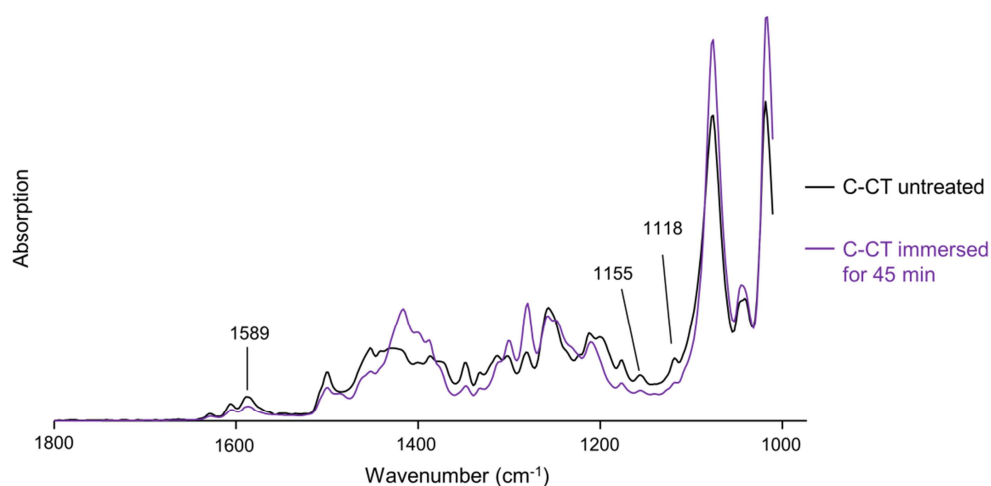
Fig. 42: FTIR spectrum (1800-1000 cm^{-1}) of C-CT after immersion in 0.1 M HCl for 45 min in comparison with the spectrum of untreated C-CT.

Therefore, the FTIR spectroscopic data were in accordance with the results of XRPD and thermal analysis, all together indicating that only during immersion of a tablet formulation containing CVD together with ASP, CVD turned amorphous. CVD and ASP formed a co-amorphous system with a high-temperature T_g, as indicated by DMA (see section 3.4.2.2.). As the FTIR spectra of the CA-CT samples revealed distinct changes after immersion in 0.1 M HCl, it may be assumed that this high-temperature T_g was the result of molecular interactions between CVD and ASP. Although it could not definitely be proven, it is very likely that the basic secondary amino group of CVD interacted with the carboxylic acid group of ASP, leading to salt formation between both compounds. Such a comparably strong molecular interaction may explain the high T_g, which was found with SD CoA CVD-ASP in the present study. In comparison to the T_g values previously reported for the co-amorphous salts of CVD with different organic acids [45] this T_g was even higher.

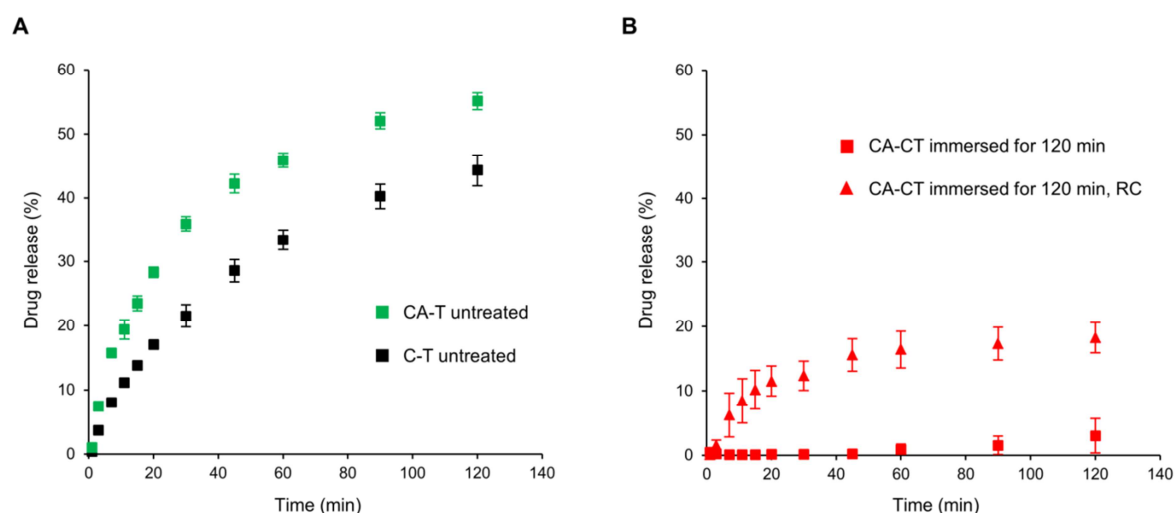*3.4.3 Drug release from the investigated tablet formulations*

After 120 min of drug release testing of CA-CT in 0.1 M HCl, the concentration of CVD detected in the medium was much lower than the quantification limit (0.18 mg/l) of the applied HPLC method. Therefore, the amount of CVD, which permeated through the coating, was less than 0.32 mg in 900 ml release medium, which corresponded to less than 0.65 % of the drug content of the investigated formulations. In contrast, for C-CT samples CVD amounts of 5.2 ± 0.3 mg in 900 ml (≙ 10.3 ± 0.6 % released CVD) were found after 120 min of release testing in 0.1 M HCl. These different release behaviours might be attributed to the slightly lower coating thickness of C-CT compared to CA-CT

(see section 3.4.1). However, with an average concentration of 10 % released CVD, this value was just about acceptable for a delayed-release dosage form according to the acceptance criteria of the Ph. Eur. (shown in Table 2.9.3.-3 of the Ph. Eur.).

The drug release behaviour of the two uncoated crystalline formulations CA-T and C-T in phosphate buffer pH 6.8 for a period of 120 min is shown in Fig. 43A. It was observed that both formulations disintegrated within the first 10 s after being placed into the dissolution medium. However, despite the similar disintegration time, CA-T and C-T showed different drug release profiles. Whilst the shapes of the drug release curves were similar, the quantified amounts of dissolved CVD during drug release of CA-T were distinctly higher than those reached by C-T (CA-T c_{max}: 55.1 ± 1.3 %; C-T c_{max}: 44.3 ± 2.4 %). This surprising result may be related to an *in situ* co-amorphisation of CVD and ASP upon contact with the dissolution medium. A similar phenomenon was previously observed for tablets containing IND and ARG, which was described in a previous study of this thesis (see section 3.1.4) as well as in a study by Lenz et al. [99,139]. Like with the crystalline IND-ARG formulations, where the improved drug release behaviour was attributed to an *in situ* co-amorphisation upon contact with the dissolution medium, the enhanced drug release of CA-T in the present study may in a similar way be related to an *in situ* co-amorphisation of CVD with ASP. In any case, as the content of ASP was the only difference between both tablet formulations, the addition of ASP had to be mandatory for the observed drug release improvement.

Fig. 43: Drug release from the investigated tablet formulations in 900 ml phosphate buffer pH 6.8 at 37 °C. (A) Drug release from untreated CA-T and C-T, respectively. (B) Drug release from CA-CT directly after immersion for 120 min in 0.1 M HCl compared to CA-CT after immersion for 120 min, subsequent drying at 40 °C, and removal of the coating. Means ± SD, n = 3.

As the solid-state analysis of the immersed samples revealed a co-amorphisation of CVD and ASP during immersion of CA-CT in 0.1 M HCl (see section 3.4.2), an altered drug release behaviour was expected for the immersed CA-CT samples. Surprisingly, almost no release of CVD from the immersed CA-CT formulations could be observed (c_{max}: 3.0 ± 2.6 %), because the coating did not dissolve upon contact with the dissolution medium (Fig. 43B). This observation was attributed to an interaction of the weakly basic drug CVD with the acidic side chains (carboxylic groups) of the enteric polymer Eudragit® L 55, which led to a changed dissolution behaviour of the coating [139]. In addition, the pre-immersion in 0.1 M HCl and the presence of ASP probably led

to the generation of an acidic microenvironmental pH in the tablet cores, which might also have led to a hindrance of the dissolution of the enteric coating.

To analyse the drug release behaviour of the immersed CA-CT formulation regardless of the above mentioned interaction, the samples immersed for 120 min were dried at 40 °C overnight and the coating was carefully removed with a razor blade. The drug release from these samples is also shown in Fig. 43B. It may be observed that the removal of the coating led to an only partial release of CVD from the immersed tablets. It was also observed that these tablets did not disintegrate during the whole 120 min of drug release testing. In contrast to the dissolution media of CA-T and C-T, which contained many undissolved particles, the medium of the immersed CA-CT samples appeared transparent. Therefore, the amount of dissolved CVD from these immersed CA-CT samples was distinctly lower than for CA-T and C-T (CA-CT immersed for 120 min c_{max}: 18.3 ± 2.4 %). This lack of disintegration may for once be explained by the fact that the use of the razor blade did not result in an entire removal of the polymer. It may be assumed that a portion of the polymer was able to permeate into the tablet cores, either during the coating process or during the immersion in 0.1 M HCl. In addition, a lack of sufficient disintegration is a well-known problem of amorphous formulations [28] and was already observed for *in situ* amorphised compacts of indomethacin and PVP, leading to a delayed drug release of the partial amorphous formulation compared to the crystalline compacts [93]. Such a lack of tablet disintegration was also observed in a previous study of this thesis, where the prepared co-amorphous IND-ARG formulation had been hardened upon storage at high humidity (see section 3.1.4) [171]. The CA-CT samples in the present study also appeared slightly harder after the immersion in 0.1 M HCl and

subsequent drying. Probably, the presented *in situ* preparation approach resulted in a hard compact with reduced porosity. Thus, the immersed CA-CT formulation showed a poor disintegration and therefore also a poor drug release behaviour. However, the presence of crystalline ASP in the untreated tablet formulation already led to an enhancement of the amount of released CVD (Fig. 43A), which was probably the result of a partial *in situ* co-amorphisation of CVD with ASP. Therefore, an entire *in situ* co-amorphised CVD-ASP tablet should theoretically show an even higher drug release of CVD, if a rapid disintegration of the formulation could be ensured.

3.4.4 Conclusion

In the present study it was shown that a co-amorphous system of the basic drug CVD and the acidic amino acid ASP may be formed *in situ*, if a film coated tablet containing both components in crystalline form is immersed in 0.1 M HCl. Thus, it was demonstrated that the previously developed concept for a controlled *in situ* co-amorphisation in the final dosage form is not only limited to systems comprising an acidic API and a basic amino acid, but is also applicable to further co-amorphous formulations. The presented approach may therefore allow the oral application of differently composed co-amorphous formulations, while simultaneously preventing the need for a long-term physical stabilisation.

However, in the present study the immersion in 0.1 M HCl led to an insufficient disintegration of the final formulation. Thus, the drug release behaviour of the *in situ* co-amorphised formulation was rather poor. To profit from the theoretically improved dissolution behaviour of a co-amorphous system, this lack of a sufficient disintegration of the immersed formulation has to be overcome. Therefore, future studies will have to investigate formulation approaches to ensure a fast disintegration of the immersed tablet upon contact with a drug release medium with a pH above 5.5.

References

[1]   S.V. Sastry, J.R. Nyshadham, J.A. Fix, Recent technological advances in oral drug delivery – a review, Pharm. Sci. Technol. Today 3 (2000) 138–145.

[2]   M. Jivraj, L.G. Martini, C.M. Thomson, An overview of the different excipients useful for the direct compression of tablets, Pharm. Sci. Technol. To. 3 (2000) 58–63.

[3]   A. Talevi, P.A.M. Quiroga, Introduction. Biopharmaceutics and pharmacokinetics, in: A. Talevi, P.A.M. Quiroga (Eds.), ADME processes in pharmaceutical sciences: Dosage, design, and pharmacotherapy success, Springer, New York, USA, 2018, pp. 3–10.

[4]   L.P. Balant, Is there a need for more precise definitions of bioavailability?, Eur. J. Clin. Pharmacol. 40 (1991) 123–126.

[5]   M.S. Ku, Use of the biopharmaceutical classification system in early drug development, AAPS J. 10 (2008) 208–212.

[6]   A. Talevi, C.L. Bellera, Drug absorption, in: A. Talevi, P.A.M. Quiroga (Eds.), ADME processes in pharmaceutical sciences: Dosage, design, and pharmacotherapy success, Springer, New York, USA, 2018, pp. 11–31.

[7]   G.L. Amidon, H. Lennernäs, V.P. Shah, J.R. Crison, A theoretical basis for a biopharmaceutic drug classification: the correlation of in vitro drug product dissolution and in vivo bioavailability, Pharm. Res. 12 (1995) 413–420.

[8]   M. Yasir, M. Asif, A. Kumar, A. Aggarval, Biopharmaceutical classification system: an account, Int. J. Pharm. Res. 10 (2010) 1681–1690.

[9]   C.A. Lipinski, F. Lombardo, B.W. Dominy, P.J. Feeney, Experimental and computational approaches to estimate solubility and permeability in drug discovery and development settings, Adv. Drug Deliv. Rev. 23 (1997) 3–25.

[10]   B.J. Aungst, Optimizing Oral Bioavailability in Drug Discovery: An Overview of Design and Testing Strategies and Formulation Options, J. Pharm. Sci. 106 (2017) 921–929.

[11]   N.J. Babu, A. Nangia, Solubility advantage of amorphous drugs and pharmaceutical cocrystals, Cryst. Growth Des. 11 (2011) 2662–2679.

[12]   H.D. Williams, N.L. Trevaskis, S.A. Charman, R.M. Shanker, W.N. Charman, C.W. Pouton, Porter, C. J. H., Strategies to address low drug solubility in discovery and development, Pharmacol. Rev. 65 (2012) 315–499.

[13]   A. Fahr, X. Liu, Drug delivery strategies for poorly water-soluble drugs, Expert Opin. Drug Deliv. 4 (2007) 403–416.

[14]   Y. Kawabata, K. Wada, M. Nakatani, S. Yamada, S. Onoue, Formulation design for poorly water-soluble drugs based on biopharmaceutics classification system: basic approaches and practical applications, Int. J. Pharm. 420 (2011) 1–10.

[15]   K. Kawakami, Modification of physicochemical characteristics of active pharmaceutical ingredients and application of supersaturatable dosage forms for improving bioavailability of poorly absorbed drugs, Adv. Drug Deliv. Rev. 64 (2012) 480–495.

[16]   K. Nagapudi, J. Jona, Amorphous active pharmaceutical ingredients in preclinical studies: preparation, characterization and formulation, Curr. Bioactive Comp. 4 (2008) 213–224.

[17]   B.C. Hancock, G. Zografi, Characteristics and significance of the amorphous state in pharmaceutical systems, J. Pharm. Sci. 86 (1997) 1–12.

[18]   H. Grohganz, K. Löbmann, P. Priemel, K.T. Jensen, K. Graeser, C. Strachan, T. Rades, Amorphous drugs and dosage forms, J. Drug Deliv. Sci. Tech. 23 (2013) 403–408.

[19]   A.M. Kaushal, P. Gupta, A.K. Bansal, Amorphous drug delivery systems: molecular aspects, design, and performance, Crit. Rev. Ther. Drug 21 (2004) 133–193.

[20]   R. Laitinen, K. Löbmann, C.S. Strachan, H. Grohganz, T. Rades, Emerging trends in the stabilization of amorphous drugs, Int. J. Pharm. 453 (2013) 65–79.

[21]   S.J. Dengale, H. Grohganz, T. Rades, K. Löbmann, Recent advances in co-amorphous drug formulations, Adv. Drug Deliv. Rev. 100 (2016) 116–125.

[22]   A. Karagianni, K. Kachrimanis, I. Nikolakakis, Co-amorphous solid dispersions for solubility and absorption improvement of drugs, Pharmaceutics 10 (2018) 1–26.

[23]   W.L. Chiou, S. Riegelmann, Pharmaceutical applications of solid dispersion systems, J. Pharm. Sci. 60 (1971) 1281–1302.

[24]   F. Qian, J. Huang, M.A. Hussain, Drug-polymer solubility and miscibility: Stability consideration and practical challenges in amorphous solid dispersion development, J. Pharm. Sci. 99 (2010) 2941–2947.

[25]   S. Baghel, H. Cathcart, N.J. O'Reilly, Polymeric amorphous solid dispersions: A Review of amorphization, crystallization, stabilization, solid-state characterization, and aqueous solubilization of biopharmaceutical classification system class II drugs, J. Pharm. Sci. 105 (2016) 2527–2544.

[26]   T. van Duong, G. van den Mooter, The role of the carrier in the formulation of pharmaceutical solid dispersions. Part II: Amorphous carriers, Expert Opin. Drug Deliv. 13 (2016) 1681–1694.

[27]   Y. Huang, W.-G. Dai, Fundamental aspects of solid dispersion technology for poorly soluble drugs, Acta Pharm. Sin. B 4 (2014) 18–25.

[28]   A.T.M. Serajuddin, Solid dispersion of poorly water-soluble drugs: early promises, subsequent problems, and recent breakthroughs, J. Pharm. Sci. 88 (1999) 1058–1066.

[29]   Y. Choudhari, H. Hoefer, C. Libatani, F. Monsuur, W. McCarthy, Mesoporous silica drug delivery systems, in: N. Shah, H. Sandhu, D.S. Choi, H. Chokshi, A.W. Malick (Eds.), Amorphous solid dispersions, Springer, New York, USA, 2014, pp. 197–230.

[30]   B. Kovačič, F. Vrečer, O. Planinšek, Solid dispersions of carvedilol with porous silica, Chem. Pharm. Bull. 59 (2011) 427–433.

[31]   Y. Huang, Q. Zhang, J.-R. Wang, K.-L. Lin, X. Mei, Amino acids as co-amorphous excipients for tackling the poor aqueous solubility of valsartan, Pharm. Dev. Technol. 22 (2017) 69–76.

[32]   K.T. Jensen, L.I. Blaabjerg, E. Lenz, A. Bohr, H. Grohganz, P. Kleinebudde, T. Rades, K. Löbmann, Preparation and characterization of spray-dried co-amorphous drug-amino acid salts, J. Pharm. Pharmacol. 68 (2016) 615–624.

[33]   O. Korhonen, K. Pajula, R. Laitinen, Rational excipient selection for co-amorphous formulations, Expert Opin. Drug Deliv. 14 (2017) 551–569.

[34]   H. Meng-Lund, G. Kasten, K.T. Jensen, A. Poso, T. Pantsar, T. Rades, J. Rantanen, H. Grohganz, The use of molecular descriptors in the development of co-amorphous formulations, Eur. J. Pharm. Biopharm. 119 (2018) 31–38.

[35]   G. Kasten, K. Löbmann, H. Grohganz, T. Rades, Co-former selection for co-amorphous drug-amino acid formulations, Int. J. Pharm. 557 (2018) 336–373.

[36]   A. D'Angelo, B. Edgar, A.P. Hurt, M.D. Antonijević, Physico-chemical characterisation of three-component co-amorphous systems generated by a melt-quench method, J. Therm. Anal. Calorim. 134 (2018) 381–390.

[37]   A.W. Lim, K. Löbmann, H. Grohganz, T. Rades, N. Chieng, Investigation of physical properties and stability of indomethacin-cimetidine and naproxen-cimetidine co-amorphous systems prepared by quench cooling, coprecipitation and ball milling, J. Pharm. Pharmacol. 68 (2016) 36–45.

[38]   K. Löbmann, R. Laitinen, H. Grohganz, K.C. Gordon, C. Strachan, T. Rades, Coamorphous drug systems: enhanced physical stability and dissolution rate of indomethacin and naproxen, Mol. Pharm. 8 (2011) 1919–1928.

[39]   A. Shayanfar, A. Jouyban, Drug–drug coamorphous systems: characterization and physicochemical properties of coamorphous atorvastatin with carvedilol and glibenclamide, J. Pharm. Innov. 8 (2013) 218–228.

[40]   S. Wairkar, R. Gaud, Co-amorphous combination of nateglinide-metformin hydrochloride for dissolution enhancement, AAPS PharmSciTech 17 (2016) 673–681.

[41]   A. Beyer, H. Grohganz, K. Löbmann, T. Rades, C.S. Leopold, Improvement of the physicochemical properties of co-amorphous naproxen-indomethacin by naproxen-sodium, Int. J. Pharm. 526 (2017) 88–94.

[42]   C. Martínez-Jiménez, J. Cruz-Angeles, M. Videa, L.M. Martínez, Co-amorphous simvastatin-nifedipine with enhanced solubility for possible use in combination therapy of hypertension and hypercholesterolemia, Molecules 23 (2018) 1–13.

[43]   K. Löbmann, H. Grohganz, R. Laitinen, C. Strachan, T. Rades, Amino acids as co-amorphous stabilizers for poorly water soluble drugs-Part 1: preparation, stability and dissolution enhancement, Eur. J. Pharm. Biopharm. 85 (2013) 873–881.

[44]   R. Laitinen, K. Löbmann, H. Grohganz, C. Strachan, T. Rades, Amino acids as co-amorphous excipients for simvastatin and glibenclamide: physical properties and stability, Mol. Pharm. 11 (2014) 2381–2389.

[45]   W. Wu, H. Ueda, K. Löbmann, T. Rades, H. Grohganz, Organic acids as co-formers for co-amorphous systems - influence of variation in molar ratio on the physicochemical properties of the co-amorphous systems, Eur. J. Pharm. Biopharm. 131 (2018) 25–32.

[46]   A. Ainurofiq, R. Mauludin, D. Mudhakir, S.N. Soewandhi, A novel
         desloratadine-benzoic acid co-amorphous solid: preparation, characterization,
         and stability evaluation, Pharmaceutics 10 (2018) 1–16.

[47]   J.-H. An, C. Lim, A.N. Kiyonga, I.H. Chung, I.K. Lee, K. Mo, M. Park, W. Youn,
         W.R. Choi, Y.-G. Suh, K. Jung, Co-amorphous screening for the solubility
         enhancement of ooorly water-soluble mirabegron and investigation of their
         intermolecular interactions and dissolution behaviors, Pharmaceutics 10
         (2018) 1–14.

[48]   Y. Hu, K. Gniado, A. Erxleben, P. McArdle, Mechanochemical reaction of
         sulfathiazole with carboxylic acids: Formation of a cocrystal, a salt, and
         coamorphous solids, Cryst. Growth Des. 14 (2014) 803–813.

[49]   A.M.A. Ali, A.A. Ali, I.A. Maghrabi, Clozapine-carboxylic acid plasticized co-
         amorphous dispersions: Preparation, characterization and solution stability
         evaluation, Acta Pharmaceut. 65 (2015) 133–146.

[50]   M. Fung, K.R. Be Rziņš, R. Suryanarayanan, Physical stability and dissolution
         behavior of ketoconazole-organic acid coamorphous systems, Mol. Pharm. 15
         (2018) 1862–1869.

[51]   W. Wu, K. Löbmann, J. Schnitzkewitz, A. Knuhtsen, D.S. Pedersen, T. Rades,
         Dipeptides as co-formers in co-amorphous systems, Eur. J. Pharm. Biopharm.
         134 (2019) 68–76.

[52]   W. Wu, K. Löbmann, J. Schnitzkewitz, A. Knuhtsen, D.S. Pedersen, H.
         Grohganz, T. Rades, Aspartame as a co-former in co-amorphous systems, Int.
         J. Pharm. 549 (2018) 380–387.

[53]   J. Mishra, A. Bohr, T. Rades, H. Grohganz, K. Löbmann, Whey proteins as
         stabilizers in amorphous solid dispersions, Eur. J. Pharm. Sci. 128 (2019)
         144–151.

[54]   S. Qian, W. Heng, Y. Wei, J. Zhang, Y. Gao, Coamorphous lurasidone
         hydrochloride–saccharin with charge-assisted hydrogen bonding interaction

shows improved physical stability and enhanced dissolution with pH-independent solubility behavior, Cryst. Growth Des. 15 (2015) 2920–2928.

[55]   R.B. Chavan, R. Thipparaboina, D. Kumar, N.R. Shastri, Co amorphous systems: A product development perspective, Int. J. Pharm. 515 (2016) 403–415.

[56]   K. Löbmann, R. Laitinen, C. Strachan, T. Rades, H. Grohganz, Amino acids as co-amorphous stabilizers for poorly water-soluble drugs-Part 2: molecular interactions, Eur. J. Pharm. Biopharm. 85 (2013) 882–888.

[57]   R. Laitinen, K. Löbmann, H. Grohganz, P. Priemel, C.J. Strachan, T. Rades, Supersaturating drug delivery systems: The potential of co-amorphous drug formulations, Int. J. Pharm. 532 (2017) 1–12.

[58]   W. Wu, K. Löbmann, T. Rades, H. Grohganz, On the role of salt formation and structural similarity of co-formers in co-amorphous drug delivery systems, Int. J. Pharm. 535 (2017) 86–94.

[59]   G. Kasten, K. Nouri, H. Grohganz, T. Rades, K. Löbmann, Performance comparison between crystalline and co-amorphous salts of indomethacin-lysine, Int. J. Pharm. 533 (2017) 138–144.

[60]   K.T. Jensen, F.H. Larsen, C. Cornett, K. Löbmann, H. Grohganz, T. Rades, Formation mechanism of coamorphous drug-amino acid mixtures, Mol. Pharm. 12 (2015) 2484–2492.

[61]   H. Ueda, W. Wu, K. Löbmann, H. Grohganz, A. Müllertz, T. Rades, Application of a salt coformer in a co-amorphous drug system dramatically enhances the glass transition temperature: A case study of the ternary system carbamazepine, citric acid, and l-arginine, Mol. Pharm. 15 (2018) 2036–2044.

[62]   J.-H. An, C. Lim, A.N. Kiyonga, I.H. Chung, I.K. Lee, K. Mo, M. Park, W. Youn, W.R. Choi, Y.-G. Suh, K. Jung, Co-amorphous screening for the solubility enhancement of poorly water-soluble mirabegron and investigation of their

intermolecular interactions and dissolution behaviors, Pharmaceutics 10 (2018) 1–14.

[63]   M. Allesø, N. Chieng, S. Rehder, J. Rantanen, T. Rades, J. Aaltonen, Enhanced dissolution rate and synchronized release of drugs in binary systems through formulation: Amorphous naproxen-cimetidine mixtures prepared by mechanical activation, J. Controlled Release 136 (2009) 45–53.

[64]   N. Chieng, J. Aaltonen, D. Saville, T. Rades, Physical characterization and stability of amorphous indomethacin and ranitidine hydrochloride binary systems prepared by mechanical activation, Eur. J. Pharm. Biopharm. 71 (2009) 47–54.

[65]   H. Ueda, N. Muranushi, S. Sakuma, Y. Ida, T. Endoh, K. Kadota, Y. Tozuka, A strategy for co-former selection to design stable co-amorphous formations based on physicochemical properties of non-steroidal inflammatory drugs, Pharm. Res. 33 (2015) 1018–1029.

[66]   A. Beyer, H. Grohganz, K. Löbmann, T. Rades, C.S. Leopold, Influence of the cooling rate and the blend ratio on the physical stability of co-amorphous naproxen/indomethacin, Eur. J. Pharm. Biopharm. 109 (2016) 140–148.

[67]   K.T. Jensen, F.H. Larsen, K. Löbmann, T. Rades, H. Grohganz, Influence of variation in molar ratio on co-amorphous drug-amino acid systems, Eur. J. Pharm. Biopharm. 107 (2016) 32–39.

[68]   K.T. Jensen, K. Löbmann, T. Rades, H. Grohganz, Improving co-amorphous drug formulations by the addition of the highly water soluble amino acid, proline, Pharmaceutics 6 (2014) 416–435.

[69]   S.J. Dengale, O.P. Ranjan, S.S. Hussen, B.S.M. Krishna, P.B. Musmade, G. Gautham Shenoy, K. Bhat, Preparation and characterization of co-amorphous Ritonavir-Indomethacin systems by solvent evaporation technique: improved dissolution behavior and physical stability without evidence of intermolecular interactions, Eur. J. Pharm. Sci. 62 (2014) 57–64.

[70]   A. Newman, S.M. Reutzel-Edens, G. Zografi, Coamorphous active pharmaceutical ingredient-small molecule mixtures: Considerations in the choice of coformers for enhancing dissolution and oral bioavailability, J. Pharm. Sci. 107 (2018) 5–17.

[71]   L. Yu, Amorphous pharmaceutical solids: preparation, characterization and stabilization, Adv. Drug Deliv. Rev. 48 (2001) 27–42.

[72]   G.P. Kumar, B.S. Kumar, Current challenges in the development and formulation of amorphous solids, Indonesian J. Pharm. 23 (2012) 65–83.

[73]   C. Ahlneck, G. Zografi, The molecular basis of moisture effects on the physical and chemical stability of drugs in the solid state, Int. J. Pharm. 62 (1990) 87–95.

[74]   S. Bates, G. Zografi, D. Engers, K. Morris, K. Crowley, A. Newman, Analysis of amorphous and nanocrystalline solids from their X-ray diffraction patterns, Pharm. Res. 23 (2006) 2333–2349.

[75]   L.I. Blaabjerg, E. Lindenberg, T. Rades, H. Grohganz, K. Löbmann, Influence of preparation pathway on the glass forming ability, Int. J. Pharm. 521 (2017) 232–238.

[76]   L.M. Martínez, M. Videa, G.A. López-Silva, de Los Reyes, Carlos A, J. Cruz-Angeles, N. González, Stabilization of amorphous paracetamol based systems using traditional and novel strategies, Int. J. Pharm. 477 (2014) 294–305.

[77]   A. Beyer, H. Grohganz, K. Löbmann, T. Rades, C.S. Leopold, Multivariate quantification of the solid state phase composition of co-amorphous naproxen-indomethacin, Molecules 20 (2015) 19571–19587.

[78]   V. Sai Krishna Anand, S.D. Sakhare, K.S. Navya Sree, A.R. Nair, K. Raghava Varma, K. Gourishetti, S.J. Dengale, The relevance of co-amorphous formulations to develop supersaturated dosage forms: In-vitro, and ex-vivo investigation of Ritonavir-Lopinavir co-amorphous materials, Eur. J. Pharm. Sci. 123 (2018) 124–134.

[79]   G. Kasten, H. Grohganz, T. Rades, K. Löbmann, Development of a screening method for co-amorphous formulations of drugs and amino acids, Eur. J. Pharm. Sci. 95 (2016) 28–35.

[80]   Z. Wang, M. Sun, T. Liu, Z. Gao, Q. Ye, X. Tan, Y. Hou, J. Sun, D. Wang, Z. He, Co-amorphous solid dispersion systems of lacidipine-spironolactone with improved dissolution rate and enhanced physical stability, Asian J. Pharm. Sci. 14 (2018) 95–103.

[81]   A. Beyer, L. Radi, H. Grohganz, K. Löbmann, T. Rades, C.S. Leopold, Preparation and recrystallization behavior of spray-dried co-amorphous naproxen-indomethacin, Eur. J. Pharm. Biopharm. 104 (2016) 72–81.

[82]   G. Craye, K. Löbmann, H. Grohganz, T. Rades, R. Laitinen, Characterization of amorphous and co-amorphous simvastatin formulations prepared by spray drying, Molecules 20 (2015) 21532–21548.

[83]   R. Ojarinta, L. Lerminiaux, R. Laitinen, Spray drying of poorly soluble drugs from aqueous arginine solution, Int. J. Pharm. 532 (2017) 289–298.

[84]   J. Mishra, T. Rades, K. Löbmann, H. Grohganz, Influence of solvent composition on the performance of spray-dried co-amorphous formulations, Pharmaceutics 10 (2018) 1–13.

[85]   E. Lenz, K. Löbmann, T. Rades, K. Knop, P. Kleinebudde, Hot melt extrusion and spray drying of co-amorphous indomethacin-arginine with polymers, J. Pharm. Sci. 106 (2017) 302–312.

[86]   G. Kasten, Í. Duarte, M. Paisana, K. Löbmann, T. Rades, H. Grohganz, Process optimization and upscaling of spray-dried drug-amino acid co-amorphous formulations, Pharmaceutics 11 (2019) 1–11.

[87]   P.A. Priemel, H. Grohganz, T. Rades, Unintended and in situ amorphisation of pharmaceuticals, Adv. Drug Deliv. Rev. 100 (2016) 126–132.

[88]   B.C. Hancock, G. Zografi, Effects of solid-state processing on water vapor sorption by aspirin, J. Pharm. Sci. 85 (1996) 246–248.

[89]   J. Wardrop, D. Law, Y. Qiu, K. Engh, L. Faitsch, C. Ling, Influence of solid phase and formulation processing on stability of Abbott-232 tablet formulations, J. Pharm. Sci. 95 (2006) 2380–2392.

[90]   P.A. Priemel, R. Laitinen, H. Grohganz, T. Rades, C.J. Strachan, In situ amorphisation of indomethacin with Eudragit® E during dissolution, Eur. J. Pharm. Biopharm. 85 (2013) 1259–1265.

[91]   M. Doreth, K. Löbmann, H. Grohganz, R. Holm, H. Lopez de Diego, T. Rades, P.A. Priemel, Glass solution formation in water - In situ amorphization of naproxen and ibuprofen with Eudragit® E PO, J. Drug Deliv. Sci. Tech. 34 (2016) 32–40.

[92]   M. Doreth, M.A. Hussein, P.A. Priemel, H. Grohganz, R. Holm, H. Lopez de Diego, T. Rades, K. Löbmann, Amorphization within the tablet: Using microwave irradiation to form a glass solution in situ, Int. J. Pharm. 519 (2017) 343–351.

[93]   M. Doreth, K. Löbmann, P. Priemel, H. Grohganz, R. Taylor, R. Holm, H. Lopez de Diego, T. Rades, Influence of PVP molecular weight on the microwave assisted in situ amorphization of indomethacin, Eur. J. Pharm. Biopharm. 122 (2017) 62–69.

[94]   M. Edinger, M.M. Knopp, H. Kerdoncuff, J. Rantanen, T. Rades, K. Löbmann, Quantification of microwave-induced amorphization of celecoxib in PVP tablets using transmission Raman spectroscopy, Eur. J. Pharm. Biopharm. 117 (2018) 62–67.

[95]   D. Maurya, V. Belgamwar, A. Tekade, Microwave induced solubility enhancement of poorly water soluble atorvastatin calcium, J. Pharm. Pharmacol. 62 (2010) 1599–1606.

[96]   M. Moneghini, B. Bellich, P. Baxa, F. Princivalle, Microwave generated solid dispersions containing ibuprofen, Int. J. Pharm. 361 (2008) 125–130.

[97]   N. Radacsi, G.D. Stefanidis, P. Szabó-Révész, R. Ambrus, Analysis of niflumic acid prepared by rapid microwave-assisted evaporation, J. Pharmaceut. Biomed. 98 (2014) 16–21.

[98]   M. Otsuka, Y. Maeno, T. Fukami, M. Inoue, T. Tagami, T. Ozeki, Solid dispersions of efonidipine hydrochloride ethanolate with improved physicochemical and pharmacokinetic properties prepared with microwave treatment, Eur. J. Pharm. Biopharm. 108 (2016) 25–31.

[99]   E. Lenz, K.T. Jensen, L.I. Blaabjerg, K. Knop, H. Grohganz, K. Löbmann, T. Rades, P. Kleinebudde, Solid-state properties and dissolution behaviour of tablets containing co-amorphous indomethacin-arginine, Eur. J. Pharm. Biopharm. 96 (2015) 44–52.

[100] S. Tanabe, K. Higashi, M. Umino, W. Limwikrant, K. Yamamoto, K. Moribe, Yellow coloration phenomena of incorporated indomethacin into folded sheet mesoporous materials, Int. J. Pharm. 429 (2012) 38–45.

[101] A. Paudel, J. Meeus, Van den Mooter, Guy, Structural characterization of amorphous solid dispersions, in: N. Shah, H. Sandhu, D.S. Choi (Eds.), Amorphous Solid Dispersions: Theory and Practice, Springer, New York, USA, 2014, pp. 421–485.

[102] P.G. Royall, C.-Y. Huang, S.-W.J. Tang, J. Duncan, G. Van-de-Velde, M.B. Brown, The development of DMA for the detection of amorphous content in pharmaceutical powdered materials, Int. J. Pharm. 301 (2005) 181–191.

[103] D. Mahlin, J. Wood, N. Hawkins, J. Mahey, P.G. Royall, A novel powder sample holder for the determination of glass transition temperatures by DMA, Int. J. Pharm. 371 (2009) 120–125.

[104] D.S. Jones, Y. Tian, O. Abu-Diak, G.P. Andrews, Pharmaceutical applications of dynamic mechanical thermal analysis, Adv. Drug Deliv. Rev. 64 (2012) 440–448.

[105] A. Heinz, C.J. Strachan, K.C. Gordon, T. Rades, Analysis of solid-state transformations of pharmaceutical compounds using vibrational spectroscopy, J. Pharm. Pharmacol. 61 (2009) 971–988.

[106] C.J. Strachan, T. Rades, K.C. Gordon, J. Rantanen, Raman spectroscopy for quantitative analysis of pharmaceutical solids, J. Pharm. Pharmacol. 59 (2007) 179–192.

[107] J. Sibik, K. Löbmann, T. Rades, J.A. Zeitler, Predicting crystallization of amorphous drugs with terahertz spectroscopy, Mol. Pharm. 12 (2015) 3062–3068.

[108] G.A. Stephenson, R.A. Forbes, S.M. Reutzel-Edens, Characterization of the solid state: quantitative issues, Adv. Drug Deliv. Rev. 48 (2001) 67–90.

[109] S. Bhattacharya, H.G. Brittain, R. Suryanarayanan, Thermoanalytical and crystallographic methods, in: H.G. Brittain (Ed.), Polymorphism in pharmaceutical solids, 2nd ed., Informa healthcare, New York, USA, 2009, pp. 327–342.

[110] R. Suryanarayanan, X-Ray Powder Diffractometry, in: H.G. Brittain (Ed.), Physical characterization of pharmaceutical solids, Informa healthcare, New York, USA, 1995, pp. 187–218.

[111] K. Shankland, An overview of powder x-ray diffraction and its relevance to pharmaceutical crystal structures, in: A. Müllertz, Y. Perrie, T. Rades (Eds.), Analytical techniques in the pharmaceutical sciences, Springer, New York, USA, 2016, pp. 293–314.

[112] B. Shah, V.K. Kakumanu, A.K. Bansal, Analytical techniques for quantification of amorphous/crystalline phases in pharmaceutical solids, J. Pharm. Sci. 95 (2006) 1641–1665.

[113] X. Ma, R.O. Williams, Characterization of amorphous solid dispersions: An update, J. Drug Deliv. Sci. Tech. (2019).

[114] P. Gabbott, A practical introduction to differential scanning calorimetry, in: P. Gabbott (Ed.), Applications of thermal analysis, 1st ed., Blackwell Publishers, New Jersey, USA, 2007, pp. 1–50.

[115] J.A. McCauley, H.G. Brittain, Thermal methods of analysis, in: H.G. Brittain (Ed.), Physical characterization of pharmaceutical solids, Informa healthcare, New York, USA, 1995, pp. 224–243.

[116] M. Saunders, Thermal analysis of pharmaceuticals, in: P. Gabbott (Ed.), Applications of thermal analysis, 1st ed., Blackwell Publishers, New Jersey, USA, 2007, pp. 286–327.

[117] E.O. Kissi, G. Kasten, K. Löbmann, T. Rades, H. Grohganz, The role of glass transition temperatures in coamorphous drug-amino acid formulations, Mol. Pharm. 15 (2018) 4247–4256.

[118] P.S. Gill, S.R. Sauerbrunn, M. Reading, Modulated differential scanning calorimetry, J. Therm. Anal. 40 (1993) 931–939.

[119] C. Tomasi, P. Mustarelli, N.A. Hawkins, V. Hill, Characterisation of amorphous materials by modulated differential scanning calorimetry, Thermochimica Acta 278 (1996) 9–18.

[120] M.M. Knopp, K. Löbmann, D.P. Elder, T. Rades, R. Holm, Recent advances and potential applications of modulated differential scanning calorimetry (mDSC) in drug development, Eur. J. Pharm. Sci. 87 (2016) 164–173.

[121] D.E. Bugay, A.C. Williams, Vibrational spectroscopy, in: H.G. Brittain (Ed.), Physical characterization of pharmaceutical solids, Informa healthcare, New York, USA, 1995, pp. 59–88.

[122] G. Reich, Mid and near infrared spectroscopy, in: A. Müllertz, Y. Perrie, T. Rades (Eds.), Analytical techniques in the pharmaceutical sciences, Springer, New York, USA, 2016, pp. 61–69.

[123] H.G. Brittain, Vibrational spectroscopy, in: H.G. Brittain (Ed.), Polymorphism in pharmaceutical solids, 2nd ed., Informa healthcare, New York, USA, 2009, pp. 347–373.

[124] G.C. Cole, J.E. Hogan, M.E. Aulton, Pharmaceutical coating technology, Taylor & Francis, London, UK, 1995.

[125] P.K. Gaur, S. Mishra, R. Gautam, A.P. Singh, M. Yasir, Film coating technology: Past, present and future, J. Pharm. Sci. Pharmacol. 1 (2014) 57–67.

[126] F. Siepmann, J. Siepmann, M. Walther, R.J. MacRae, R. Bodmeier, Polymer blends for controlled release coatings, J. Controlled Release 125 (2008).

[127] H. Sohi, Y. Sultana, R.K. Khar, Taste masking technologies in oral pharmaceuticals: Recent developments and approaches, Drug Dev. Ind. Pharm. 30 (2004) 429–448.

[128] O. Bley, J. Siepmann, R. Bodmeier, Characterization of moisture-protective polymer coatings using differential scanning calorimetry and dynamic vapor sorption, J. Pharm. Sci. 98 (2009) 651–664.

[129] C.T. Rhodes, S.C. Porter, Coatings for controlled-release drug delivery systems, Drug Dev. Ind. Pharm. 24 (1998) 1139–1154.

[130] C.S. Leopold, Coated dosage forms for colon-specific drug delivery, Pharm. Sci. Technol. Today 2 (1999) 197–204.

[131] G. van Savage, C.T. Rhodes, The sustained release coating of solid dosage forms: A historical review, Drug Dev. Ind. Pharm. 21 (2008) 93–118.

[132] N. Debotton, A. Dahan, Applications of polymers as pharmaceutical excipients in solid oral dosage forms, Med. Res. Rev. 37 (2017) 52–97.

[133] K.O.R. Lehmann, Chemistry and application properties of polymethacrylate coating systems, in: J.W. McGinity (Ed.), Aqueous polymeric coatings for

pharmaceutical dosage forms, Marcel Dekker, New York, USA, 1989, pp. 153–245.

[134] BASF Aktiengesellschaft, Technical information, Kollicoat® Protect, 2012.

[135] S. Bose, R.H. Bogner, Solventless pharmaceutical coating processes: A review, Pharm. Dev. Technol. 12 (2007) 115–131.

[136] C.R. Steuernagel, Latex emulsions for controlled drug delivery, in: J.W. McGinity (Ed.), Aqueous polymeric coatings for pharmaceutical dosage forms, Marcel Dekker, New York, USA, 1989, pp. 1–61.

[137] J. Siepmann, F. Siepmann, Stability of aqueous polymeric controlled release film coatings, Int. J. Pharm. 457 (2013) 437–445.

[138] L.A. Felton, Mechanisms of polymeric film formation, Int. J. Pharm. 457 (2013) 423–427.

[139] Evonik Industries, EUDRAGIT® Application Guidelines, 12 ed., Darmstadt, Germany, 2018.

[140] L.D. Bruce, J.W. McGinity, Polymer interactions with drugs and excipients, in: J.W. McGinity, L.A. Felton (Eds.), Aqueous polymeric coatings for pharmaceutical dosage forms, 3rd ed., Informa healthcare, New York, 2008, pp. 369–408.

[141] L. Carpentier, R. Decressain, S. Desprez, M. Descamps, Dynamics of the amorphous and crystalline alpha-, gamma-phases of indomethacin, J. Phys. Chem. B 110 (2006) 457–464.

[142] V. Andronis, G. Zografi, Crystal nucleation and growth of indomethacin polymorphs from the amorphous state, J. Non-Cryst. Solids 271 (2000) 236–248.

[143] N. Kaneniwa, M. Otsuka, T. Hayashi, Physicochemical characterization of indomethacin polymorphs and the transformation kinetics in ethanol, Chem. Pharm. Bull. 8 (1985) 3447–3455.

[144] S.A. Surwase, J.P. Boetker, D. Saville, B.J. Boyd, K.C. Gordon, L. Peltonen, C.J. Strachan, Indomethacin: new polymorphs of an old drug, Mol. Pharm. 10 (2013) 4472–4480.

[145] R. Ojarinta, A.T. Heikkinen, E. Sievänen, R. Laitinen, Dissolution behavior of co-amorphous amino acid-indomethacin mixtures: The ability of amino acids to stabilize the supersaturated state of indomethacin, Eur. J. Pharm. Biopharm. 112 (2017) 85–95.

[146] A. Cipiciani, C. Ebert, P. Linda, F. Rubessa, G. Savelli, Kinetics and mechanism of the basic hydrolysis of indomethacin and related compounds: A reevaluation, J. Pharm. Sci. 72 (1983) 1075–1076.

[147] N.R. Goud, S. Gangavaram, K. Suresh, S. Pal, S.G. Manjunatha, S. Nambiar, A. Nangia, Novel furosemide cocrystals and selection of high solubility drug forms, J. Pharm. Sci. 101 (2012) 664–680.

[148] M. Banik, S.P. Gopi, S. Ganguly, G.R. Desiraju, Cocrystal and salt forms of furosemide: Solubility and diffusion variations, Cryst. Growth Des. 16 (2016) 5418–5428.

[149] G. Murtaza, S.A. Khan, M. Najam-ul-Haq, I. Hussain, Comparative evaluation of various solubility enhancement strategies for furosemide, Pak. J. Pharm. Sci. 27 (2014) 963–973.

[150] G.J. Fernandes, L. Kumar, K. Sharma, R. Tunge, M. Rathnanand, A review on solubility enhancement of carvedilol—a BCS class II drug, J. Pharm. Innov. 4 (2018) 1387.

[151] J. Mishra, K. Löbmann, H. Grohganz, T. Rades, Influence of preparation technique on co-amorphization of carvedilol with acidic amino acids, Int. J. Pharm. 552 (2018) 407–413.

[152] E.P. Serjeant, B. Dempsey, Ionisation constants of organic acids in aqueous solution, Pergamon Press, New York, USA, 1979.

[153]   K.G. Pitt, J.M. Newton, P. Stanley, Tensile fracture of doubly-convex cylindrical discs under diametral loading, J. Mater. Sci. 23 (1988) 2723–2728.

[154]   J.E.K. Schawe, T. Hütter, C. Heitz, I. Alig, D. Lellinger, Stochastic temperature modulation: A new technique in temperature-modulated DSC, Thermochim. Acta 446 (2006) 147–155.

[155]   R.L. Danley, New heat flux DSC measurement technique, Thermochim. Acta 395 (2003) 201–208.

[156]   I. Youm, B.-B.C. Youan, Validated reverse-phase high-performance liquid chromatography for quantification of furosemide in tablets and nanoparticles, J. Anal. Methods Chem. 2013 (2013) 1–9.

[157]   P. Tong, G. Zografi, Effects of water vapor absorption on the physical and chemical stability of amorphous sodium indomethacin, AAPS PharmSciTech 5 (2004) 9-16.

[158]   W.L. Hulse, R.T. Forbes, M.C. Bonner, M. Getrost, The characterization and comparison of spray-dried mannitol samples, Drug Dev. Ind. Pharm. 35 (2009) 712–718.

[159]   B.C. Hancock, M. Parks, What is the True Solubility Advantage for Amorphous Pharmaceuticals?, Pharm. Res. (2000) 397–404.

[160]   D.E. Alonzo, G.G.Z. Zhang, D. Zhou, Y. Gao, L.S. Taylor, Understanding the behavior of amorphous pharmaceutical systems during dissolution, Pharm. Res. 27 (2010) 608–618.

[161]   S.A. Raina, D.E. Alonzo, G.G.Z. Zhang, Y. Gao, L.S. Taylor, Impact of polymers on the crystallization and phase transition kinetics of amorphous nifedipine during dissolution in aqueous media, Mol. Pharm. 11 (2014) 3565–3576.

[162]   H. Konno, T. Handa, D.E. Alonzo, L.S. Taylor, Effect of polymer type on the dissolution profile of amorphous solid dispersions containing felodipine, Eur. J. Pharm. Biopharm. 70 (2008) 493–499.

[163] F. Tanno, Y. Nishiyama, H. Kokubo, S. Obara, Evaluation of hypromellose acetate succinate (HPMCAS) as a carrier in solid dispersions, Drug Dev. Ind. Pharm. 30 (2004) 9–17.

[164] D.E. Alonzo, Y. Gao, D. Zhou, H. Mo, G.G.Z. Zhang, L.S. Taylor, Dissolution and precipitation behavior of amorphous solid dispersions, J. Pharm. Sci. 100 (2011) 3316–3331.

[165] T. Sato, A. Okada, K. Sekiguchi, Y. Tsuda, Difference in physico-pharmaceutical properties between crystalline and noncrystalline 9,3-diacetylmidecamycin, Chem. Pharm. Bull. 29 (1981) 2675–2682.

[166] S. Janssens, H.N. de Armas, J.P. Remon, G. Van den Mooter, The use of a new hydrophilic polymer, Kollicoat IR, in the formulation of solid dispersions of Itraconazole, Eur. J. Pharm. Sci. 30 (2007) 288–294.

[167] T. Le Minh, Designing crystallization based-enantiomeric separation for chiral compound-forming systems in consideration of polymorphism and solvate formation, Dr. Hut, München, 2014.

[168] A. Barth, Infrared spectroscopy of proteins, Biochim. Biophys. Acta 1767 (2007) 1073–1101.

[169] A. Barth, The infrared absorption of amino acid side chains, Prog. Biophys. Mol. Bio. 74 (2000) 141–173.

[170] J.F. Pearson, M.A. Slifkin, The infrared spectra of amino acids and dipeptides, Spectrochim. Acta 28 (1972) 2403–2417.

[171] I. Petry, K. Löbmann, H. Grohganz, T. Rades, C.S. Leopold, Solid state properties and drug release behavior of co-amorphous indomethacin-arginine tablets coated with Kollicoat® Protect, Eur. J. Pharm. Biopharm. 119 (2017) 150–160.

[172] P. Tong, G. Zografi, Solid-state characteristics of amorphous sodium indomethacin relative to its free acid, Pharm. Res. 16 (1999) 1186-1192.

[173]   B.R. Hajratwala, J.E. Dawson, Kinetics of indomethacin degradation I: Presence of alkali, J. Pharm. Sci. 66 (1977) 27–29.

[174]   www.drugs.com/dosage/indomethacin, Indomethacin dosage (2018).

[175]   www.drugs.com/dosage/furosemide, Furosemide dosage (2018).

[176]   R. C. Rowe, P. J. Sheskey, M. E. Quinn, Handbook of Pharmaceutical Excipients, Pharmaceutical Press, London, 2010.

[177]   G.A. Agyilirah, G.S. Banker, Polymers for controlled drug delivery, CRC Press, Boca Raton, USA, 1991.

[178]   A. Burger, J.-O. Henck, S. Hetz, J.M. Rollinger, A.A. Weissnicht, H. Stöttner, Energy/Temperature diagram and compression behavior of the polymorphs of d-mannitol, J. Pharm. Sci. 89 (2000) 457–468.

[179]   I. Petry, K. Löbmann, H. Grohganz, T. Rades, C.S. Leopold, In situ co-amorphisation of arginine with indomethacin or furosemide during immersion in an acidic medium - a proof of concept study, Eur. J. Pharm. Biopharm. 133 (2018) 151–160.

[180]   J. Hildesheim, S. Finogueev, B.-Z. Dolitzky, S. Ben-Valid, US6699997B2 - Carvedilol (2004).

[181]   IPCS, www.inchem.org/documents/icsc/icsc/eics1439, L-aspartic acid, 2018.

[182]   R.N. Shamma, M. Basha, Soluplus®: A novel polymeric solubilizer for optimization of Carvedilol solid dispersions: Formulation design and effect of method of preparation, Powder Technol. 237 (2013) 406–414.

[183]   L. Jagannathan, R. Meenakshi, S. Gunasekaran, S. Srinivasan, FT-IR, FT-Raman and UV–vis spectra and quantum chemical investigation of carvedilol, Mol. Simulat. 36 (2010) 283–290.

Appendix

A Hazardous materials

Substance	Supplier	Danger symbol	Hazard statements	Precautionary statements
Acetic acid	VWR, USA		H226, H290, H314	P210, P280, P301 + 330 + 331, P305 + 351 + 338, P308 + 310
Acetone	Biesterfeld, Germany		H225, H319, H336, H373	P210, P235, P260, P305 + 351 + 338
Acetonitrile	VWR, USA		H225, H302 + H312 + H332, H319	P210, P240, P302 + P352, P305 + P351, P403 + P233
Arginine	Merck, Germany		H319	P305+P351+P338
Carvedilol	TCI, Germany		H411	P273
4-Chlorobenzoic acid	Merck, Germany		H302, H315, H319, H335	P261, P305 + 351 + 338

Citric acid	Carl Roth, Germany		H319	P280, P305 + 351 + 338, P337 + 313
Hydrochloric acid 1.0 mol/l	Carl Roth, Germany		H290	P234, P390
Furosemide	Fagron, Germany		H360	P201, P308 + P313
Indomethacin	Fagron, Germany TCI, Germany		H300, H317, H360	P201, P280, P301 + 310 + 330, P302 + 352, P308 + 313
Isopropyl alcohol	BCD Chemie, Germany		H225, H319, H336	P210, P261, P305 + 351 + 338
Phosphoric acid 85 %	Carl Roth, Germany		H290, H314	P280, P310, P301 + P330 + P331, P303 + P361 + P353, P305 + P351 + P338

B Curriculum vitae

Name: Petry, Ina Zainabu   Date of birth: Dec 24th, 1990

Marital status: unmarried   Place of Birth: Kassel

Education	since 10/2015	Ph.D.student, Division of Pharmaceutical Technology, Universität Hamburg, Supervisor: Prof. Dr. C.S. Leopold Co-Supervisor: Prof. Dr. Dr. h.c. T. Rades
	06/2015	Licensure as a pharmacist (Approbation)
	09/2012 – 01/2013	Semester abroad (Study of Pharmacy), University of Bath, England
	10/2009 – 04/2014	Study of Pharmacy, Universität Hamburg
Specialization	since 03/2016	"Fachapotheker für Pharmazeutische Technologie"
Internships	11/2014 – 04/2015	Intern, Nikolai Apotheke, Hamburg
	05/2014 – 10/2014	Intern, Pfizer Deutschland, Freiburg
School	06/2009	A-level diploma, Kaiser Wilhelm- und Ratsgymnasium, Hannover

C Acknowledgements

This thesis was prepared at the University of Hamburg, at the Department of Chemistry in the division of Pharmaceutical Technology on the initiative and under supervision of Professor Dr. Claudia S. Leopold. In this part of the thesis, I would like to thank all those people who made an important contribution to this work.

First of all, I would like to thank Prof. Dr. Leopold for leaving me with this highly interesting research topic and for giving me the opportunity to be a member of her research group. I deeply appreciate her provided freedom in my research and thank her for the guidance and the inspiring scientific discussions.

Furthermore, I would gratefully acknowledge Prof. Dr. Dr. h.c. Thomas Rades, Prof. Dr. Korbinian Löbmann and Prof. Dr. Holger Grohganz from the University of Copenhagen for the co-supervision of this work. They motivated and supported me and gave me a warm welcome in their working group during my research stays at the University of Copenhagen. I really enjoyed the inspiring discussions with them and deeply appreciate their effort for the joint research projects.

Moreover, I am grateful to Prof. Dr. Ralph Holl for evaluating this thesis. Furthemore, I would like to thank Prof. Dr. Sebastian Wicha and Dr. Axel T. Neffe for being members of the examination committee.

I also thank Dr. Albrecht Sakmann for his help with student's supervision as well as for enabling my attendance to conferences or training courses, even during student's supervision. In addition, I would like to thank Petra Borbe and Kai Braunschweig for their kind assistance with regard to TGA and HPLC analysis. Also, I would like to thank

<u>Declaration on oath (affirmation in lieu of oath)</u> / Eidesstattliche Versicherung

Hiermit versichere ich an Eides statt, die vorliegende Dissertation selbst verfasst und keine anderen als die angegebenen Hilfsmittel benutzt zu haben. Die eingereichte schriftliche Fassung entspricht der auf dem elektronischen Speichermedium. Ich versichere, dass diese Dissertation nicht in einem früheren Promotionsverfahren eingereicht wurde.

Datum, Unterschrift